

Author's Response:

We wish to thank both referees for their comprehensive and elaborated comments. Despite some mistakes they have revealed in the manuscript, the referees took the time and effort to explain the source of the inaccuracies and offer good advice and practical solutions.

Overall, we have received extensive comments on all sections and figures by both referees. Therefore, we've decided to combine the referees' comments and write our point to point response along the manuscript sections:

- Abstract
- Introduction
- Instruments
- Results
- Conclusions and discussion
- References

We hope this structure is acceptable and easy to follow.

Sincerely,

Leenes Uzan, Dr. Smadar Egert and Prof. Pinhas Alpert

Abstract: lines 39-51

Referees Comments:

Referee #2: *The abstract does not just summarize the paper properly. The abstract should be compact, i.e., as short as possible and just cover the contents of the paper: The main goal, the instruments and methods used, and main findings.... no outlook..., no unnecessary (motivating) statements that can be given in the introduction....*

Author's response: Comments accepted.

Author's changes in manuscript: The abstract was rewritten as recommended.

Introduction: lines 56-145

Referees Comments:

Referee #1: *line 61: I recommend to add a short paragraph here introducing the scientific objectives and the benefit of the paper. Something like "One of the strongest events ever... It was investigated already by several studies... However, ... is missing. Therefore, in our investigation we focus on...". Then the short description of the event and the review of the existing publications can follow as is.*

Referee #2: *The introduction could be more straight forward, as follows: There was a huge dust storm in the Middle East, however, the dust forecast models failed. The question was then: Why? This question motivated Solomos et al. (2017) to run a cloud resolving model system. They found the most probable reasons. Please state their findings in the introduction! Afterwards, Gasch et al. (2017) used the new IKON/ART model system with rather high resolution (a global cloud-process-resolving model!!!) and also investigated this dust storm... and discussed the storm in even larger detail.... and concluded.... Please read the final version and present their final conclusions. This would be a nice introduction, very informative, so that the reader would learn a lot. And then you could provide the motivation for your own ceilometer study.... Because open points remained, and this historical dust storm must be documented for a variety of regions in the Middle East.*

Author's response: Comments accepted.

Author's changes in manuscript: Keeping in thought this paper is supplementary and an important insight of the extreme September 2015 dust storm, we significantly expanded the overview of previous studies describing the origin of the dust storm, analysis of observations and posteriori model runs. On our behalf, we added information describing the weather conditions and analyzed the dust event evolution over Israel in the lower atmosphere (up to 1 km). The data we present can support verification of state of the art model simulations (actually already been done by Gasch et al., which cited our presentation from the EGU conference).

Referees Comments:

Referee #1: line 62: Fig. 1 seems to be the justification that it is worthwhile to study the event. A detailed explanation of Fig. 1 is however missing.

line 71 (figure caption): The AOD derived from MSG (mention the sensor!) is shown. Make clear that Fig. 6 shows the AOD from AERONET for comparison.

Referee #2: Page 3, Fig. 1: The shown AOD range... is that the range of trustworthy values? Because the dust AODs were much higher than 2.7. So one could enlarge the color scale... How large is the uncertainty in the MSG data, source for the data (<http...>) should be mentioned.

Author's response: Comments accepted.

Author's changes in manuscript: Fig 1. was moved to the " Results and discussion" section where it was discussed. The caption was updated with the MSG SEVIRI sensor and source of the MSG data. The uncertainty of AOD measurements from MSG SEVIRI can rise up to 15% (Mei et al, 2012). The Sede-Boker AERONET AOD values at 12 UTC were added upon Fig.1 in the location of the Sede-Boker site.

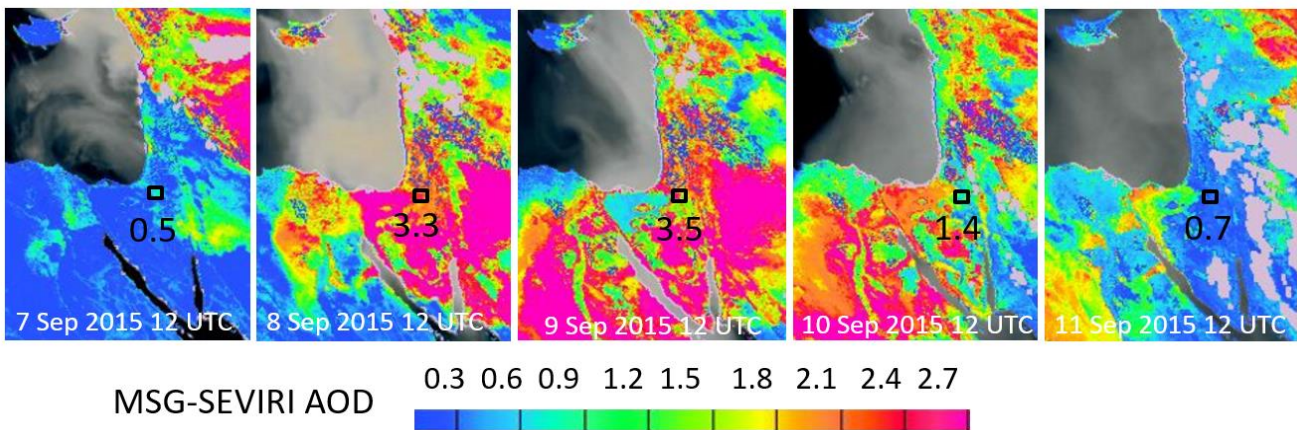


Figure 1. Aerosol Optical Depth (AOD) at 12 UTC analyzed by NAScube (Université de Lille) based on imagery from the Meteosat Second Generation (MSG) Satellite (by a combination of the SEVIRI IR8.7, IR10.8 and IR12.0 channels). The map includes indication of the Sede Boker AERONET site (black square) and its AOD value at 12 UTC.

Referees Comments:

Referee #1: line 68: How does the visibility and the reference to AERONET fit together? Give a citation for AERONET.

Author's response: Comments accepted.

Author's changes in manuscript: The referee is correct. AOD from AERONET could not be a reference to visibility. The AERONET reference was erased. We added a citation for the AERONET data.

Referees Comments:

Referee #1: *lines 78 ff: Give citations for Meteoinfo, MODIS, EARLINET, ICON-ART.*

Referee #2: *P3, L78, reference for Meteoinfo or http.*

Author's response: Comments accepted.

Author's changes in manuscript: Citations were added.

Referees Comments:

Referee #1: *line 91: Avoid acronyms in cases when it is only used once or twice, e.g. RST and SBF.*

Author's response: Comment accepted.

Author's changes in manuscript: Acronyms used up to twice were deleted.

Referees Comments:

Referee #1: *Use a common format for dates: "8. September 2015" instead of "08.09.15" is certainly a better option.*

Author's response: Comment accepted.

Author's changes in manuscript: The format of all dates was changed in to the suggested format.

Referees Comments:

Referee #1: *line 98: When referring to CALIPSO, mention that it was found that the top of the dust layer was at about 3–4 km (though the overpass was several hundreds of kilometers east of Israel). Even better: include a (short?) discussion of CALIPSO measurements (hopefully closer to Israel than in Gasch et al., 2017) into the results-section showing where the upper boundary of the dust layer has been. For this purpose, quick looks from the CALIPSO website could be sufficient. Then, the measurement range of the ceilometers can be highlighted (it is doubtful that the ceilometers can fully penetrate the dust layer at all times).*

Author's response: Comments accepted.

Author's changes in manuscript: We added two images (total backscatter and extinction coefficient) from the only passage of CALIPSO over Israel, on 10 September 2015. The images reveal a dust layer between 2-4 km ASL (see Fig.X below).

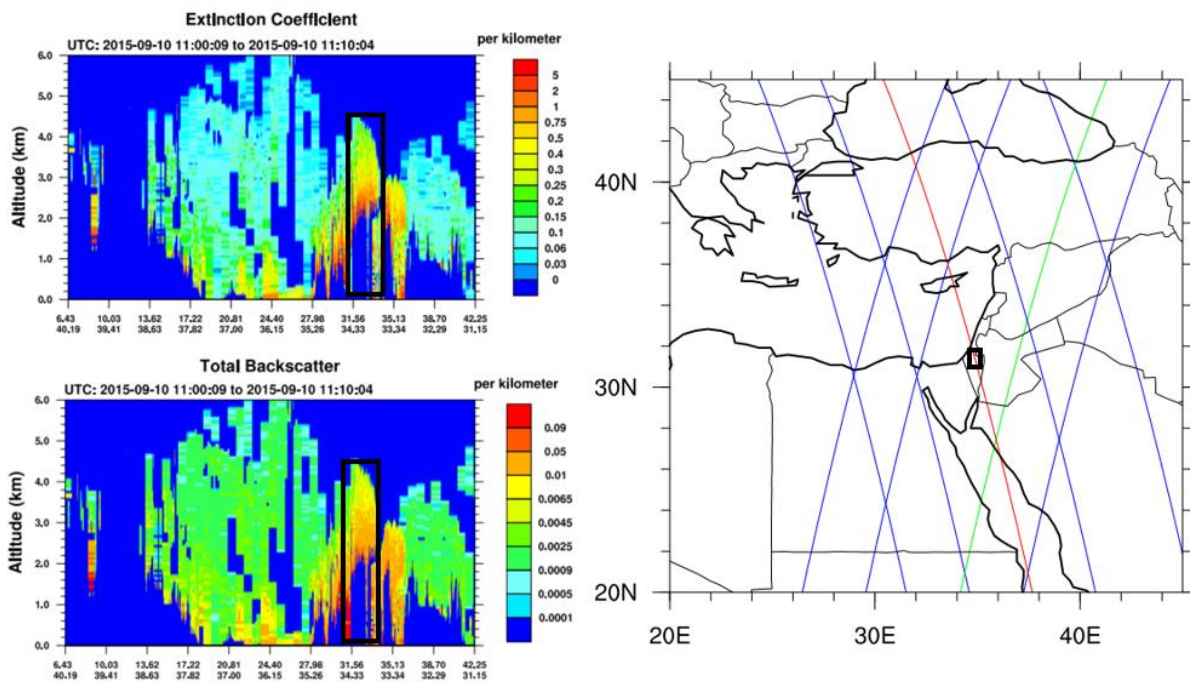


Figure X. A map of CALIPSO satellite overpasses (right panel). The only overpass above Israel was on 10 September 2015 at 11:00-11:10 UTC (indicated by a red line). On the left panel are the CALIOP lidar products of total backscatter and extinction coefficient. Indications of the overpass over Israel is given by a black rectangle.

Referees Comments (overview of Gasch et al.):

Referee #2:

P3, L94, the model better explained..... compared to what?

P3, L94, ART, give reference.

P4, L100, please check the finally revised version of the Gasch paper. I asked these authors, the final version should be out soon."

Author's response: Comments accepted.

Author's changes in manuscript: We expanded the summary of the Gasch et al. (2016) paper, explaining the model set up, ART model reference and the conclusions of the dust storm process. The final version of the Gasch et al (2016) was approved on the 15 November 2017 and will be cited accordingly.

Referees Comments (overview of Stavros et al.):

Referee #1:

line 115: Where was the lidar located?

line 118: Were the model results compared to CALIPSO or EARLINET (both are lidars)?

line 120: "...but the ability to predict the details were partial..": I don't understand this sentence. Is this relevant for this paper?

line 122: Lidars don't provide "aerosol concentration", but backscatter coefficients (or extinction coefficients, depended on the system).

Author's response: Comments accepted.

Author's changes in manuscript: We extended the summary of the Stavros et al., research and referred to the lidar located (Limassol Cyprus), the comparison of the EARLINET lidar to the model results and the estimation of the aerosol concentration based on the lidar ability to reproduce the strength of the dust event.

Referees Comments:

Referee #1: Use "lidar" instead of "LIDAR".

Referee #2: P4, L115, L118, L122: lidar... not LIDAR

Author's response: Comments accepted.

Author's changes in manuscript: "LIDAR" was changed to "lidar" throughout the text.

Referees Comments:

Referee #1:

line 130: What is meant by "scattering properties"?

Author's response: Comment accepted.

Author's changes in manuscript: " Scattering properties" was corrected to "optical properties".

Referees Comments:

Referee #1:

124: Give citation to " deep blue algorithm".

Author's response: Comment accepted.

Author's changes in manuscript: A citation for deep blue algorithm was added (Hsu et al., 2013).

Referees Comments:

Referee #2: P5, L134, *Is there no discussion in the literature on dust-radiation-dynamics relationship? I believe, the SAMUM group (Tellus 2011 special issue) investigated the relationship between dust (and smoke) and the radiation field and changes in the air flow (dynamics) as a result of the impact of dust and smoke on the radiative fluxes. Such dense dust layers as in September 2015 certainly had a huge impact on the radiation budget and significantly changed the weather pattern and thus air mass transport. This may explain why the routine dust forecast models failed because the forecasted dust concentration was too low to produce a significant radiation effect on the weather pattern (and dynamics) and dust transport in the model.*

Author's response: Comments accepted.

Author's changes in manuscript: The cited reference of Pu et al., (2016) did not discuss the effect of dust particles on the thermal radiation. Following the referees' remark, an elaborated discussion based on ground level radiation was added to "Results and discussion" section.

Referees Comments:

Referee #1: line 139: *"So far, no attempt has been done to relate the models findings..."*. *This seems to be in contradiction to the previous review of publications. The benefit of this paper is the provision of vertical profiles of the dust in the lower part of the troposphere and the continuous measurements at 8 sites. This helps to obtain a more complete picture (with high resolution) of the event over Israel: this is a valuable contribution. "...spatial, temporal and vertical...": vertical can be omitted because it is "included" in spatial.*

line 140: *"display" - "discuss"*.

Referee #2: P5, L138-L142: *You must clearly say in the beginning how the ceilometer network can contribute: Ceilometers can detect the dust layer base and provide some information about the lower part of the dust layer and, very important, the downward transport towards the ground. This is a good and valuable contribution to atmospheric science. On the other hand, not more than that! But this is fine! Nevertheless, you need to provide the limits of such systems! Very clearly! At these high AODs, there is no chance to detect most of the dust and the dust layer top.*

Author's response: Comments accepted.

Author's changes in manuscript: We rephrased the paragraph referring to the ceilometers' contribution (lines 138-142) and listed the limitation of the ceilometers in general and under high AOD conditions.

Manuscript lines 148-273 (Sect.2 Instruments):

Referees Comments:

Referee #1: *A (short) section on the satellite data used in this study is missing and might be included.*

Author's response: Comments accepted.

Author's changes in manuscript: A section of satellite data regarding imagery from MSG (SEVIRI), Terra (MODIS), Aqua (MODIS) and CALIPSO (CALIOP) satellites was added to the "Instruments" section.

Referees Comments:

Referee #2: *The description of the instruments and data sets on the one hand, and the presentation and discussion of scientific results on the other hand should be clearly separated. Presently e.g. the "radiosonde section" includes results (lines 211 ff.) that should be moved to Sect. 3*

Author's response: Comments accepted.

Author's changes in manuscript: Presentation and discussion of scientific results were moved to the "Results and discussion" section.

Referees Comments:

Referee #1: *line 152: "... to the atmosphere above its measuring point". Must be "top of the atmosphere". Omit "above its measuring point": strictly it is a slanted column.*

line 159: "...to add the vertical aerosol distribution...". The distribution is not added, but information on the distribution. Check the whole paper for similar wordings that are not fully correct.

Author's response: Comments accepted.

Author's changes in manuscript: We rephrased these sentences as recommended.

Referees Comments:

Referee #1: *The role of the scaling factor (lines 282 ff) should be moved to the description of the instruments and data sets. In particular, the ceilometer section must include more relevant information.*

line 165: To be more precise the first sentence and the corresponding citations should be modified: Start with a general statement on the potential of lidars to observe (dust) aerosols: here you can cite Mona et al. (already mentioned, but missing in the list of references), more papers from the EARLINET community such as Wiegner et al. (2011), Papayannis et al. (2008), Ansmann et al., (2003), all in J. Geophys. Res., or other papers. Then, you can state that with recent improvements of the ceilometers' hardware these eyesafe single-wavelength systems are getting more and more important in particular when implemented as network (move the citation of Wiegner et al., 2014, to this place). The

Weitkamp-paper is also missing in the reference list – so I don't know why it is included here. Finally, Vaisala's CL31 can be introduced but note that the cited Muenkel-paper from 2004 is on the CT25k-ceilometer, not on the CL31. So replace this citation by e.g. Muenkel et al., (2011)¹. Kotthaus et al. (2015) (cited later) is indeed on the CL31. Subsection "ceilometers": This paragraph needs major revisions. A few points: Make clear what you want to measure/determine: mixing layer heights, general structure of layers, heights of lower and upper boundaries, attenuated backscatter, particle backscatter coefficients or whatever. Depending on the desired output the requirements on the data evaluation are different.

Referee #2: *It seems to me that the authors try to avoid to clearly state: The ceilometer is of rather limited use in dust plume tracking. We were not able to see the full dust layer. But such a statement is required! ..and will not disturb the main goal of the paper. As reviewer I have to say: This is not acceptable and has to be improved! In cases with thick dust layer with optical depth >1 the transmitted (rather weak) radiation pulses of these ceilometers are immediately attenuated in the lowest part of the dust layers".*

Author's response: Comments accepted.

Author's changes in manuscript: The ceilometer paragraph was changed. We described the ceilometers limitations including the instrument specific characteristics which affect the quality and availability of the attenuated backscatter profiles, calibration methods, range detection limitations by the overlap function and determination of the sensitivity of the attenuated backscatter signal to relative humidity. Nevertheless, we portrayed the contribution of the ceilometers in the analysis of dust plume development in the lower part of the troposphere (up to 1 km AGL).

Instruments - Ceilometers: lines 164-188

Referees Comments:

Referee #1: *Include the discussion of the "scale factor" here: it is given by the manufacturer and it is unknown to the user where it comes from and how accurate it is. What is the purpose of it? Is it just a "mean" conversion factor of counts (no unit) to attenuated backscatter in $m^{-1} sr^{-1}$?*

Author's response: The ceilometer attenuated backscatter profiles are automatically corrected by:

*An internal calibration to convert signal counts to attenuated backscatter multiplying by 10^{-9} . The internal algorithm (resulting in 10^{-9}), unknown to the user, is suitable for all ceilometer types (C. Muenkel, private communication, September 2017).

*A cosmetic shift of the backscatter signal to better visualize the clouds base.

*An obstruction correction when the ceilometers' window is blocked (by an obstacle).

*An overlap correction to the height where the receiver field of view reaches complete overlap with the emitted laser beam.

Author's changes in manuscript: Data referring to the automatic correction of the ceilometer output profiles was added to the "Instruments" section.

Referees Comments:

Referee #1: *When you mention the wavelength of 910 nm, you should also mention that the signals must be corrected for water vapor absorption whenever you want to quantitatively derive any aerosol related quantity (e.g. link to AOD); here the citation of Weigner and Gasteiger (already included in the reference list) should be added.*

Author's response: Following Wiegner et al., (2014, 2015), the ceilometer wavelength range (given as 905 ± 3 nm) is influenced by water vapor absorption. However, in the case of aerosol layer detection, the water vapor distribution has a small effect on the signal change (indicating the MLH or an elevated mixed layer) because the aerosol backscatter itself remains unchanged. Consequently, except for a case of a dry layer in a humid mixed layer height, the water vapor is unlikely to lead misinterpretation of the aerosol stratification.

Author's changes in manuscript: The aforementioned explanation was added to the "Ceilometers" subsection. In our study we did not attempt to derive aerosol quantity as our ceilometers were not calibrated. We have rephrased all sentences that could have mislead the reader in this manner.

Referees Comments:

Referee #1: *As a consequence of Kotthaus et al. you should give the firmware version of your ceilometers.*

Author's response: Unfortunately, 6 out of the 8 ceilometers belong to a governmental office which does not allow to publicize their firmware data. Yet, we have been confirmed by the exclusive supplier of the ceilometers in Israel that the combination of firmware and hardware was done according to Kotthaus et al., recommendations.

Author's changes in manuscript: For the remaining 2 ceilometers we have added technical data summarized in Table X:

Table X. Ceilometer technical information

Location	Type	Engine board	Receiver	Transmitter	Firmware
Beit Dagan	CL31	CLE311	CLR311	CLT311	1.72
Weizmann	CL51	CLE321	CLRE321	CLT521	1.03

Moreover, the title of Table 2 in the manuscript referred to all ceilometers as CL31 type, while ceilometer Weizmann (Rehovot) is a CL51. Therefore, we added Table X1 as follows:

Table X1. Ceilometer configuration

Location	Type	Time resolution(sec)	Height resolution (m)	*Height range (km)
Mount Meron	CL31	16	10	7.7
Ramat David	CL31	16	10	7.7
Hadera	CL31	16	10	7.7
Tel Aviv	CL31	16	10	7.7
Beit Dagan	CL31	15	10	7.7
Rehovot (Weizmann)	CL51	16	10	15.4
Nevatim	CL31	16	10	7.7
Hazerim	CL31	16	10	7.7

* Height range depends on sky conditions and is limited as AOD increases.

* In all ceilometers but in Beit Dagan site, data acquisition was limited to 4.5 km based on the BLview firmware.

Referees Comments:

Referee #1: *You should mention that the overlap correction is automatically performed by the proprietary software and that it is not disclosed to the user. If the overlap correction creates signal artefacts (at 50–100 m), different for each ceilometer, is this crucial for your scientific objectives (if yes, what are the consequences?).*

Author's response: In our study we focused on the downward motion of the dust plume and its effect on the creation of the mixed layer height which did not reach below 200 m AGL. Therefore, artefacts up to 100 m AGL were not crucial.

Author's changes in manuscript: An explanation of the automatic overlap correction was added to the text.

Referees Comments:

Referee #1: *Be clear with the temporal resolution (it can be selected by the user in the range from ... to ... s; in this paper 16 s was selected, is there a special reason for 15 s for some ceilometers?). 7.7 km applies to all ceilometers, not only that at Beit Dagan. Do you know the pulse energy of the CL31?*

Referee #2: *P7, L178: ...up to 7.7 km height AGL. Yes the ceilometer may measure up to 7.7 km height, but only for clear sky conditions with AOD of the order of 0.2, at least clearly below 1. One has to state that. In case of the dust storm, all delivered 'counts' above 1 km were more or less just background noise!.*

P7, L188 ... The Beit Dagan Ceilometer measures up to 7.7 km. Yes, as mentioned, under clear sky conditions. At dust storm conditions with AODs from 2 to probably 5 and more, the ceilometer measures just noise from 1 to 7.7 km height. So this is an unacceptable statement. Please change.

Author's response: All ceilometers were capable to measure up to 7.7 km with a range gate of 10 m under the limitations of sky condition and a decrease in SNR with height. The data acquisition was limited to 4.5 km by BLview default except for ceilometer Beit Dagan.

Ceilometer Beit Dagan has a temporal resolution of 15 s set by the manufacturer. The pulse energy of the CL31 $1.2 \mu\text{Ws} \pm 20\%$.

Author's changes in manuscript: We rephrased the sentence and pointed out the limitations of the ceilometers to measure up to the maximum height range declared by the manufacturer.

Referees Comments:

Referee #2: *In the radiosonde plots there is always written: ... launching sites... please improve!*

Author's response: Comment accepted.

Author's changes in manuscript: The radiosonde plots were changed. We have omitted the profiles from the Cyprus site and concentrated on the low level (up to 1200 m ASL) of the temperature and relative humidity profiles from Beit Dagan in order to better visualize the MLH descent once the dust storm prevailed.

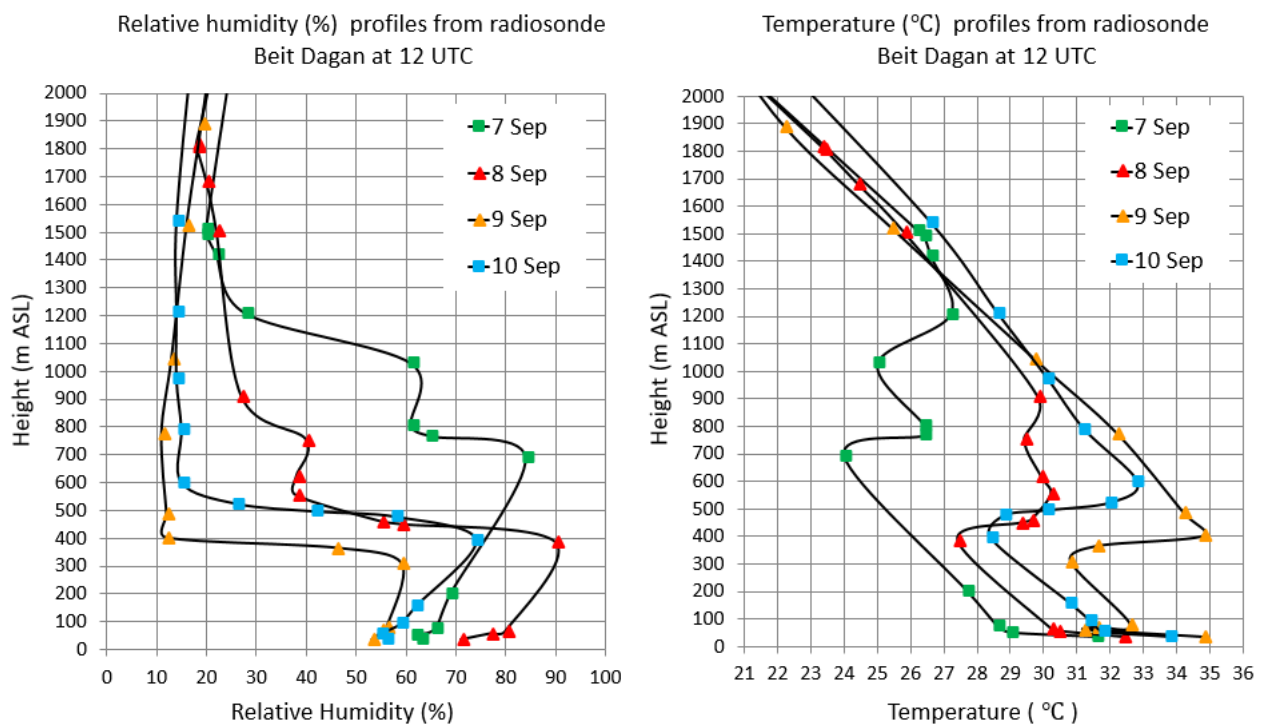


Figure X2. Radiosonde Beit Dagan profiles at 12 UTC between 7-10 September 2015 of relative humidity (left panel) and temperature (right panel).

Referees Comments:

Referee #2: P7, L173: Do you think that you would find the true mixing layer height (when applying the wavelet analysis) under such dense dust conditions? I am not sure! Usually you have the polluted mixing layer and the clear free troposphere on top. At these conditions, the wavelet technique works well. Now you have the opposite. And there was almost no solar heating of the ground (almost no convection), just a residual (less dust laden) layer below the dust layers. What you detect and interpret as mixing layer top is to my opinion just the other way around: the dust layer base height. One should state and discuss this point more clearly. At AODs of 2 and more there is no convection left to lead to well mixed conditions. The dust layer is warmer than the lowest, near-surface tropospheric layer and produces the temperature inversion observed with radiosonde.

Author's response: Ground level measurements of global radiation and ground temperature (measurements 10 cm AGL) from 33 sites (Fig. X3-X7) revealed the process of ground heating on 9 September was possible as the maximum global radiation measured at 12 (UTC+2) reached 500-700 (W m⁻²) in 19 out of 22 sites (Fig. X8) and the ground temperature reached the values measured prior to the dust storm. Nevertheless, WCT method (seeking the derivative which is the peak value) on the 8 September was probably a result of subsidence of the dust plume as suggested by the referee.

Fig. X3 Ground temperature (10 cm AGL) from northern Israel.

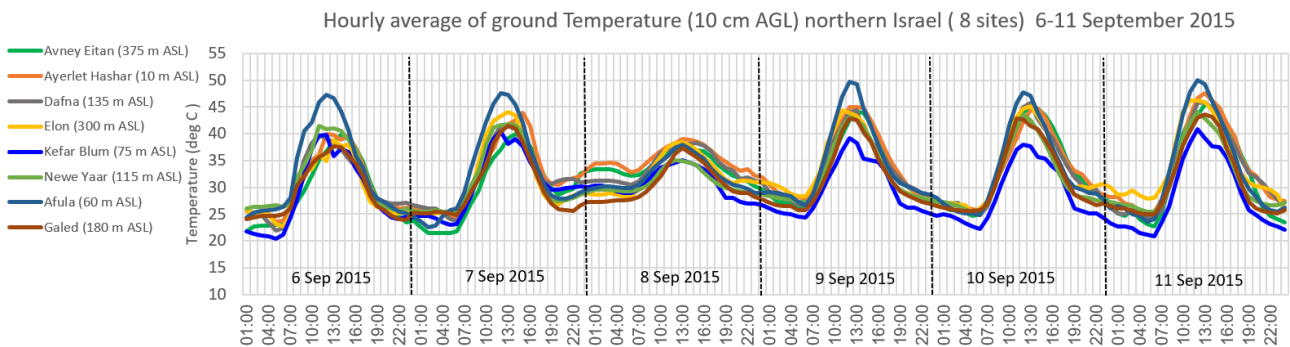


Fig. X4 Ground temperature (10 cm AGL) from mountain sites in Israel.

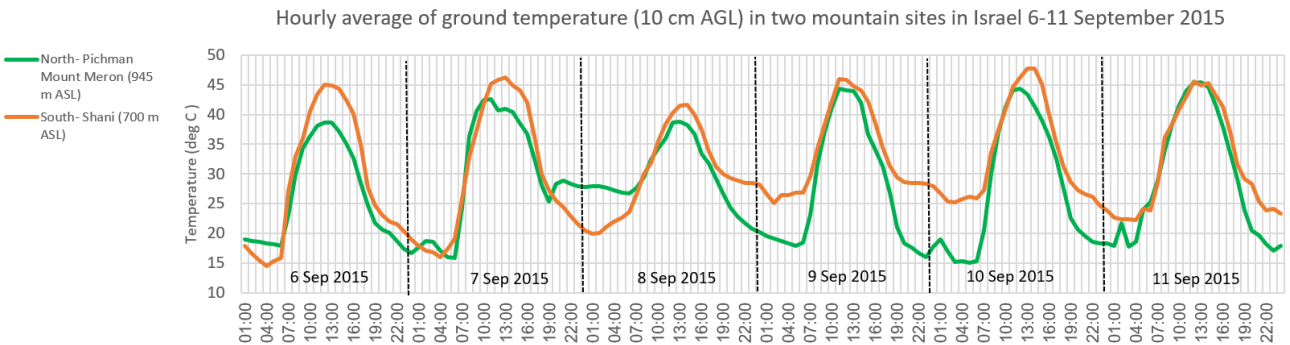


Fig. X5 Ground temperature (10 cm AGL) from valley sites in Israel.

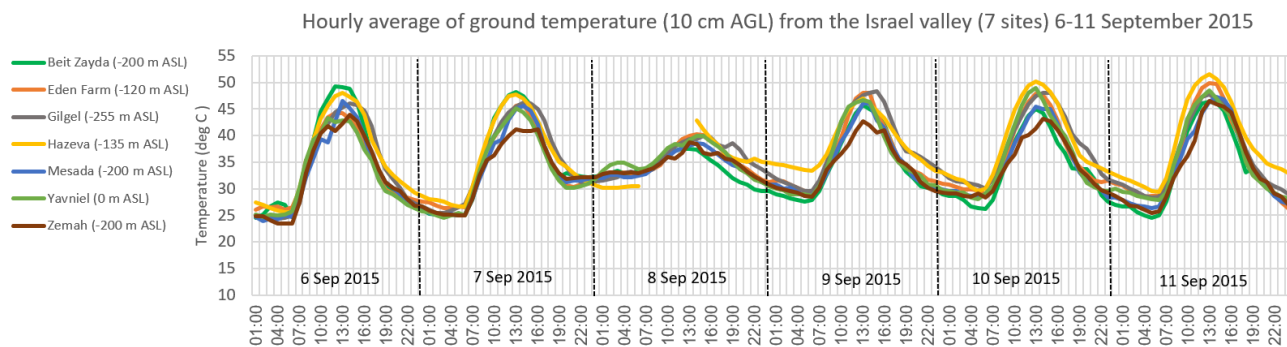


Fig. X6 Ground temperature (10 cm AGL) along the coast of Israel.

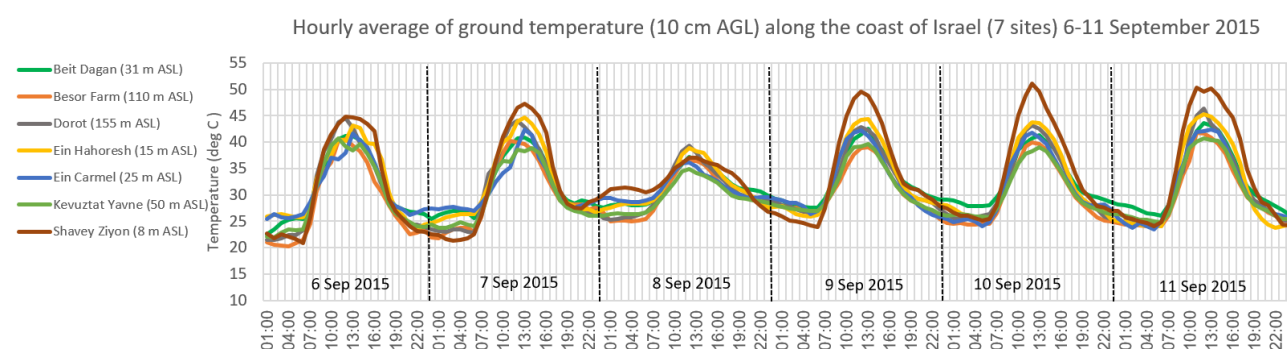
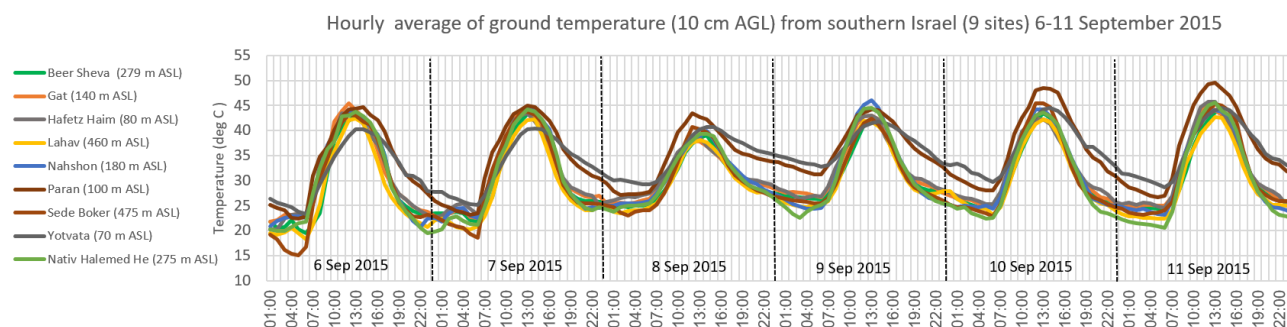


Fig. X7 Ground temperature (10 cm AGL) from southern Israel.



Author's changes in manuscript: We have omitted the figure comparing the MLH as identified by the the ceilometer and radiosonde from Beit Dagan site. Instead we dedicated an anlysis referring to the spatial and temporal variations in solar radiation supplemented Fig. X8-X9:

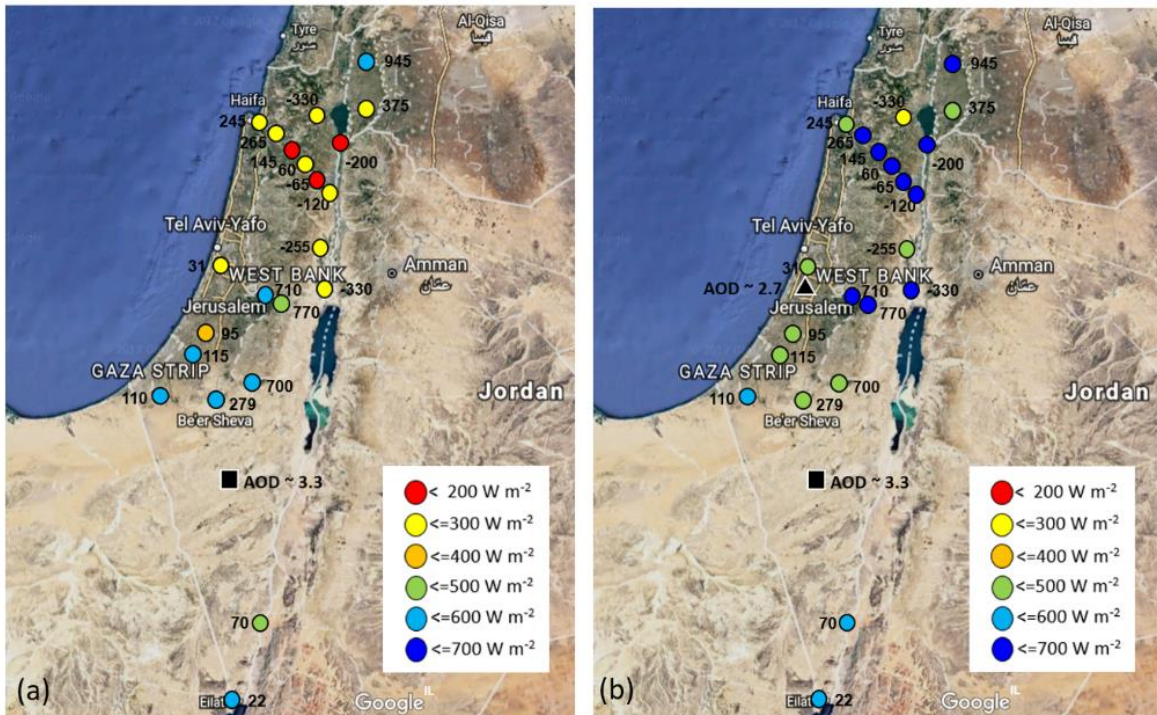


Figure X8. A map maximum global solar radiation from 22 sites measured at 10 UTC (midday) on 8 September 2015 (a) and 9 September 2015 (b). The map includes indications of radiation range (see legend), height of measurement site (numbers in black) and AERONET AOD from Sede Boker site (black square) and Weizmann site (black triangle). On 8 September Weizmann AERONET did not operate.

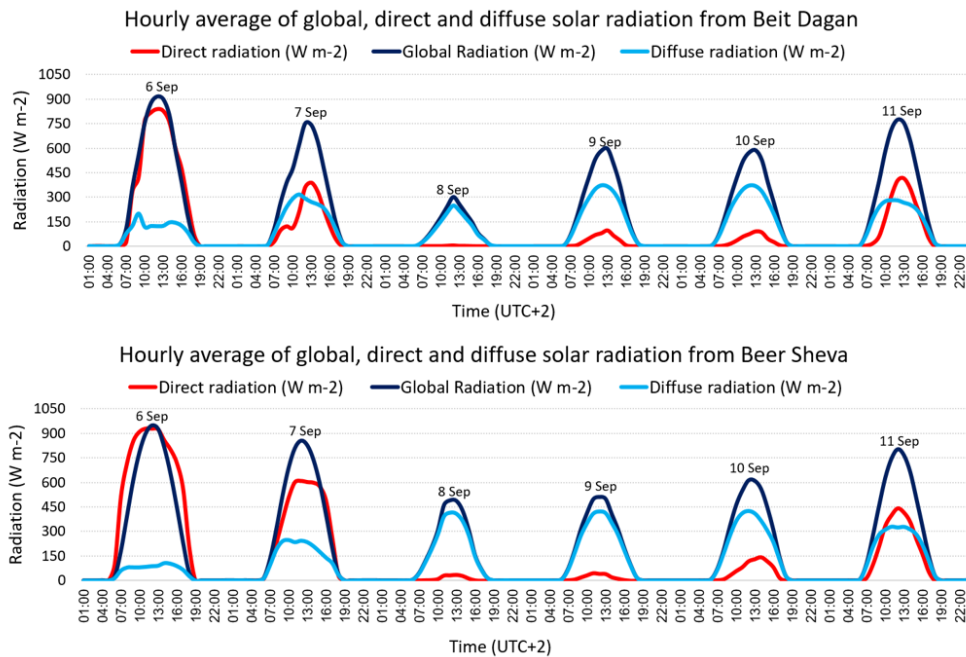


Figure X9. Hourly average of global, direct and diffuse solar radiation between 6-11 September 2015 from Beit Dagan and Beer Sheva.

Referees Comments:

Referee #2: P7, L183: Now a critical issue: I checked the Kotthaus paper. According to this paper and as it is well known, the ceilometer delivers range-corrected signals in arbitrary units. The measured counts are converted by using a conversion factor to obtain useful signal profiles, when the background is subtracted. We may denote these range corrected signals as level-0 data. Vaisala uses a 'conventional' conversion factor to transfer the background-corrected signals into lidar backscatter signals. But this is NOT the attenuated backscatter coefficient! To obtain the attenuated backscatter coefficient (something like the Rayleigh-calibrated range-corrected signal) you need an actual calibration (to obtain an actual conversion factor). This actual conversion factor however can only be derived under clear sky conditions (so that clear sky backscatter in the free troposphere becomes visible and an accompanying sunphotometer delivers the total OD (aerosol plus water vapor absorption) at around 910 nm, and the aerosol related AOD at 910nm by using interpolation between the measured 870 and 1020nm AOD). At these favorable conditions, the range-corrected signal may be calibrated to deliver the attenuated (aerosol) backscatter profile, and by using the Klett method and adjustment of the lidar ratio (that has to take care of water vapor absorption in addition in case of the Vaisala ceilometer) even the total particle backscatter coefficient. But all this was not possible under these dust storm conditions. In conclusion, you just present range-correct signals in arbitrary units. All the plots have to be changed accordingly. The paper is unacceptable if this important changes are not done.

Author's response: Comments accepted.

Author's changes in manuscript: The plots present signal counts. The term "backscatter coefficient" was deleted from the text. We apologize for the mistake. Thank you for the detailed explanation.

Instruments- Radiosonde: lines 197-213

Referees Comments:

Referee #1: "...disclosing the different meteorological conditions...": This is a too short statement: explain, what is shown. Explain the differences that can be seen from Fig. 4. What are the conclusions with respect to the overall topic of the paper?

Referee #2: P7, L198: Please remove the trivial statement about the radiosonde ascents. Please provide just information on radiosonde type and company, and meteorological parameters measured.

lines 208 ff: Move all results to Sect. 3.

Author's response: Comments accepted.

Author's changes in manuscript: A discussion on radiosondes profiles was moved to the "Results and discussion" section. The radiosonde is a Vaisala type RS41-SG producing profiles of humidity, temperature, pressure, and wind measurement.

Instruments- Particulate matter measurements: lines 221-247:

Referees Comments:

Referee #1: *Note, that the titles of the subsections are inconsistent: "ceilometers" are instruments, but "PM10" is not.*

Author's response: Comment accepted.

Author's changes in manuscript: The title of Sect. 2.3 was changed from "PM10" to "Particulate matter monitoring (PM10, PM2.5)". In the text, PM10 was mentioned as the type of measurement and not as the name of the instrument itself.

Referees Comments:

Referee #1:

line 223: Give the manufacturer (and type) of the instruments.

Author's response: The particulate matter measurements were taken from the air monitoring network directed by the Israel ministry for environmental protection. Unfortunately, the ministry does not publicize in their internet site the type of instrument they use. Nevertheless, all monitoring stations were granted ISO17025 meaning the calibration method of measurement is approved by European standards. Based on private communication with the ministry, the manufacturer of the majority of particulate matter instruments is Thermo Fisher Scientific. Two main types are used: FH 62 C14 (beta attenuation method) and 1405 TEOM (tapered element oscillating microbalance method).

Author's changes in manuscript: The instrument type and manufacturer were added to the text.

Referees Comments:

Referee #1:

line 235: If the availability is given for the PM10-monitors it would be consistent to mention the availability of the other instruments as well (certainly a minor point).

line 236:" (87% of the monitoring stations" can be omitted.

Author's response: The PM10 continuous measurements are 5 min average based on instantaneous measurements of 1 min. Data is automatically defined "invalid" if among the average time based (e.g., 30 min, 1 hr) more than 25% of the data is missing. Therefore, it was possible to evaluate the availability of the PM10 measurements. In the other instruments (AERONET, ceilometers), there isn't a defined method to objectively evaluate the availability of the data, thus it was not stated. For instance, AERONET also availability depends on the daylight hours and the degree of AOD (at high AODs the instruments shuts down). Overall, the ceilometers data (not referring to the quality of the data along the profile) was 100% except for the Weizmann (Rehovot) site with 6 hours missing on 7 September (shown in the figure) due to a local power failure. Fig. 6 presented instantaneous data from the AERONET sites, was an attempt to show the extent of the daily availability as it changed from day to day.

Author's changes in manuscript: We added comments referring to the availability of the data from each instrument but avoided presenting absolute values. The AERONET figure was changed to daily values shown in Fig X10:

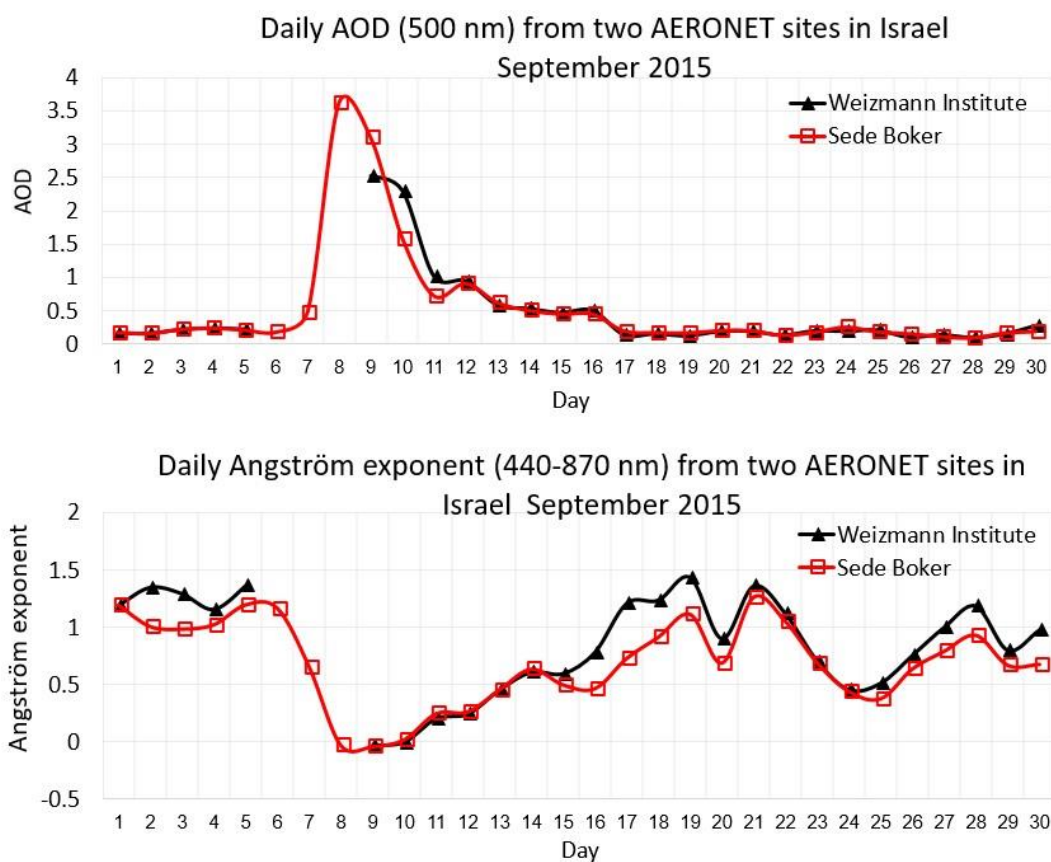


Figure X10. September 2015 daily average of AOD (top panel) and Angström exponent (bottom panel) from two AERONET sites in Israel (Sede Boker and Weizmann). The Weizmann AERONET did not operate on 6-8 September due to power failure.

Referees Comments:

Referee #1:

lines 237/38: This is also a result and should be moved to the corresponding section. The same is true for Fig. 5a. Add a xy-grid to facilitate the interpretation of Fig. 5a. Figs. 5a ... also belong to the results.

Referee #2: P9, Figure 5 caption: *Please clearly state what the yellow curve shows. It took me some time, to see that it belongs to the southern region. The curves show the mean of all sites of a given region? Hard to see the ceilometer stations. Give them a yellow full circle and plot them last (after plotting everything else). Then one should clearly see the sites.*

Author's response: Following the comments we decided to present the data from 31 monitoring sites (Table X3) and present the spatial and temporal PM10 dispersion by Fig. X11.

Author's changes in manuscript: We replaced the PM10 plots to Table X4 and Fig X11:

Table X4. Hourly maximum concentration of PM10, collected from 31 monitoring sites, between 7-10 September 2015. The values are ranked from low (dark green) to high (dark red) values.

No.	Site	Height (m ASL)	Region	PM10 ($\mu\text{g m}^{-3}$)			
				7-Sep-15	8-Sep-15	9-Sep-15	10-Sep-15
1	Galil Maaravi	297	North	114	3130	1987	1562
2	Karmelia	215	North	39	1120	1008	765
3	Newe Shaanan	240	North	104	3459	2471	1518
4	Haifa Port	0	North	78	1600	1965	1699
5	Nesher	90	North	117	3265	2746	1270
6	Kiryat Haim	0	North	82	1161	1625	1088
7	Afula	57	North	97	3239	2322	1961
8	Um El Kotof	0	Coast	99	2025	2028	1630
9	Orot Rabin	0	Coast	58	1152	1455	999
10	Barta	0	Coast	112	2540	2345	1612
11	Qysaria	19	Coast	54	1067	2116	1272
12	Rehuvot	70	Coast	88	2236	3045	1257
13	Givataim	0	Coast	112	1909	4014	1484
14	Yad Avner	77	Coast	61	1738	2902	1252
15	Ameil	20	Coast	96	2027	3472	1321
16	Shikun Lamed	17	Coast	51	1701	3244	1097
17	Station	29	Coast	87	1420	2176	998
18	Ashkelon	29	Coast	117	953	1692	551
19	Ariel	546	Mountain	128	2723	1481	1358
20	Jerusalem Efrata	770	Mountain	273	7820	1630	1437
21	Jerusalem Bar Ilan	749	Mountain	181	5588	1191	966
22	Jerusalem Safra	797	Mountain	491	10280	2389	1780
23	Gush Ezion	960	Mountain	310	6230	1679	1119
24	Erez	80	South	44	1000	1000	718
25	Beit Shemesh	350	South	115	2097	1943	1788
26	Carney Yosef	260	South	85	1047	784	594
27	Modiin	267	South	185	2701	2245	1980
28	Bat Hadar	54	South	65	1342	2563	841
29	Nir Galim	0	South	94	1479	2292	1027
30	Negev Mizrahi	577	South	183	9031	2806	1730
31	Eilat	0	South	275	1867	1592	1684

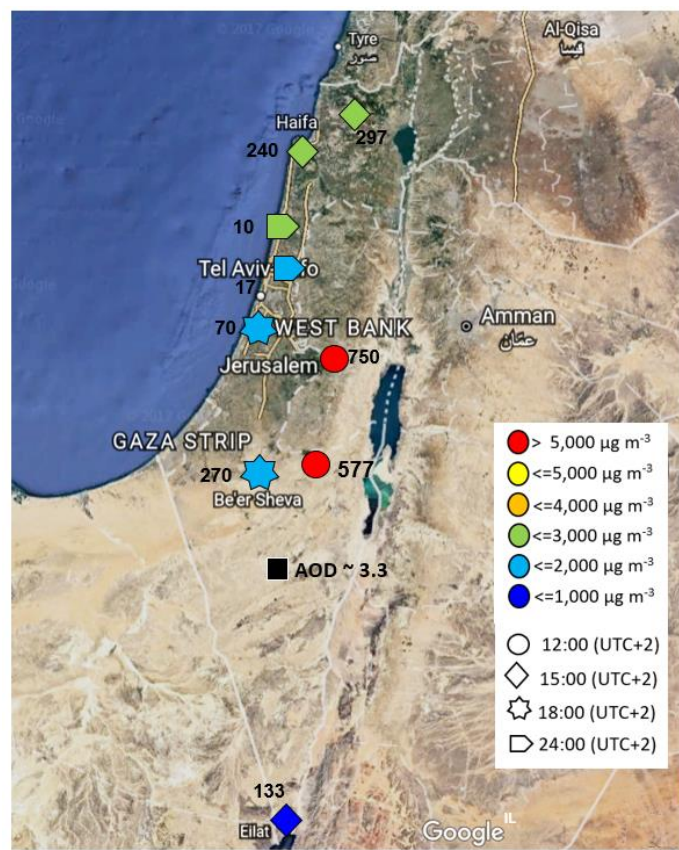


Figure X11. A map of PM₁₀ maximum hourly concentration from 9 sites measured at 10 UTC on 8 September 2015. The map includes indications of the time of measurement (symbol shape), concentration range (symbol color), height of measurement site (numbers in black) and AERONET AOD from Sede Boker site.

Referees Comments:

Referee #2: I asked colleagues from Israel to help me with... the following..., I am not familiar with Hebrew language... for example: <http://www.svivaaqm.net/>. Technically, you have at <http://www.svivaaqm.net/> 'reports from numerous sites'... The dust storm: at September 7, around 22:00 values above 100 are already recorded for two sites (cities): Kiriya Ata and Nesher (next to Haifa). Haifa region (Northern part of Israel) must be included for more comprehensive analyses. The authors stated that: "Unfortunately, there are no PM₁₀ measurements in northern Israel". (Line 233) During the dust event there were seven sites that measure PM₁₀ that were available. Figure 5 is not correct therefore, it covers more area, than depicted in Figure 5, including the Haifa Bay area.

Author's response: All PM₁₀ measurements, including the Haifa region, were included in our calculations. Nevertheless, these stations do not cover what we define as the northeast region in Israel named "Golan heights" (also referred by Gasch et al.). Measurements from the Golan heights would have given us a perspective whether the dust plume prevalence over Israel on 8 September 2015, had gradually progressed inland from northeast, or rather

unified but measured mainly by the elevated monitoring sites since the dust plume hadn't thus far subsided.

Author's changes in manuscript: Following the comments we decided to present the data from 31 monitoring sites (Table X3) and present the spatial and temporal PM10 dispersion by Fig. X11.

Referees Comments:

Referee #2: *Why did the authors not include PM2.5 sites data.*

Author's response: We did not include the PM2.5 measurements although we've already analyzed them) since the intensity of the dust storm was less profound in PM2.5 measurements (see Fig. X13) an with less monitoring sites compared to PM10 measurements.

Author's changes in manuscript: We can add a summary (Table X5) of PM2.5 maximum hourly averages from all sites available between 1-10 September.

Table X5. Hourly maximum concentration of PM2.5, collected from 21 monitoring sites, between 7-10 September 2015. The values are ranked from low (dark green) to high (dark red) values.

No.	Site	Height (m ASL)	Region	PM2.5 ($\mu\text{g m}^{-3}$)			
				7-Sep-15	8-Sep-15	9-Sep-15	10-Sep-15
1	Kefar Masarik	8	North	52	378	389	378
2	Ahuza	280	North	36	743	650	419
3	Newe Shaanan	240	North	43	400	466	525
4	Nesher	90	North	43	564	496	349
5	Kiryat Biyalic	25	North	53	424	703	447
6	Kiryat Binyamin	5	North	40	223	412	256
7	Kiryat Tivon	201	North	47	413	416	300
8	Afula	57	North	44	836	550	405
9	Raanana	54	Coast	38	173	291	229
10	Antolonsky	34	Coast	32	470	626	386
11	Ashdod	25	Coast	36	303	750	332
12	Ironi D	12	Coast	34	424	507	327
13	Tel aviv Central Station	29	Coast	41	716	803	451
14	Ashkelon	25	Coast	61	182	537	119
15	Jerusalem Efrata	749	Mountain	106	2285	434	403
16	Jerusalem Bar Ilan	770	Mountain	107	3063	641	518
17	Gedera	70	South	34	433	683	308
18	Nir Israel	30	South	25	363	638	228
19	Kiryat Gvaram	95	South	42	376	870	300
20	Sede Yoav	105	South	45	323	245	228
21	Negev Mizrahi	577	South	42	1748	526	317

Instruments- AERONET : lines 254-273

Referees Comments:

Referee #1: "...within a 1 min period": maybe it is better to remove this. From this statement the measurement cycle is not clear: 8 s measurements, 22 s break, 8 s measurements, 22 s break, 8 s measurements? This is more than 1 minute.

Author's response: Comment accepted.

Author's changes in manuscript: The sentence was omitted.

Referees Comments:

Referee #1: Figs.. 6 also belong to the results.

line 262: As this is a result it should be moved to Sect. 3. Fig. 6: to be moved to Sect. 3.

Author's response: Comments accepted.

Author's changes in manuscript: AERONET figure was moved to the "Results and discussion" section.

Referees Comments:

Referee #1: I don't understand the x-axis of Fig.6 ? Why is the length of the days different? Where are the night measurements of AERONET from (do you deploy a lunar photometer?)? Is there a specific reason for not choosing a line plot in Fig. 6a (as in Fig. 6b)?

Referee #2: P10, Figure 6: the time axis ... the day scale (width) is changing from day to day. E.g., the 8 September is very narrow, the 7 September has a factor of 4 more space..., why?

Author's response: All the data available from the Israeli AERONET sites was delineated in Fig. 6. The length of the days is different due to missing data. Fig. 6 was an attempt to present the availability of the AODs as the extent of available data changed from day to day. We found the presentation of Fig. 6 more informative than a line plot.

Author's changes in manuscript: The AERONET figure was changed to daily values shown in the aforementioned Fig X10.

Referees Comments:

Referee #2: P10, L264. The Rehovot station did not work, the instrument was out of order? or did the station not allow useful data analysis because the AOD was too high? Please clarify and state what was the case...

Author's response: The instrument was out of order due to power failure in the Weizmann institute.

Author's changes in manuscript: We mentioned the instrument was out of order.

Results: lines 276-472

Referees Comments:

Referee #1: *In the "results" -section the discussion should be more elaborated and linked to the findings from the other data sets (provided in part when the MLH is discussed). The discussion of the scientific results must be improved and extended. In the present state the paper is sort of a collection of (useful) pieces of information, but their relationship and their interpretation is not sufficiently elaborated.*

Author's response: Comments accepted.

Author's changes in manuscript: The "Results" paragraph was rewritten according to the overall comments of the referees.

Referees Comments:

Referee #1: *From Fig. 6a it seems that after 11. September 2015 the AOD was still relatively large (by the way: can you give the annual mean AOD of the sites in Israel?). How "typical" are the ceilometer profiles between 11. and 14. September 2015?*

Author's response: Annual mean of 2015 of AOD from Sede-Boker : 0.22 . AERONET Weizmann started operating on 6 June 2015, thus the half year mean is: 0.25. Although Sede Boker is situated in the southern Negev desert of Israel, the Average AOD of the dusty and windy season (Oct- Nov) remained 0.25. Therefore, the AODs above 3 are rare. Between 11-14 September 2015, AODs are large although the PM10 measurements and ceilometer signals infer differently since they do not include the whole air column. This finding may justify the results of Stavros et al. (2016) and the CALIPSO measurements on the 10 September of an elevated layer of the dust plume at about 3-4 km.

Author's changes in manuscript: We added a discussion on the comparison between measurements (AERONET, particulate matter, global radiation, ceilometers, Satellite pictures) after 10 September 2015.

Referees Comments:

Referee #1: *line 281 ff: Move lines 281–283 to Sect. 2.*

Author's response: Comment accepted.

Author's changes in manuscript: The sentences were moved to the ceilometer discussion in the "Instruments" section.

Referees Comments:

Referee #1: *The absolute values of the attenuated backscatter must be checked: some of the numbers are unrealistic and the corresponding figures are not clear. For example, the labels of Fig. 7c (e.g. 0.000029 in units of $10^{-9} \text{ m}^{-1} \text{ sr}^{-1}$) are confusing. lines 281–283: Check carefully the following numbers of the attenuated backscatter; some of them are unrealistic ($7 \cdot 10^{-1} \text{ m}^{-1} \text{ sr}^{-1}$).*

lines 281–283: See also general remarks at the beginning. Add a xy-grid to Fig. 7. Figs. 8–16: What is the unit of the color code? It does not agree with the values given for attenuated backscatter. Are these numbers the "counts"?

Referee #2: P12, Figure 7, We need a clear statement, that the range-corrected signals shown in Figure 7 decrease rapidly and is close zero at about 700 to 750m in b,c,d because of the strong laser light attenuation in the dust layer! As long as such a statement is missing the reader may believe to see the full dust layer and the top is at 750-1000m height. To repeat: This is unacceptable. This is simply wrong and unacceptable. Please improve! The basic ceilometer data are signals (let us say ... in units... counts per second), and if they are then range corrected... then you get the dimension 'counts per second times m^2 '. So the values are not unitless, but usually given in arbitrary units. Next, by dividing these data by 10^{-9} ... does not change anything. You still have just range-corrected signals. You can only obtain a profile of the attenuated backscatter coefficient if you are able to calibrate this range-corrected signal profile in the tropospheric region with pure Rayleigh backscattering or in the way as described above. So, you show range corrected signals!!! And not attenuated backscatter!!! As mentioned already, you must change to range corrected signals in all ceilometer plots!

Author's response: A fundamental mistake. The attenuated backscatter presented in Fig. 7 had already been divided by 10^9 , therefore, 10^9 should have been omitted from the x-axis label. The numbers shown in the ceilometer plots are signal counts.

Author's changes in manuscript: Ceilometer profiles were correct to units of attenuated backscatter in the order of $10^{-5} m^{-1} sr^{-1}$. the title "Signal counts" was added to the legend in all ceilometer plots.

Referees Comments:

Referee #1: The authors should be aware that a comparison of brown vs. brown color or brown vs. blue color (Figs. 10–16) is not suitable for a scientific publication. Please use quantitative numbers! Think about plotting coincident attenuated backscatter profiles of the 8 sites (similar to Fig. 7), this may help to see temporal delays in the arrival and decay of the plume.

Referee #2: P12. Figure 8, x-axis please show data always from 0-24 local time (or UTC). Again we need proper text for the x-axis and y-axis, as it is the case in Figure 7. P12-15: All the Figures 8, 10-16 have no x-axis and y-axis description. This is poor and unacceptable. And again, all these ceilometer color plots suggest that the dust layer was just a few hundred meter thick. This is dangerous! The reason is simply the almost total attenuation of the ceilometer radiation pulses by the rather dense dust layers. This must be made very clear.

line 320: "the time corrected from local time to" can be removed.

Author's response: After several trials we found the current plot contours are the most informative. However, supplemented plots of attenuated backscatter profiles from all ceilometers at specific hours given in Fig. X12.

Author's changes in manuscript: Supplement figure X12:

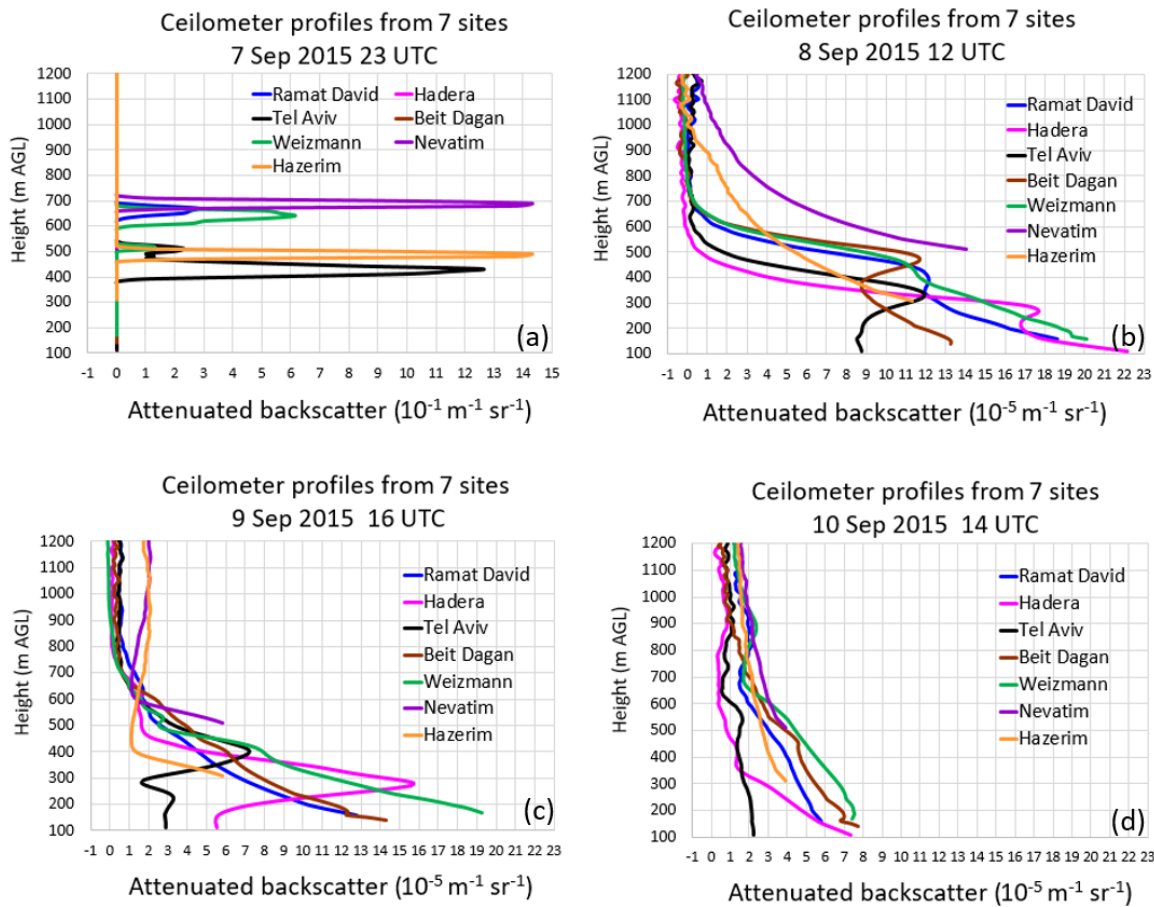


Figure X12. Ceilometer attenuated backscatter profiles from 7 sites (Ramat David, Hadera, Tel Aviv, Beit Dagan, Weizmann, Nevatim and Hazerim, Fig. 3) at 23 UTC 7 Sep 2015 (a), 8 September 2015 at 12 UTC (b), 9 September 2015 at 16 UTC (c) and 10 September 2015 at 14 UTC (d). Notice each profile begins relative to the height of its' measuring site (ASL) including a deletion of the first 100 m AGL due to inaccuracies in the first range gates of the CL31 ceilometers (for details see Sect. 2.1). Fig (a) shows cloud detection therefore it has a different scale ($10^{-1} \text{ m}^{-1} \text{ sr}^{-1}$) and a different x-axis range.

Referees Comments:

Referee #2: P13, L324: again and again: you were able to track the dust layer base only, this must be clearly said. In Figure 8, the numbers for 'your' attenuated backscatter are suddenly up to 15000, compared to values of about 10^{-14} in Fig 7 (b,c,d)? Then in Figs 10-12: up to 10000. And in Fig 13, suddenly only up to 800..., Fig. 14 up to 15000, and Fig15-16 up to 10000. So all this is rather strange...and only reasonable and understandable if we switched to range corrected signals (arbitrary units). So, please change..... to range corrected signals.

P13, L347: *Plots are given in different scales to highlight the dust features. This is ok, because range corrected signals are shown and the ceilometer performance changes from site to site (from ceilometer to ceilometer). So again, there is a clear need to work with range corrected signals.*

Author's response: 6 Out of the 8 of the ceilometers belong to a governmental office. We were not informed whether the "message profile noise h2" was off or on therefore whether an automated range correction was done.

Author's changes in manuscript: No changes.

Referees Comments:

Referee #1: *lines 328 ff: Obviously attenuated backscatter is converted into particle extinction coefficient (with a relatively large uncertainty inherent in all CL31 measurements; see water vapor absorption mentioned above, unknown lidar ratio, unknown accuracy of the scaling factor) with an estimated lidar ratio. Then, the visibility is estimated according to Koschmider. Which altitude was selected for this conversion? The problem is, that if it is done for a large altitude (maybe 100 m or more) it is difficult to compare this visibility to independent ground based measurements. If it is done for the ground, then the overlap problem is critical. Nevertheless, an order of magnitude agreement should be possible, but please extend this paragraph by explaining all aspects of this comparison.*

Referee #2: *P13, L330: A visibility of 200m (visual meteorological range is defined by an AOD of 3, after Koschmieder for an AOD of 4) according to an AOD of 3 means that the particle extinction coefficient was 15 km⁻¹ or 0.015 m⁻¹ and the backscatter coefficient is then 0.0003 m⁻¹ sr⁻¹ if the dust lidar ratio is 50sr. All your 'numbers' are far far away from these value. This corroborates: It is impossible and dangerous (and thus not justified) to convert the range-corrected signals into optical properties just by taking 'some' conversion factor!*

Author's response: We took the visibility observations under 100 m AGL and compared to the attenuated backscatter received at ~500 m AGL. We understand it is misleading and therefore we decided to omit this paragraph.

Author's changes in manuscript: The paragraph was deleted.

Referees Comments:

Referee #1: *lines 334 ff: "Ceilometers are not provided with an AOD...": I don't understand this paragraph. AOD and MLH are mentioned but it is unclear what the message is. The retrieval of the MLH from ceilometer data is completely different from a retrieval of the AOD (provided that can be determined at all). So, how is the validation ("verify ceilometer") of the ceilometer's performance achieved? Please rephrase and extend this part.*

Referee #2: *P13, L334-L337. I would remove this text on the ceilometer and the AOD upper limit. This is useless. The Vaisala ceilometers are not built for aerosol profiling. The wavelength is bad, the signals are corrupted by water vapor absorption.*

Author's response: We intended to explain that we do not know the detection limit of the attenuated backscatter signals at high AODs. Therefore, we cannot put a direct limit to the ceilometer threshold. Instead we tried to use other methods to verify the first layer height. In this subsection we attempted to retrieve the inversion height from the ceilometers and radiosonde. Since aerosols are usually trapped under the inversion height and this height is similar in the radiosonde and WCT calculation as a tool to define the height of the first dust layer.

Author's changes in manuscript: We rephrased the sentences.

Referees Comments:

Referee #2: P19, L490: *Again, you have to mention the limits of a ceilometer. It was too weak to see the layers higher up. No chance to see the main part of the dust layers and dust layer top.*

Author's response: Comment accepted.

Author's changes in manuscript: We have listed the ceilometers limits in the Instruments section and referred to these limits in the results.

Referees Comments:

Referee #2: P13, Fig. 9 shows the dust base height. *To my opinion it is misleading to denote the near-surface layer a 'mixed layer' at these conditions with no vertical exchange*
P13: *The text on this page is poor and needs to be significantly improved.*

Author's response: We accept the referee's opinion on the 8 September since the global radiation (Fig. X2) was marginal for a significant thermal creation.

Author's changes in manuscript: The "Results and discussion" paragraph was rewritten according to the overall comments of the referees.

Referees Comments:

Referee #1: *line 381 ff: A short paragraph should be included here to prepare the reader: The event is divided into several phases (not necessarily split into single days, one phase can be shorter, another can last for more than one day; development, main phase, decay can be an alternative) according to certain criteria and to highlight consistencies/inconsistencies of different data sets/models (by doing this "Next, we describe the decrease of aerosols aloft on mid-day" in line 299 can be omitted). Then, each subsection such as "Entrance of dust into Israel – 7 Sep 2015" should include the full discussion and interpretation of all available data sets for the corresponding period, i.e., parts from Sect. 2 should be included here whenever applicable.*

Author's response: Comments accepted.

Author's changes in manuscript: We changed the results section and described the dust storm evolution along its generation rather than by dates.

Referees Comments:

Referee #2: P15, L383: Please clearly state where the dust layer top was found by Solomos et al. (2017).

Author's response: Stavros et al (not Solomos, my mistake) analyzed by CALIPSO overpass two layers, 2 km (total attenuation was reported up to 1.5 km) and between 3-4 km.

Author's changes in manuscript: The summary of Stavros et al. was extended.

Referees Comments:

Referee #2: "The AERONET (Fig. 6) and ceilometer plots (Fig. 8, 11-16) reveal that the first dust plume penetrated Israel at approximately 04:00 UTC". What day? Sept. 7 or Sept 8?

Author's response: 7 September 2015.

Author's changes in manuscript: The "Results and discussion" paragraph was rewritten according to the overall comments of the referees.

Referees Comments:

Referee #1: line 401: What is meant by "decrease"? Concentration or altitude?

Author's response: We meant the subsidence of the dust plume.

Author's changes in manuscript: The "Results and discussion" paragraph was rewritten according to the overall comments of the referees.

Referees Comments:

Referee #1: line 405:" clearly shown in Fig. 13-16 between 08-16 UTC)": This is indeed hard to see. Can you explain this in a more quantitative way?

Author's response: We based our conclusions on the wind direction profiles from radiosonde launches in Beit Dagan. Apart the radiosonde, we do not have auxiliary measurements to prove our assumption. Therefore, if the referee could not relate to our conclusions, we decided to omit this hypothesis.

Author's changes in manuscript: The sentence was erased.

Referees Comments:

Referee #1: line 408: Please clarify what "these model findings" are? The vertical distribution of dust (backscatter)?

Author's response: We were referring to the hydraulic jump upstream the dead sea rift valley explained by Gasch et al., as the dust plume entered from northeast and progressed southwest. In contrary, the ceilometers plots revealed the penetration of the dust plume

occurred at once from north (Ramat David site) to south (Hazerim and Nevatim sites) and to west (Hadera, Tel Aviv, Beit Dagan and Weizmann sites).

Author's changes in manuscript: The "Results and discussion" paragraph was rewritten according to the overall comments of the referees.

Referees Comments:

Referee #1: line 422: 2000 $\mu\text{g}/\text{m}^3$: is this in contradiction to 9800 $\mu\text{g}/\text{m}^3$ in line 416?

Author's response: We were referring to the second "jump" in PM10 measurements which occurred simultaneously in all monitoring stations on the 8 September at ~17:00 (UTC+2) after the extreme values of 9800 $\mu\text{g}/\text{m}^3$ were measured only in the high altitude stations on the 8 September at ~ 12:00 (UTC +2).

Author's changes in manuscript: We rephrased the sentence in the scope of the "Results and discussion" section.

Referees Comments:

Referee #1: line 437: "...limited radiative transmitted...": what does this mean?

Author's response: We meant the decrease in the global solar radiation.

Author's changes in manuscript: The sentence was rephrased.

Referees Comments:

Referee #2: P17, L435: At very high optical depth as on 9 Sep, I would assume that convective motions in the PBL as well as a sea breeze winds cannot develop. Are you sure that sea breeze developments were possible at these days with almost no sun and differential sea/land heating? Please keep the discussion free of speculation.

Author's response: On the 8 September, the maximum wind speed was below 3m/s and maximum global solar radiation up to 264 W m⁻². The ability to generation of thermals under these would be rather weak. on the next day, on the 9 of September the maximum global radiation more than doubled reaching 621 (w m⁻²) and wind speed increased to a maximum of 5 m s⁻¹ at 13:00 (UTC+2). At these conditions, convection and creation of thermals is possible.

Author's changes in manuscript: We've added an explanation regarding the possibility of thermals creation on the 9 September.

Referees Comments:

Referee #1: Fig. 17: This figure is misleading as the range of the color code is different from Fig. 14. This should be pointed out clearly. As long as the inter-comparison with the AOD (AERONET) is qualitative only, it would be helpful to show the typical(?) background(?) values of the AOD and attenuated backscatter of the days before the event for comparison.

Referee #2: P17.... Figure 17 indicates that there was dust higher up. The AOD decreased towards 0.5-1 on 12-14 Sep. A perfect mixing layer could develop now up to 750 m, as seen on 13 and 14 Sep. Nice to see, that the aerosol dried in the PBL during the morning hours and thus the color of the range corrected signals changed from red to green and blue (for dry particles producing less backscatter later on).

Author's response: In order to visualize the maximum information from each ceilometer plot, the plot scale varied from site to site in reference to the ceilometer type (CL51, CL31) and installation definitions (e.g. ceilometer Beit Dagan produces significantly less signal counts for the same phenomena).

Author's changes in manuscript: New ceilometer plots with a unified scale of 0-10,000 signal counts (Fig. X13-X18) except for the CL51 Weizmann ceilometer plots (0-15,000 signal counts, Fig. X19) and Beit Dagan ceilometer (0-800 signal counts, Fig. X20).

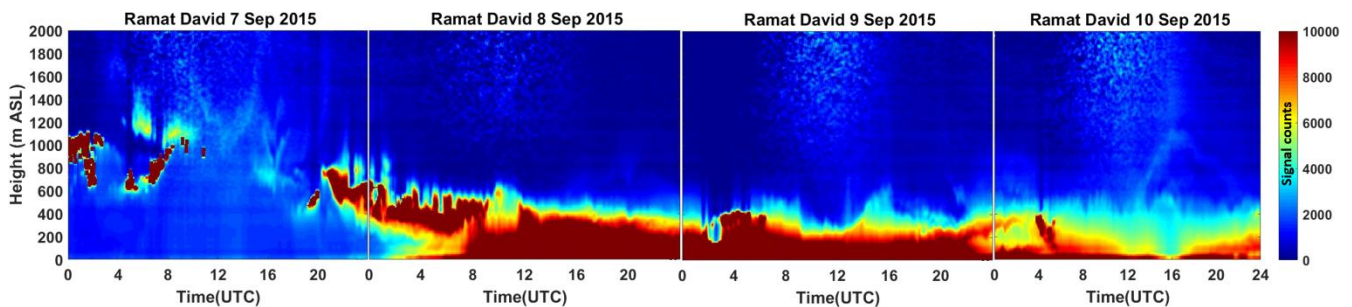


Figure X13. Ramat David ceilometer signal counts plots for 7-9 September 2015. Y-axis is the height up to 2000 m ASL, X-axis is the time in UTC, signal counts scale range between 0-10,000.

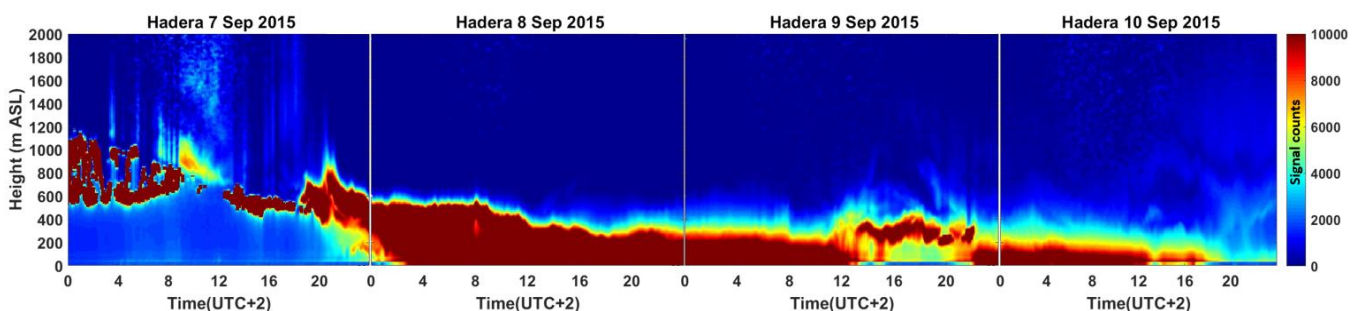


Figure X14. Hadera ceilometer signal counts plots for 7-9 September 2015. Y-axis is the height from site deployment to 2000 m ASL, X-axis is the time in LST (UTC+2), signal counts scale range between 0-10,000.

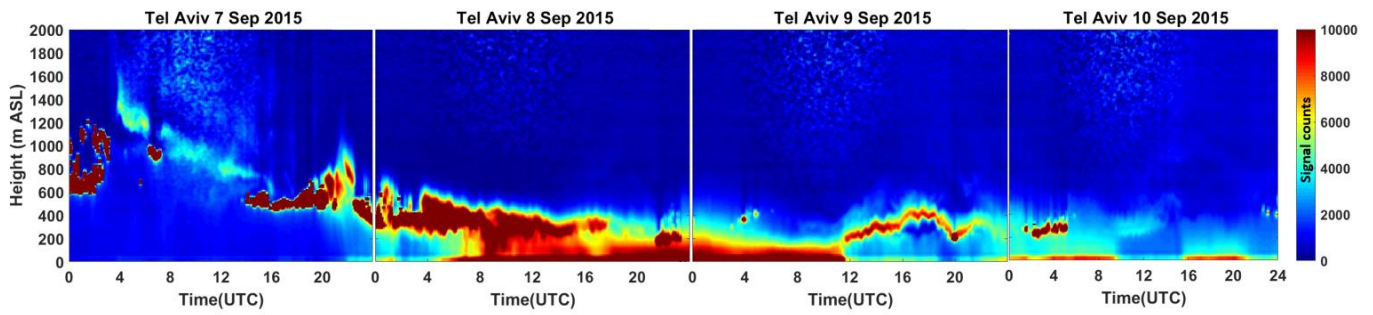


Figure X15. Tel Aviv ceilometer signal counts plots for 7-9 September 2015. Y-axis is the height from site deployment to 2000 m ASL, X-axis is the time in UTC, signal counts scale range between 0-10,000.

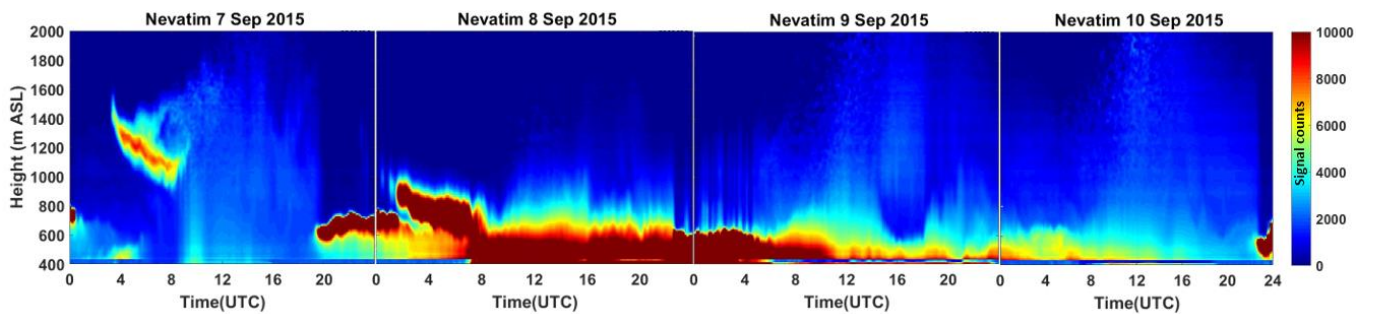


Figure X16. Nevatim ceilometer signal counts plots for 7-9 September 2015. Y-axis is the height from site deployment to 2000 m ASL, X-axis is the time in UTC, signal counts scale range between 0-10,000.

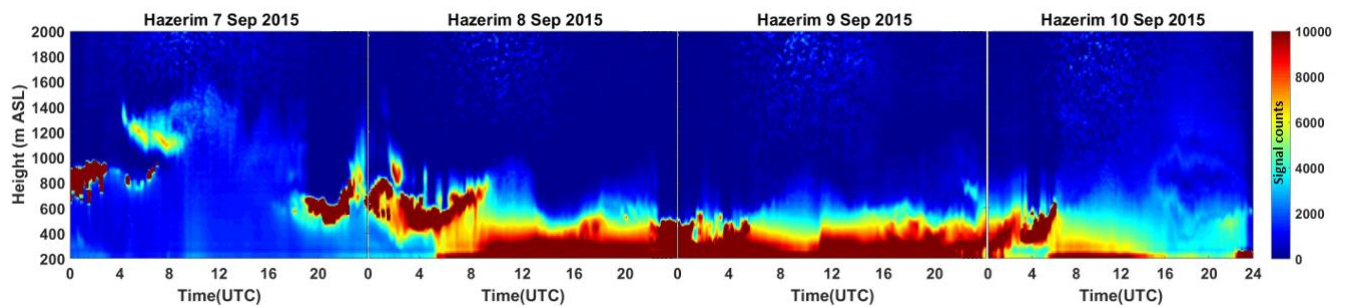


Figure X17. Hazerim ceilometer signal counts plots for 7-9 September 2015. Y-axis is the height from site deployment to 2000 m ASL, X-axis is the time in UTC, signal counts scale range between 0-10,000.

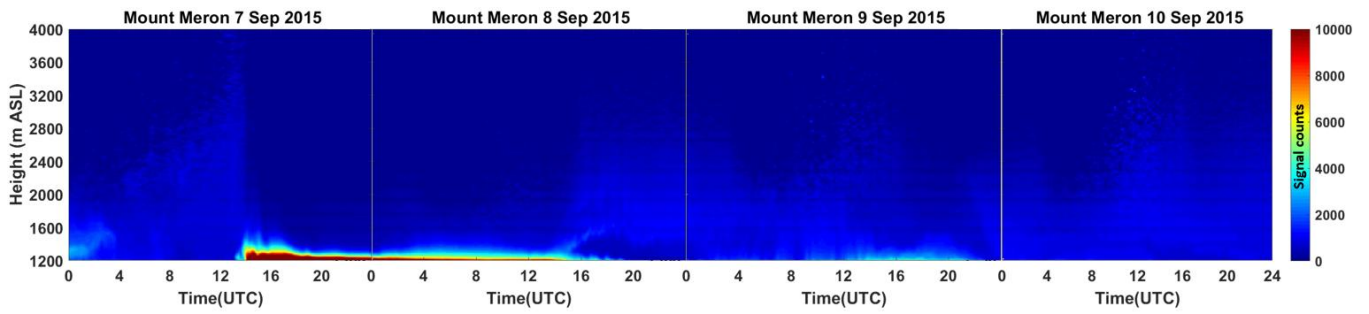


Figure X18. Mount Meron ceilometer signal counts plots for 7-9 September 2015. Y-axis is the height from site deployment to 2000 m ASL, X-axis is the time in UTC, signal counts scale range between 0-10,000.

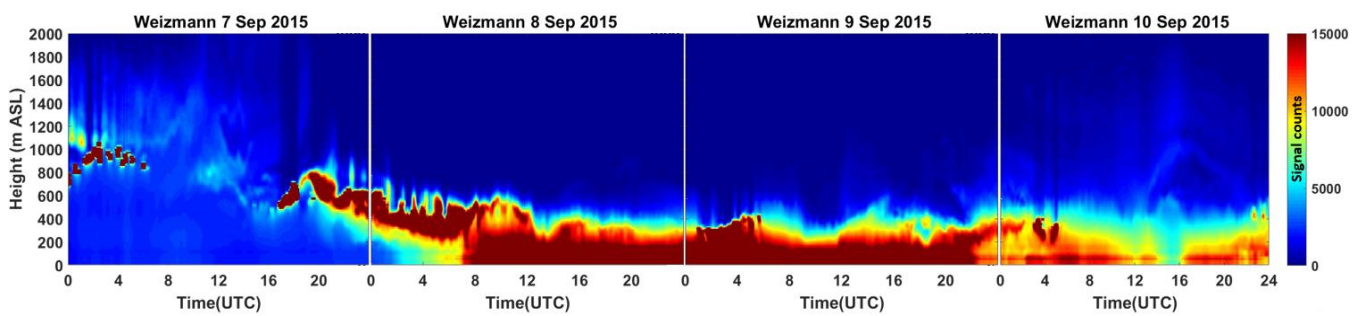


Figure X19. Weizmann ceilometer signal counts plots for 7-9 September 2015. Y-axis is the height from site deployment to 2000 m ASL, X-axis is in UTC, signal counts scale range between 0-15,000.

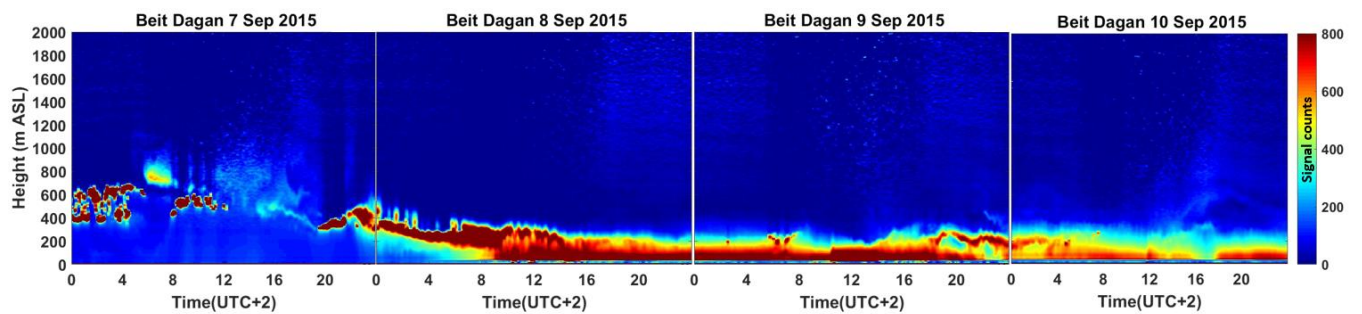


Figure X20. Beit Dagan ceilometer signal counts plots for 7-9 September 2015. Y-axis is the height from site deployment to 2000 m ASL, X-axis is in LST (UTC+2), signal counts scale range between 0-800.

Referees Comments:

Referee #2: P17, L444: *You state: The ceilometer reveals total clearance on 10 Sep! But the Weizmann Institute AERONET shows AODs of 2 and more on 10 Sep! What is wrong, what is true? Please clarify?*

P18, L461: *The AOD was >1.0 all the time on 9 and 10 Sep...until 12 Sep. What do you thus mean with dissipation of dust?*

P19, L498-499: *When were the AE values high again? They were continuously <0.5 even on 14 Sep (Weizmann AERONET).*

Author's response: The "clearance" we mentioned was referred to the lower part of the atmosphere (up to ~1 km), as the PM10 values decreased considerably and the amount of signal counts from all 8 ceilometers declined. On 10 September, the dust plume motion continued southwest to Egypt, with indication of a dust layer between 2-4 km measured by CALIPSO. The progression of the dust storm southwest over Israel, from the Syria-Iraqi border to Egypt, continued in two separated levels. The lower level (up to 1 km ASL) dissipated at 13 September while the level aloft (above 1 km ASL) was observed until 17 September.

Author's changes in manuscript: Supplementary results and a discussion on the dust dissipation.

Referees Comments:

Referee #1: *line 454: 250 m: is this the vertical extent or the altitude?*

Referee #2: P18, L454: *...as a dust layer of 250 m thickness (fig 11-13, 15-16) penetrated Israel at a height of 1000-1500m.... How do you know the depth of the dust layer? The ceilometer fails to see higher up.... So, how do you know? I would leave out to mention any dust layer depth.*

Author's response: Comments accepted.

Author's changes in manuscript: Considering the ceilometers limitations to detect attenuated backscatter signals above a dense dust layer, we omitted the assumptions regarding the vertical extent of the dust layer.

Referees Comments:

Referee #1: *line 486: The PM10 measurements are considered as in-situ measurements, not remote sensing.*

Author's response: Comments accepted.

Author's changes in manuscript: We corrected the sentence referring to PM10 measurements as in situ.

Conclusions and discussion: lines 480-514

Referees Comments:

Referee #2: P19: The conclusions have to be rewritten completely after improving all the text before along the lines this review and the other review.

Author's response: Comment accepted.

Author's changes in manuscript: We rephrased the "Conclusions " section according to the referees' comments.

Referees Comments:

Referee #2: What sources of errors do they have when using the ceilometers? They should critically state the limitations, disadvantages and advantages. Including comparison between different ceilometers that authors used for the analyses. Without this comprehensive critical discussion on authors findings, the outcome of the paper is doubtful.

Author's response: Comments accepted.

Author's changes in manuscript: We listed the ceilometers limitations in the Instruments sections. In the discussion section we referred to these limitations in the as part of the process of evaluation.

Referees Comments:

Referee #2: *Figure 18: The major claim - the dust penetrates from the East. But- combining PM10 from the Haifa Bay area, there is a "jump" towards values of 2500-3000 micrograms/m³ at 8 of September, similarly to East, which means it has two entrances/sources. Do the authors see the "North region" dust entrance using ceilometer data? The authors must justify what new information they get using ceilometer more clearly than in Figure 18, what new insights they get about the extreme dust event? And number/summarize all "new insights" about the event that they discover*

Author's response: We analyzed PM10 and PM2.5 measurements from all available monitoring stations in Israel. Unfortunately, we did not recognize a second jump from northern region. To emphasize our conclusions, we prepared Fig. X21 presenting PM10 values from monitoring sites the referee mentioned: Haifa Bay, and the northeast station in Israel (Karmiel). We added three more stations: Hadera (central shoreline), (Jerusalem (mountains) and Arad (south). To our opinion, it is difficult to define a second "jump" on the 8 September exclusively in the northern sites.

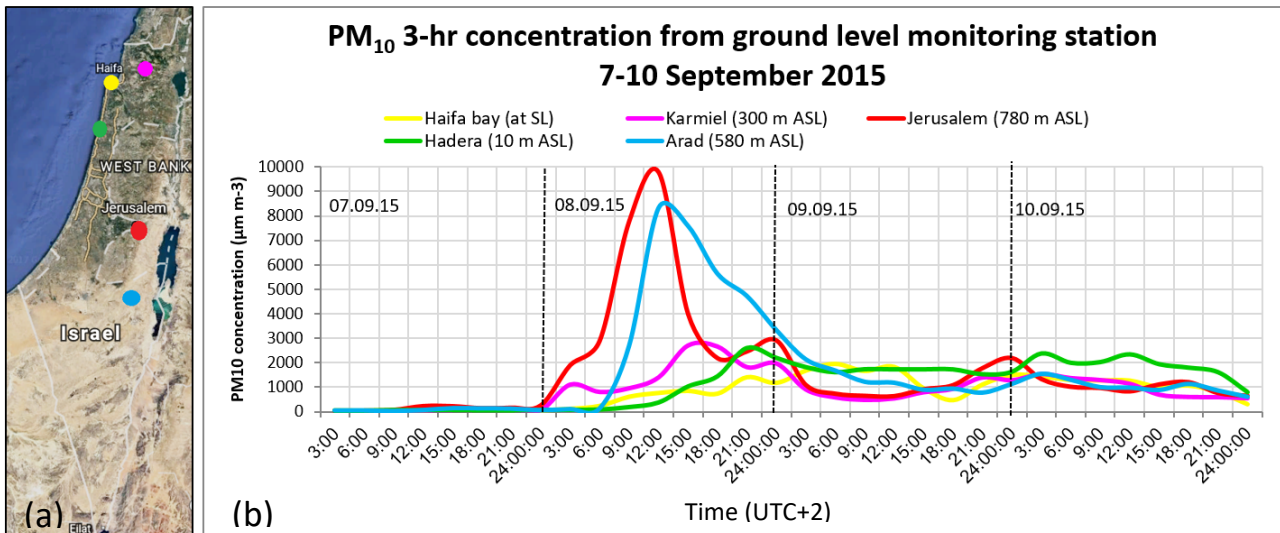


Fig. X21. (a) Map of PM10 monitoring sites (Karmiel, Haifa Bay ,Hadera, Jerusalem, Arad) (b) 3 hourly average values of PM10 measured at each site during 7-10 September 2015.

Author's changes in manuscript: Figure 18 was replaced by additional solar radiation figures and a discussion on the contribution of the ceilometers to understand the evolution of the dust storm in the lower atmosphere (under 1 km ASL).

Referees Comments:

Referee #1: line 488:” ...for the first time, such an event is vertically analyzed using an array of ceilometers...”. On the one hand this is true, on the other hand it is slightly misleading as the vertical structure (by other means) has already been investigated. So it might be advisable to use a less strong statement in the next sentence (a note on the limited measurement range).

Referee #2: P19, L488: for the first time such an event is vertically analyzed..... this is misleading because Mamouri et al. already used lidar to characterize the dust storm. You probably wanted to say, for the first time with a ceilometer network. However, you should mention that there were already lidar studies with Cyprus lidar and CALIOP lidar, and now you come with a ceilometer network study..... Then this would be more clear, and of course this is a new aspect.

Author's response: Comments accepted.

Author's changes in manuscript: We rephrased the sentence and emphasized the contribution of the ceilometer measurements to the analysis of the lower part of the atmosphere (from ground level up to ~1 km) as a completion to previous studies concentrating on the generation and propagation of the dust plume down to ~1.5 km.

Referees Comments:

Referee #1: lines 492, 497:” plume”!

Author's response: Comment accepted.

Author's changes in manuscript: Typing mistakes were corrected.

Referees Comments:

Referee #1: *line 494:* "mainly of mineral dust": where is this information coming from?

Author's response: We based our conclusions on Sede-Boker AERONET Angström exponent (Fig. X10). Mamouri et al., (2016) studied the dust layer particle linear depolarization by an EARLINET lidar stationed in Limassol Cyprus. They concluded the linear depolarization ratio of 0.25-0.32 on 7, 10 September, indicated the dominance of mineral dust (the lidar was inoperative on 8 September).

Author's changes in manuscript: We added the citation to the AERONET Angström exponent measurements in Israel and referred to the conclusions from Mamouri et al., (2016).

Referees Comments:

Referee #2: *P19, L494:* As a result, of what?

Author's response: As a result of the low boundary layer.

Author's changes in manuscript: We rephrased the "Conclusions and discussion" section according aforementioned overall comments of the referees.

Referees Comments:

Referee #2: *P19, L502-504:* This is speculation, at least to my opinion. Be more save with your statements.

Author's response: Comment accepted.

Author's changes in manuscript: The sentence was omitted and a comprehensive analysis of the meteorological measurements (global radiation, direct radiation, diffused radiation, ground temperature, wind speed) and environmental measurements (PM10, PM2.5, TSP) were added in the attempt to explain and reveal the meteorological conditions held as the dust storm prevailed in Israel.

Referees Comments:

Referee #2: *P19, L506-511:* Again, dangerous statements. I would remove. Otherwise, you need to check the CALIPSO overflight over Israel to corroborate your speculative suggestions. However, the modeling papers of Solomos et al and Gasch et al. (partly based on model plus CALIOP results) do not leave room for statements like ... who knows to what height the dust plumes reached over Israel. To my opinion, in the Middle East dust layer top was up to 4-5 km height everywhere.

Author's response: We accept the comment. Additional data from the CALIPSO passage over Israel on the 10 September (given here in Fig. X) indeed shows a dust plume between ~2.5-4.5 km.

Author's changes in manuscript: We omitted the statement and referred to the ceilometers data in the context of the evolution of the dust plume at the lowest level of the

troposphere. We stated the ceilometers' limited ability to detect attenuated backscatter signals above the dust layer detected at ~ 1 km.

References: lines 546-637

Referees Comments:

Referee #2: P21, L554: No authors.

Author's response: The reference is a report edited and distributed by the U.S Environmental protection Agency with no specific authors mentioned upon the report.

Author's changes in manuscript: No change.

Referees Comments:

Referee #2: P23, L621: TOASJ...?

Author's response: Acronym for The open atmospheric science journal.

Author's changes in manuscript: The acronym was converted to the full name of the journal.

A list of relevant changes made in the manuscript:

1. Updated abstract
2. Updated introduction (Sect. 1) including an expanded review of previous studies.
3. Updated "Instruments" section (Sect. 2) including new instrument (solar radiation and satellite imagery).
4. The structure of the "Results and discussion" section had been changed. Each day (7-10 September 2015) had been analyzed by the same set of tools (instruments).
5. Updated conclusions.
6. Previous figures have been either deleted or updated.
7. Supplement of new figures and tables.

Formatted: Font: 18 pt, Font color: Auto

1 **New insights into the vertical structure of the September 2015**
2 **dust storm employing 8 ceilometers over Israel**

Formatted: Font color: Auto

3
4 Leenes Uzan^{1,2}, Smadar Egert¹, Pinhas Alpert¹

5
6 ¹Department of Geosciences, Raymond and Beverly Sackler Faculty of Exact Sciences,
7 Tel-Aviv University, Tel Aviv, 6997801, Israel.

8 ²The Israeli Meteorological Service, Beit Dagan, Israel.

9
10 Correspondence to: Leenes Uzan (Leenesu@gmail.com)

Formatted: Font color: Auto

11
12
13
14
15
16
17
18
19
20
21
22
23
24
25
26
27
28
29
30
31
32
33
34
35

36

Formatted: Font: 18 pt, Font color: Auto

Formatted: Font: 16 pt, Font color: Auto

Formatted: Font color: Auto

37 **Abstract**

38

39 On September 7th 2015, an unprecedented dust storm approached the East Mediterranean (EM) basin.
40 The storm origin was in the Iran, Iraq, Syria and the Turkey border. The Israeli meteorological service
41 considered the storm as exceptional due to its extent of over 6 days, occurrence time in early September
42 and concentrations reaching values 100 times the normal. Previous studies examined the formation and
43 evolution of the dust storm synoptic scale and explained why aerosol models often failed to simulate it.
44 This study concentrates on spatial and vertical meso-scale dust spreading over Israel based on several
45 remote sensing instruments including eight micro light detection and ranging (LIDAR) ceilometers. The
46 ceilometers high resolution attenuated backscatter profiles (every 10 m and 15 s) reveal the downward
47 motion of elevated dust plume as it penetrated Israel, ground coverage and gradual dispersion. The
48 additional data of spectral radiometers and ground particulate matter under 10 micro-meter aero-diameter
49 (PM10) as well as meteorological data made it possible to verify the dust properties and the differences
50 between its ground deposition and elevated dispersion. Further investigations of dust storms in the EM
51 by the ceilometer array will help improve the regional forecast models.

52 On 7 September 2015 an unprecedented and unexceptional extreme dust storm struck the Eastern
53 Mediterranean (EM) basin. Here, we provide an overview of the previous studies and describe the dust
54 plume evolution over a relatively small area, i.e., Israel. This study employs multiple tools including an
55 array of eight ceilometers, spectral radiometers (AERONET), ground particulate matter concentrations,
56 satellite images, global/diffuse/direct solar radiation measurements and radiosonde profiles. Main
57 findings reveal that the dust plume penetrated Israel on the 7 September from the northeast in a downward
58 motion to southwest. On 8 September, the lower level of the dust plume reached 200 m above ground
59 level, generating aerosol optical depth of $AOD > 3$, and extreme particulate matter concentration measured
60 on ground level up to $\sim 10,000 \mu\text{m}^{-3}$. A most interesting feature on 8 September was the very high
61 variability in the surface solar radiation in the range of $200\text{--}600 \text{ W m}^{-2}$ (22 sites) over just a distance of
62 several hundred km in spite of the thick dust layer above. Furthermore, 8 September shows the lowest
63 radiation levels for this event. On the following day, 9 September, the surface solar radiation increased,
64 thus enabling a late ($\sim 11 \text{ UTC}$) sea breeze development mainly in the coastal zone along with 5 m s^{-1}
65 surface winds associated with arc-shaped dust layers. On 10 September the AOD values started to drop
66 to ~ 1.5 , the surface concentrations of particulate matter decreased as well as the ceilometers aerosol
67 indications; Still, as indicated by CALIPSO a 2-4 km dust layer remained.

Formatted: Font color: Auto

68

69

Formatted: Font: 18 pt, Font color: Auto
Formatted: Font color: Auto
Formatted: Font: 14 pt, Font color: Auto
Formatted: List Paragraph, Indent: Before: 0.25"

1. Introduction

Dust storms in the East Mediterranean (EM), defined as Sharav cyclones, are common through the months of April, May, October and December (Alpert and Ziv, 1989). As the Sharav cyclone travels rapidly eastwards from North Africa to the EM, dry hot air enters Israel generating dust plumes which typically last 1-2 days, doubling the monthly average surface dust concentration (Israeli Environmental ministry air quality, monthly reports).

The September 2015 dust storm was created north east to Israel, in the beginning of September (Fig. 1). Dust advections from the northeast do not occur in the summer season nor do they result with such a major dust impact (Israeli Meteorological Service monthly reports). In the September dust storm, high ground-level particulate matter concentrations were measured for over 3 days with the highest levels of 100 times above the hourly average of $60 \mu\text{g}/\text{m}^3$ in Jerusalem (Israeli Environmental ministry air quality monthly reports). Low visibility of 0.5-3 km was measured across the county for four consecutive days during 8-11 Sep 2015 (Israel Meteorological Service monthly reports, Aerosol RObotic NETwork (AERONET) radiometers).

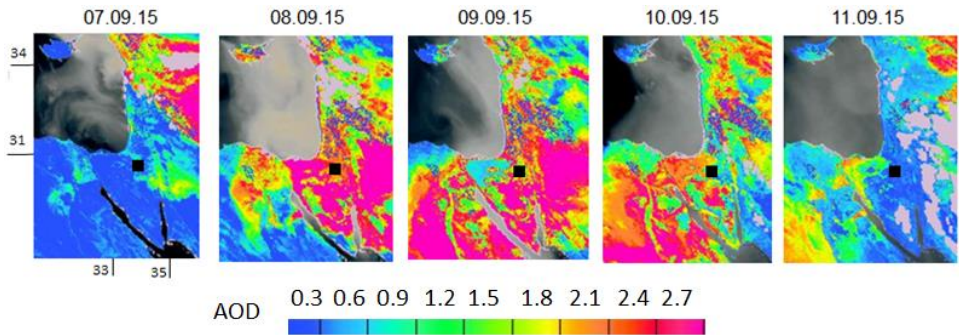
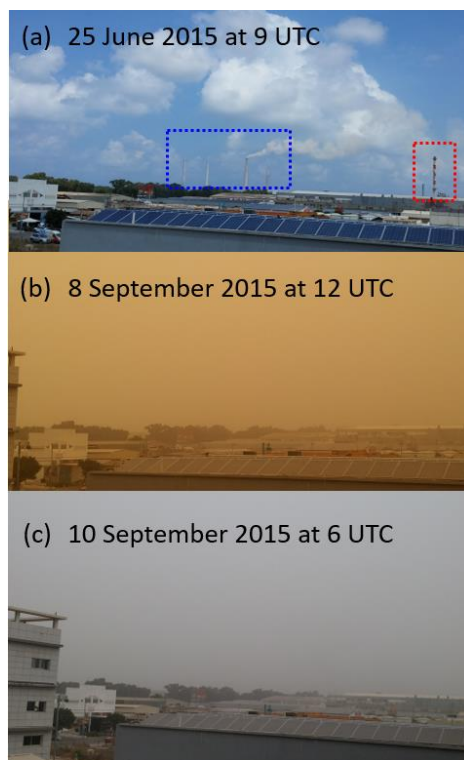


Figure 1. Aerosol Optical Depth (AOD) at 12 UTC from Meteosat Second Generation (MSG) spacecraft. The black square indicates the location of the Sede Boker AERONET unit measuring AOD from ground level. The AOD measurements are given in Fig. 6.

An exceptionally extreme dust storm prevailed over the Eastern Mediterranean (EM) on September 2015. The Israeli meteorological service (IMS) declared the dust storm to be extraordinary as it occurred on early September (7-10 September), extended over a time span of 100 hours creating extreme ground level particulate matter (PM) concentrations (e.g. 100 times above the hourly average of PM10 in Jerusalem). On 7 September, prior to the penetration of the dust storm over Israel, IMS reported (<http://www.ims.gov.il/IMS/CLIMATE>; in Hebrew) a heat wave which prevailed over Israel causing

97 harsh weather conditions of 80-90% relative humidity, 42 °C in valleys, 38 °C in mountains. On 8
98 September, visibility decreased below 3 km and consequently, inland aviation was prohibited until the 9
99 September (Fig.1). Concurrently, severe ground level PM concentrations resulted a public warning from
100 outdoor activities, issued by the environmental protection ministry. Finally, on 11 September, as visibility
101 increased, the IMS confirmed the dust storm ended, whereas the heat wave was over only two days later,
102 on 13 September, subsequent to a profound change in weather conditions. The PM concentrations
103 declined to values measured prior to the dust storm (<http://www.svivaqam.net/Default.rtl.aspx>; in
104 Hebrew) only on 14 September, though the AERONET measurements (<https://aeronet.gsfc.nasa.gov>)
105 stationed in central and southern Israel reveal that the aerosol optical depth (AOD) resumed to values
106 prior to the dust storm only on 17 September.

107
108
109



110
111
112

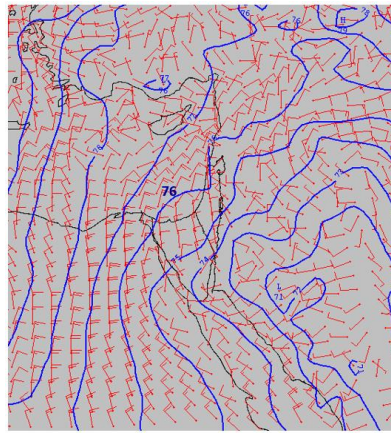
Figure 1. Photographs taken from the central coast of Israel, adjacent to the Hadera ceilometer, 3.5 km southeast to the stacks of a power plant (indicated by a blue rectangle) and 600 m north to a

113 factory stack (indicated by a red rectangle). The photographs were taken prior to the dust storm, on
114 25 July 2015 (a) and during the dust storm, on 8 September 2015 (b) and 10 September 2015 (c).
115 Notice that during the dust event (b,c) the stacks clearly seen in (a) from the same spot, are invisible.

116
117 Investigation of the mechanisms leading the severe dust storm was performed by Gasch et al. (2017)
118 using a state of the art dust transport model ICOSahedral Nonhydrostatic (ICON) with the Aerosol and
119 Reactive Trace gases (ART) (Rieger, et al., 2015). The model concentrated on the EM with one global
120 domain (40 km grid spacing, and 90 vertical levels from 20 m to 75 km) and 4 nested grids (20, 10, 5
121 and 2.5 km grid spacing and 60 vertical levels from 20 m to 22.5 km). Simulations were done for three
122 consecutive days from 6-8 September. Model results delineated an unusual early incidence of an active
123 Red Sea Trough (Fig.2; Alpert et al. 2004) over Mesopotamia, followed by meso-scale convective
124 systems over the Syrian-Iraqi border generating three cold-pool outflows. On the night between 5 and 6
125 September, a convective system fueled by an inflow along the eastern side of the Red Sea Trough, moved
126 northeast over the Turkish-Syrian border region. The convective system intensified overnight and
127 generated a first weak cold pool outflow on the 6 September. After sun rise, as the nocturnal boundary
128 layer dissipated, an increase of downward mixing lead to an increase of surface wind speeds consequently
129 causing dust to pick up over Syria. The high surface wind speeds sustained during the day due to a strong
130 and shallow heat low whereas sea breeze transported dust to the south towards Jordan. At this point, the
131 atmospheric instability over the Syrian-Iraqi border created a second convective cool outflow from the
132 Zagros mountain range west into Syria. The gust from the second cool pool outflow ignited a third cool
133 pool outflow at 20 UTC. The third outflow moved southerly along the eastern flank of the Red Sea
134 Trough and shifted warm and moist air masses along the way. Past midnight, on 7 September, the
135 intensified third cool pool outflow shifted to the west. At 10 UTC 7 September, rainfall and an increase
136 of surface wind speeds north-west of Syria strengthened the third cool pool outflow. Consequently,
137 enormous dust emissions transported southwest up to 5 km. The aged second cool pool outbreak re-
138 intensified over Jordan and southwestern Syria and merged with the third outflow with the nightfall of 7
139 September. After midnight, on 8 September, the dust transported over Israel and was mostly influenced
140 by local circulation systems in the EM. Model simulations were compared to in-situ measurements and
141 satellite images: visible electromagnetic spectrum from Moderate Resolution Imaging Spectroradiometer
142 (MODIS: <https://modis.gsfc.nasa.gov/>) aboard the Aqua satellite; AOD from the Terra satellite; RGB
143 dust product from the Spinning Enhanced Visible and InfraRed Imager (SEVIRI) upon the Meteosat
144 Second Generation (MSG) satellite; total attenuated backscatter from Cloud-Aerosol Lidar upon the
145 Infrared Pathfinder Satellite Observations (CALIPSO: <https://www-calipso.larc.nasa.gov/>). Ground level
146 meteorological measurements (3 sites) and PM concentration (3 sites) in Israel were employed. Results

147 revealed the model lacked sufficient development of a super critical flow, which in effect produced the
148 excessive surface wind speeds. Eventually, this misled the forecast of the dust advection southwest into
149 Israel.

150
151



152

Formatted: Font color: Auto

153

154 ~~Jasmin (2016) compared the dust storm aerosol content provided by Meteosat Second Generation (MSG)~~
155 ~~by the Spinning Enhanced Visible and InfraRed Imager (SEVIRI) observations, to the results of the open~~
156 ~~source Meteoinfo model. The Meteoinfo model was based on meteorological variables from the~~
157 ~~European Centre for Medium Range Weather Forecasts (ECMWF). The meteorological conditions~~
158 ~~generated by the model suggested a formation of two dust storms simultaneously, from northern Syria~~
159 ~~and the Egyptian Sinai desert as a result of updrafts created by low pressure systems.~~

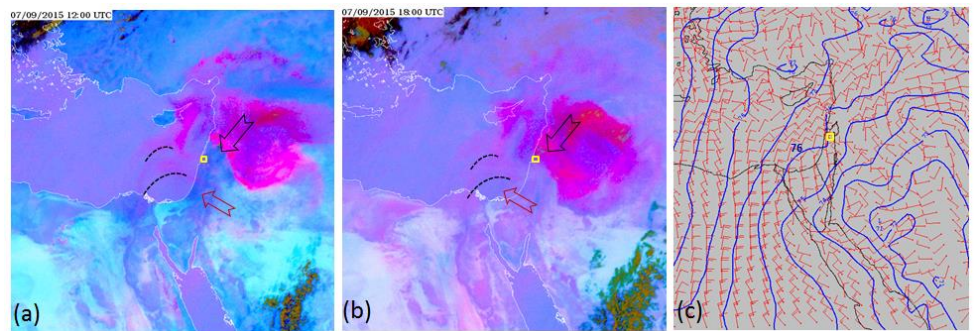
160

161 Mamouri et al (2016), analyzed the dust storm development in the Cyprus region based on Moderate
162 Resolution Imaging Spectroradiometer (MODIS) aboard the Aqua satellite (MODIS Aqua). Aerosol
163 Optical Depth (AOD) satellite pictures, backscatter and attenuation profiles based on a multispectral
164 LIDAR from the European Aerosol Research LIDAR Network (EARLINET), and ground level
165 measurements of PM10. They concluded that the dust plumes from Syria entered the EM in a double
166 layer structure, 1.5 and 4 km above sea level (ASL), pointing out to the possibility of multiple dust
167 sources.

168

169 Gasch et al. (2016) claimed an unusual early incidence of an active Red Sea Trough (RST, Fig. 2c)
170 (Alpert et al, 2004) followed by meso-scale convective systems generating cold-pool outflows producing

171 the dust storms (Fig. 2c). They applied the ICOSahedral Nonhydrostatic (ICON) modelling system with
 172 the Aerosol and Reactive Trace gases (ART). This model better explained the dust evolution but lacked
 173 sufficient development of a super-critical flow in order to produce the excessive surface wind speeds.
 174 These eventually misled the forecast of the dust advection southwest into Israel.
 175 The model results were related to two Cloud Aerosol LIDAR and Infrared Pathfinder Satellite
 176 Observation (CALIPSO) LIDAR overpasses (Winker et al., 2009). They suggested that the dust plume
 177 expanded north-west and then turned south-east as the trough collapsed penetrating Israel and Egypt from
 178 the east. In addition, they related the model findings with three particulate matter ground station
 179 measurements in Israel.



181
 182 Figure 2. MSG-SEVIRI satellite pictures of dust RGB component at 07.09.15 12 UTC (a) and 18 UTC (b). The
 183 dust appears in pink colors. Indications of the Mount Meron site (Yellow Square at Lon 33.0° Lat 35.4°) the first
 184 dust plume (red arrow and dashed line) and second dust plume (black arrow).

185 (c) Synoptic 925 mb 12 UTC map from 7 September 2015 12 UTC of the geopotential height with 1
 186 dm interval (the 76 dm line is passing over Israel; blue lines) and wind (10 kt, each line; red arrows).

187 Source: IMS from UKMO British Met Office model.

188
 189
 190 Parolari et al. (2016), conducted simulations using the Weather Research and Forecasting (WRF) model
 191 that disclosed an unusual low-level westerly wind spread to the EM, enhancing surface wind shear stress
 192 to reversely transport the previously eastward particles back to the EM.

193
 194 Solomos et al. (2016) investigated the dust event by an EARLINET LIDAR, satellite aerosol content
 195 observations from MSG, and the CALIPSO. In addition, they ran the high regional atmospheric modeling
 196 system (RAMS) in order to reanalyze the progression of the dust event. The model results were compared
 197 with the satellite pictures and LIDAR measurements. The model predicted a few events of dust outbreaks
 198 resulting from different synoptic conditions. They have succeeded to improve the plumes extent and front

199 ~~directions compared to the original forecasts, but the ability to predict the details were partial, probably~~
200 ~~due to inaccuracies in the model physical processes. Eventually, the aerosol concentration profile of the~~
201 ~~improved model was lower than the actual LIDAR measurements.~~

202
203 The fact that forecast models did not succeed in predicting this outstanding dust event motivated
204 Mamouri et al. (2016) to study its origin and development. Their research presented dust load
205 observations in the Cyprus region. Luckily, at the time of the dust storm, an EARLINET (European
206 Aerosol Research lidar Network: <https://www.earlinet.org/>) Raman lidar stationed in Limassol provided
207 vertical dust profiles and valuable optical dust properties of backscatter, extinction, lidar ratio and linear
208 depolarization ratio. They analyzed the optical thickness (AOT) and Angström exponent derived from
209 the MODIS Aqua satellite. MODIS Aqua AOT measurements were compared to the Limassol lidar
210 observations, AOD measurements from two AERONET sites (Cyprus and Israel) and ground level PM10
211 concentration from four Cyprus sites. On 7 September, EARLINET lidar observations measured two dust
212 layers (extending up to 1.7 km ASL and between 1.7-3.5 km ASL). The dust particle extinction
213 coefficient measured in Limassol had reached 1000 Mm^{-1} followed by high PM10 concentration of 2000
214 $\mu\text{m m}^{-3}$. Extreme values over Limassol, were reported on the 8 September as MODIS Aqua AOT
215 observations exceeded 5 (assuming overestimation up to 1.5) and hourly PM10 concentration of about
216 $8,000 \mu\text{m m}^{-3}$ (with uncertainties in the order of 50%). Unfortunately, on the 8 September, the lidar was
217 intentionally shut down to avoid potential damage to the instrument. Nevertheless, lidar observations
218 indicated another dense dust outbreak (1-3 km ASL) reaching Limassol on the 10 September, also visible
219 by the MODIS Aqua AOT imagery. The researchers concluded the scale of the dust storm features was
220 too small for global and regional dust transport models. They presumed that the initiation of the dust
221 plume was due to an intense dust storm (Habbob) in northeastern Syria and northern Iraq, leading to
222 vigorous downbursts which consequently pushed huge amounts of dust and sand to the atmosphere. The
223 lidar observations indicated a double layer structure of the dust, 1.5 and 4 km above sea level (ASL),
224 pointing to multiple dust sources.

225
226 Stavros et al., (2016) continued the investigation of the formation and mechanism of the dust storm
227 over Cyprus by a high regional atmospheric model of the integrated community limited area modeling
228 system (RAMS-ICLAMS). The model simulations focused on the generation of the dust storm on 6 and
229 7 September. Model results were fine-tuned by observations from EARLINET lidar stationed in
230 Limassol, radiosonde data from five sites (Cyprus, Israel, Jordan, and two from Turkey) and satellite
231 imagery from MSG SEVIRI and CALIPSO CALIOP. The model was set to three grid space domains:
232 an external grid of 12×12 km, (over the EM) an inner set at 4×4 km (over northern EM) and 2×2 km

267 AOD were compared to the monthly average of 2000-2015. The monthly average of September 2015
268 vegetation status in the region was estimated by MODIS normalized difference vegetation index (NDVI).
269 Historical data was divided into two periods: none-drought (2001-2006) and drought (2007-2010). Wind
270 shear stress was calculated to estimate wind erosion. Their findings reveal that the enhanced dust uplift
271 and transportation of the September 2015 dust storm was due to meteorological conditions rather than
272 the land-use changes because of the civil conflict in Syria. WRF simulations revealed the well-known
273 Shamal winds and cyclone associated with dust storms in the Middle East (Rao et al., 2003) were
274 characterized by northwesterly winds west of the low pressure zone in the Syrian-Iraqi border. However,
275 the source of elevated dust concentrations over the EM coast on the 7 and 8 September were attributed
276 cyclone front movement. On 6 September low level winds (700 hPa) were opposite to the northwesterly
277 high level (300 hPa) winds, consequently, generating enhanced surface shear stress and transported re-
278 suspended PM westward. Furthermore, based on the past 20 years, the Israeli summer of 2015 was
279 unusually dry and hot and therefore enabled easier updraft of dust soil increasing the probability of dust
280 emissions.

Formatted: Font color: Auto 281 Jasmin (2016) compared the dust storm aerosol content provided by A summary of the aforementioned
282 studies is given in Table 1.

283
284
285 To this point, the forecast and reanalysis models were found to be incapable of reproducing the details
286 of this extreme dust storm event. So far, no attempt has been done to relate the models findings to a
287 continuous spatial, temporal and vertical set of profiles measurements. The goal here is to display the
288 evolution of this extreme event by several local remote sensing devices available in Israel, particularly
289 the eight ceilometers spread across Israel in order to describe the plume evolution.

290
291 An overview of the instruments and location of the measuring sites is given in Sect. 2. Section 3
292 presents the results. MSG SEVIRI observations, to the results of the open source Meteoinfo model
293 (Wang, 2014). The Meteoinfo model was based on meteorological variables from ECMWF. The model
294 meteorological conditions suggested a formation of two simultaneous dust storms, from northern Syria
295 and from the Egyptian Sinai desert, resulting from updrafts created by low pressure systems.

296
297 The aforementioned studies (summarized in Table 1) focused on the generation of the dust storm in
298 the Syria region based on transport models, satellite imagery and in situ measurements. In our study we
299 focus on the evolution of the dust plume over Israel in the lower atmosphere based on an array of 8
300 ceilometers, 52 in situ PM measurements, two AERONET sites and satellite imagery. We do not

301 investigate the reasons of the models frailer to predict this extraordinary storm, but rather attempt to
302 present details of the evolution of the dust plume passage over Israel. The data presented here can be
303 used as a tool to verify state of the art model simulations and provide a different point of view to the
304 meteorological conditions governing the dust plume advection over the EM.

305
306 In the following section we describe the measuring sites and instruments in this study. The list of
307 instruments includes; ceilometers, PM measurements, AERONET, radiosonde, solar radiation and
308 satellite imagery. Sect. 3 presents the results of the dust plume spatial and temporal scheme delineated
309 by the ceilometer plots on 7 September through the 10 September 2015. We discuss and compare
310 between the ceilometer plots and the aforementioned auxiliary measurements. In Sect. 4 we conclude our
311 main findings of the dust plume advection in the lower atmosphere above Israel and the downward
312 transport towards the ground.

313 **Conclusions** and discussion are given in Sect. 4.

316 2. Instruments

317
318 Continuous measurements of aerosols in Israel are conducted by PM10 ground monitoring stations
319 managed by the Israeli Environmental Protection ministry (IEPM). While the monitoring stations provide
320 the temporal and spatial dispersion of the aerosols on ground level, AERONET measurements portrays
321 several parameters of the aerosol content in the column of air from ground level to the atmosphere above
322 its measuring point. Despite the progress with the satellite products from MODIS Terra, MODIS Aqua
323 and MSG-SEVIRI, the 2D pictures cannot delineate the vertical evolution of the dust plume highly
324 influenced by the spatial orography and particle distribution, governed by the synoptic system and meso-
325 meteorological conditions (Su and Toon, 2011).

326
327 Fortunately, the ability to add the vertical aerosol distribution by ground remote sensing ceilometers is
328 available in Israel. These instruments use the LIDAR principle as a tool for mapping worldwide dust
329 movements (Ansmann et al., 2011; Mona et al., 2014).

332 2.1 Ceilometers

333

Ceilometers ~~The~~, initially intended for cloud level height detection, are automatic low cost lidars widespread in airports and weather stations worldwide. As single wavelength lidars, ceilometers cannot produce the information aerosol properties such as size distribution, scattering and absorption coefficients (Ansmann et al., 2011; Papayannis et al., 2008). Nevertheless, with improvement of hardware and firmware over the years, ceilometers have become a valuable tool in the study of the atmospheric boundary layer and the vertical distribution of aerosols layers (Haeffelin and Angelini, 2012; Ansmann et al., 2003). Furthermore, in 2013 ceilometers been assimilated in the EUMETNET (European Meteorological Services network) Profiling Program (E-profile) to develop a homogeneous dataset from automatic lidars and state-of-the-art ceilometers across Europe (<http://eumetnet.eu/activities/observations-programme/current-activities/e-profile/alc-network/>).

Vaisala ceilometers type CL31 ceilometer (Wiegner et al., 2014; Mona et al., 2014; Weitkamp, 2005; Muenkel et al., 2004), are commonly deployed worldwide, and the main research tool in this study as well. CL31 is a pulsed elastic micro LIDAR lidar, employing an Indium Gallium Arsenide (InGaAs) laser diode transmitter of near infrared wavelength (of 910 nm \pm 10 nm at 25°C). In order to compensate the low pulse energy of the laser (defined "eye-safe") and to provide sufficient signal to noise ratio (SNR), the pulse repetition rate is of 10 kHz of short pulses are emitted to the atmosphere, in a measuring interval of every two seconds (Vaisala ceilometer CL31 user's guide at: <http://www.vaisala.com>). The backscatter transmissions signals are collected by an avalanche photodiode (APD) receiver, are averaged to produce an individual and designed into attenuated backscatter profile profiles within a reporting interval of 2 to 120 s. (determined by the user). The attenuated backscatter profiles are automatically corrected by an internal calibration (resulting in a multiplication factor of 10^{-8} to convert the signal count to attenuated backscatter), a cosmetic shift of the backscatter signal (to better visualize the clouds base), an obstruction correction (when the ceilometers' window is blocked by a local obstacle) and an overlap correction (to the height where the receiver field of view reaches complete overlap with the emitted laser beam).

Kotthaus et al., backscattering relative signals (profiles) were used in this study to verify the trends in the vertical distribution of the dust and its spreading over Israel. The diurnal (2016) examined the Vaisala CL31 ceilometer by comparing the attenuated backscatter profiles from 5 units with different specification of sensor hardware, firmware and operation settings (noise, height and time reporting interval). They have concluded the instrument characteristics that affect the quality and availability of the attenuated backscatter profiles in the following manner: At high altitudes, a discontinuity in the attenuated backscatter profile is evident at two height points, ~ 4949 and 7000 m. Background signals

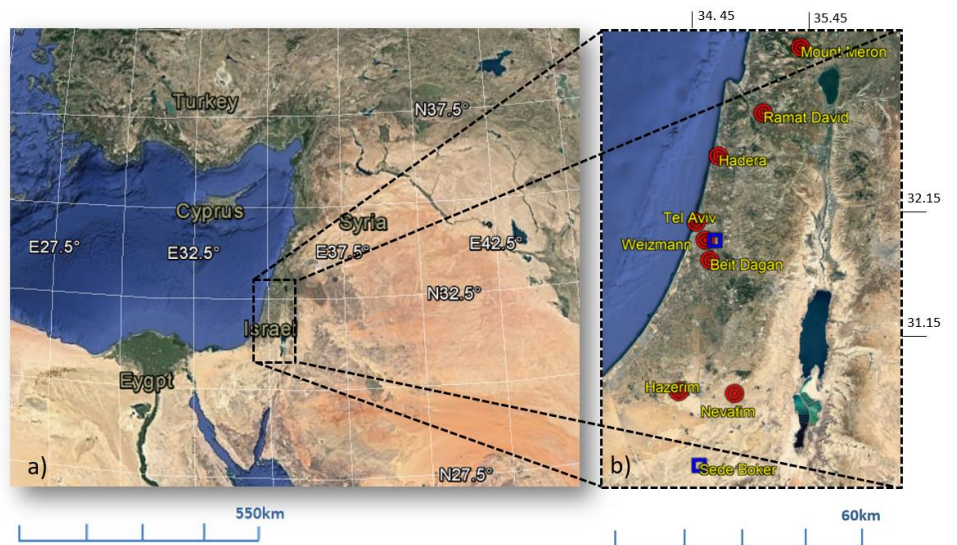
368 (instrument related) and cosmetic shift (firmware dependent) tend to be either negative or positive up to
369 6000m and then switch signs above ~ 6000 m. Below 70 m an overlap correction is applied internally by
370 the ceilometer sensor as well as an obstruction correction (below 50 m). Between 50-80 m hardware
371 related perturbation cause a slight offset in the attenuated backscatter values. The authors advise the user-
372 defined reporting interval should be no shorter than 30s to avoid consecutive profiles partial overlap.
373 However, they emphasize the internal calibration applied to convert the signal count output to “attenuated
374 backscatter” does not always fully represent the actual lidar constant, therefore, it is not accurate enough
375 for meteorological research. Nevertheless, since ceilometers are not sensitive to molecular scattering and
376 solar radiation contributes to the random noise, a background correction can be derived by a 4 hr round
377 of midnight attenuated backscatter profiles. Furthermore, a range corrected attenuated backscatter can be
378 derived by the attenuated backscatter profiles during an existence of a stratocumulus cloud.

379
380 Furthermore, Weigner et al, (2014) studied different retrieval methods to derive the aerosol backscatter
381 coefficient from the ceilometers' attenuated backscatter profiles based on a comparison to auxiliary
382 collocated instruments such as a sunphotometer or a multiwavelength lidar. They focused on calibration
383 methods, the range detection limitations by the overlap function and the sensitivity of the attenuated
384 backscatter signal to relative humidity. Although, the ceilometer wavelength range (given as 905 ± 3 nm)
385 is influenced by water vapour absorption, in the case of aerosol layer detection, water vapour distribution
386 has a small effect on the signal change, indicating the mixed layer height (MLH) was evaluated by the
387 or an elevated mixed layer, as the aerosol backscatter itself remains unchanged. Consequently, except for
388 a case of a dry layer in a humid MLH, the water vapour is unlikely to lead misinterpretation of the aerosol
389 stratification. Fortunately, most algorithms are based on a significant signal slope to define the aerosol
390 layers, therefore, can be determined from uncelebrated ceilometer attenuated backscatter profiles. The
391 wavelet covariance transform (WCT) method was the method used in this study to evaluated the MLH
392 (Uzan, et al, 2016). Using this data together with the satellites pictures AOD and the spectral integrated
393 AEROSOL ROBOTIC NETWORK (AERONET) measurements described below, made sure that only dust,
394 whether determined by the creation of thermals or the subsidence of the dust plume.

395
396 In this study, we address the aforementioned limitations as we refer to the ceilometer signal count
397 profiles between 100-1000 m AGL. The ceilometer array is comprised of 8 units in different sites (Fig 3
398 and Tables 2-3), 6 of which are owned by a governmental office. The ceilometers are CL31 type apart
399 for ceilometer CL51 stationed in the Weizmann Institute which has a higher backscatter profile range (up
400 to 15.4 km, Munkel et al., 2011). Unfortunately, calibration procedures were not held and maintenance
401 (cleaning of the ceilometer window) was addressed done regularly only for the Beit Dagan ceilometer.

402 Apart from the Beit Dagan and Weizmann ceilometers (Table 4), we could not retrieve the technical
403 information of firmware and hardware type. However, we have been confirmed (personal
404 communication) that the combination of hardware and firmware had been done following Kotthaus et al
405 (2016). The Beit Dagan ceilometer signal count were found to be weaker (up to 800 signal count
406 compared to 10,000 in the other CL31 ceilometers) due to different hardware definitions. Therefore, in
407 order to present the Beit Dagan attenuated backscatter profiles aligned with the profiles of the other
408 ceilometers (given in Fig. 17), the Beit Dagan attenuated backscatter values were multiplied by 12.5
409 (10,000/800).

411 ~~Based on the CL31 specifications it should measure linearly from ground level up to 7.7 km AGL.~~
412 ~~However, when the signals are analyzed it is clear that the instruments have a structured feature of an~~
413 ~~artificial peak around 50-100 m AGL (the exact location is instruments dependent). Since this feature is~~
414 ~~repeatable, it is possible to verify relative changes in the signal strength below this height, but linear~~
415 ~~measurements should be analyzed only above it. The CL31 features and their dependence on the~~
416 ~~instruments electronics and software version were studied in details by the TOPROF group (~~



417 ~~Kotthaus et al., 2016).~~

420 ~~The location of the ceilometers deployed in Israel is given in Fig. 3 and Table 2. The ceilometers transmit~~
421 ~~every 16 sec and with height resolution of 10 m between 0-4.5 km. The shoreline ceilometers, however,~~
422 ~~transmit every 15 sec. The Beit Dagan Ceilometer measures up to 7.7 km.~~

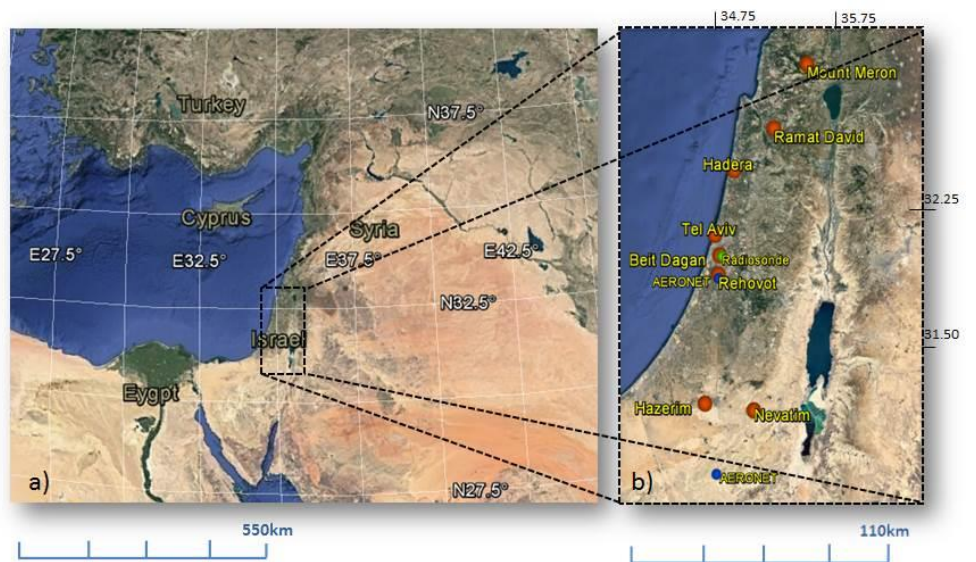


Figure 3. Google Earth map of the large domain (a) and Israel (b) with indications of 8 ceilometer deployment in Israel in 2015 (orange sites (red circle; detail in Table 2) and two AERONET sites (blue square).

2.2 Radiosonde

A radiosonde (RS) is a small instrument package suspended by a large hydrogen or helium gas balloon. As the radiosonde rises (~300 m/min) sensors on the radiosonde transmits pressure, temperature, relative humidity, pressure, and wind speed, and wind direction and GPS position data each second. In Israel the radiosonde is launched twice a day (00 UTC and 12 UTC) by the IMS, adjacent to the Beit Dagan ceilometer. The radiosonde launching site in Beit Dagan (green circle) at the site of Beit Dagan ceilometer.

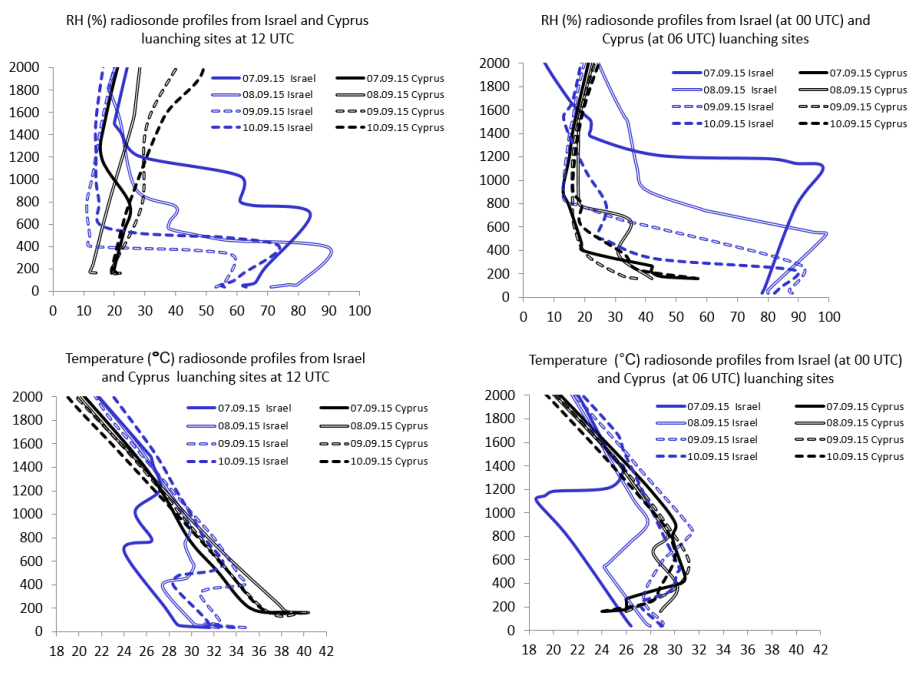
2.2.2 produces profiles of humidity, Radiosonde

A radiosonde (RS) is a small instrument package suspended by a large hydrogen or helium gas balloon. As the radiosonde rises (~300 m/min) sensors on the radiosonde transmits pressure, temperature, relative humidity, pressure, and wind speed, and wind direction and GPS position data each second. In Israel the radiosonde is launched twice a day (00 UTC and 12 UTC) by the IMS, adjacent to the Beit Dagan ceilometer. The radiosonde. The output files were downloaded from the University of Wyoming site (<http://weather.uwyo.edu/upperair/sounding.html>, station number 40172). With respect to Stull (1988), the

Formatted: Font color: Auto
 Formatted: Font color: Auto

446 MLH was defined by the RS profiles as the height where the following phenomena ~~where~~ identified:
 447 an inversion ~~layer~~ in the temperature ~~profile~~, a significant drop in the relative humidity ~~profile~~, strong wind
 448 shear ~~in the wind speed profile~~ and an increase in the virtual temperature ~~profile~~ (Uzan et al., 2016; Levi et
 449 al., 2011).
 450

451 ~~Although the large scale and intensity of the event, the dust storm dynamics was quite different between~~
 452 ~~neighboring countries. For example, the Israeli radiosonde profiles were compared to the nearest~~
 453 ~~available radiosonde site in Cyprus (station number 17607). Details on launching sites are given in Table~~
 454 ~~3. Fig. 4 presents the temperature and relative humidity profiles from 07.09.15 to 10.09.15 between the~~
 455 ~~heights of 100-1,500 m AGL disclosing the different meteorological conditions in Israel and Cyprus in~~
 456 ~~spite of a relatively short distance of about 350 km.~~
 457



458
 459
 460
 461
 462
 463

464 **Particulate** ~~Figure 4. Radiosonde Temperature and Relative humidity (RH) profiles at 12 and 00 UTC from~~
465 ~~the Israeli launching site (blue profiles) and at 12 and 06 UTC from the Cyprus launching site (black profiles)~~
466 ~~between 07.09.15-10.09.15.~~

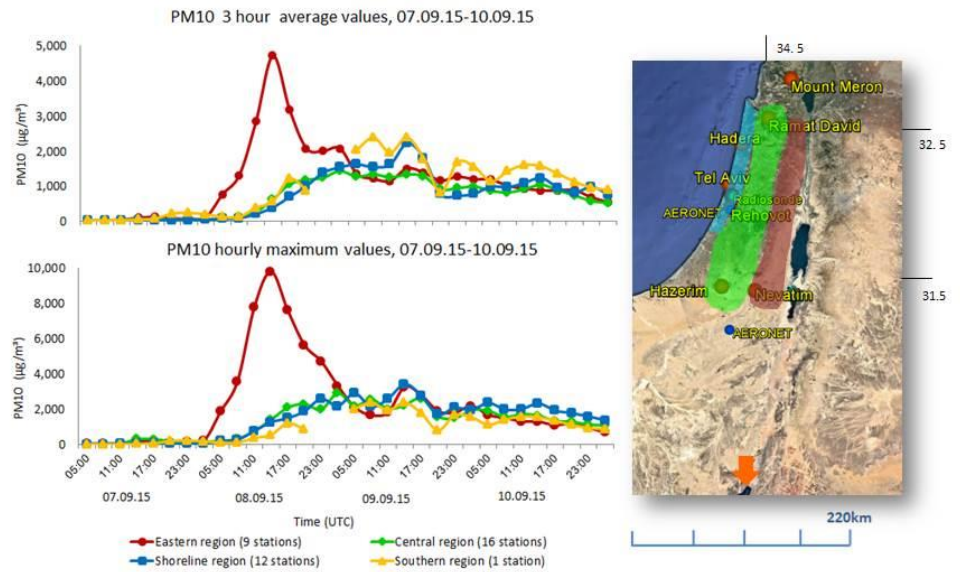
469 **2.3 PM10**

470 **2.3** ~~The majority of the ground particulate~~ **matter** ~~measurements in Israel are done by method of the~~
471 **monitors (PM10, PM2.5)**

473 ~~PM monitors are low-volume flow rate Thermo Fisher Scientific type FH 62 C14 (beta attenuation-~~
474 ~~method) and type 1405 TEOM (Tapered Element Oscillating Microbalance method). In the~~ beta
475 ~~attenuation monitor samples at ambient temperatures in a low volume flow rate. Low~~
476 ~~method~~ ~~(<https://www3.epa.gov/ttnamti1/files/ambient/inorganic/overwv1.pdf>) low-energy beta rays are focused~~
477 ~~on deposits on a filter tape and attenuated according to the approximate exponential function of~~
478 ~~particulate mass (i.e., Beer's Law). These automated samples employ a continuous filter tape. Typically,~~
479 ~~the~~ ~~The~~ ~~attenuation through an unexposed portion of the filter tape is measured, and~~ the tape is then
480 ~~exposed to the ambient sample flow where a deposit is accumulated. The beta attenuation is repeated,~~
481 ~~and the difference in attenuation between the blank filter and the deposit is a measure of the accumulated~~
482 ~~concentration. The PM10 monitors report 5 min average mass concentrations (IEPM monthly report).~~
483 ~~The weighing principle used in the TEOM method~~
484 ~~(<https://tools.thermofisher.com/content/sfs/manuals/EPM-TEOM1405-Manual.pdf>) is based on a mass~~
485 ~~change detected by the sensor as a result of the measurement of a change in frequency. The tapered~~
486 ~~element at the heart of the mass detection system is a hollow tube, clamped on one end and free to~~
487 ~~oscillate at the other. If additional mass is added, the frequency of the oscillation decreases. An electronic~~
488 ~~control circuit senses oscillation adds sufficient energy to the system to overcome losses. An automatic~~
489 ~~gain control circuit maintains the oscillation at a constant amplitude. A precision electronic counter~~
490 ~~measures the oscillation frequency with a 10-second sampling period. Both instruments report PM~~
491 ~~concentration every 5 min. The location of PM measurement sites is given in Tables 5,~~

492 ~~An ensemble of 3 hourly average of PM10 concentration from 38 monitoring stations was analyzed. For~~
493 ~~convenience, we divided the monitoring stations into 4 geographical regions: east, center, shoreline and~~
494 ~~south (Fig. 5). Unfortunately, there are no PM10 measurements in northern Israel. The eastern region~~
495 ~~includes the highest monitoring stations up to 960 m ASL. Further detail of the PM10 measurement sites~~
496 ~~is given in Table 4. The average availability of PM10 data throughout the period of the dust storm, from~~
497 ~~07.09.15 to 10.09.15, was relatively high, i.e., over 90% from 33 stations (87% of the monitoring stations~~

498 Surprisingly, in all the geographical regions (except the east Mountain region, PM10 measurements
499 indicated the dust event began on the 8.9.15. This will be discussed in detail in Sect. 3.
500
501



502
503
504
505

Formatted: Font: 12 pt, Font color: Auto

506 **Figure 5.** Map of PM10 geographical regions right panel map: east (red), center (green), shoreline (blue) and
507 south (orange arrow). The regions were overlaid upon the 8 ceilometer deployment map. The left panels are the
508 PM10 measurements for the four regions with the same colors. The 3 h average concentration (upper panel) and
509 1 h maximum (lower panel). Notice the different PM10 concentration scale (double for the maximum). Time
510 period is 07.09.15-10.09.15, time in UTC.
511

512
513
514
515
516

Formatted: List Paragraph, Outline numbered + Level: 2 +
Numbering Style: 1, 2, 3, ... + Start at: 1 + Alignment: Right
+ Aligned at: 0" + Indent at: 0.31"

Formatted: Font color: Auto

Formatted: Font color: Auto

Formatted: Font color: Auto

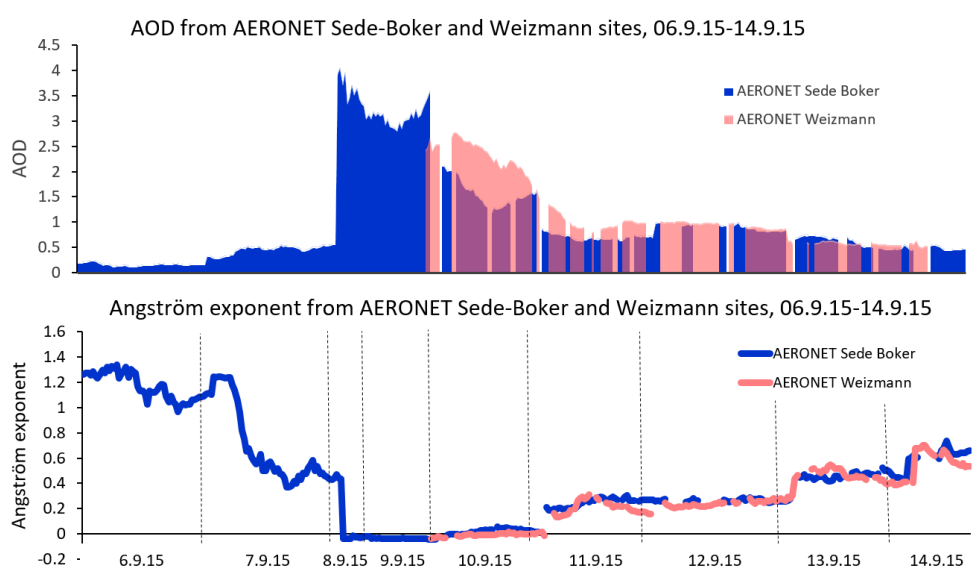
Formatted: Font color: Auto

517 **2.4.2.4 AERONET**

518
519 Aerosol RObotic NETwork (AERONET) is multiband photometer with an automatic sun tracking
520 radiometer which makes for direct sun measurements every 15 min at 340, 380, 440, 500, 675, 870, 940,

521 and 1020 nm with a spectral range of 340 to 1640 nm wavelengths. The cycle of 8 wavelengths is scanned in
 522 8 sec. Sequences of three measurements taken 30 s apart produce three measurements at each wavelength
 523 within a 1 min period. These The photometer measures the solar extinction measurements are then used
 524 in each wavelength to compute aerosol optical depth at each wavelength except for the 940 nm channel,
 525 which is used to retrieve precipitable water in centimeters (Holben et al., 1998).

527 In Israel two AERONET units are operated type CE318-N (<https://aeronet.gsfc.nasa.gov>) operate in Sede-
 528 Boker and the Weizmann Institute in Rehovot (Fig. 3), but only). Unfortunately, the Sede Boker unit
 529 measured throughout the whole event (Fig. 6 in blue). The AERONET unit in Rehovot did not operate
 530 on the first two days of the dust storm (Fig. 6 in orange). The combination of high AOD and low
 531 Angström number indicate the dust event was comprised mainly by coarse particles of mineral dust
 532 (Dubovik et al., 2000; Kaskaoutis et al., 2008).



535
 536 in Figure 6. A combination of AERONET observations for 6.9.15-14.9.15 of AOD (top panel) and Angström
 537 exponent (bottom panel) from two measuring sites: Sede Boker (southern Israel) and Weizmann Institute in
 538 Rehovot (central Israel). Both units did not operate consecutively. The Sede Boker site operated throughout the
 539 dust event while the AERONET Weizmann site began operating from 9.9.15.

542 **3. Results**

543

544 The data collected by the ceilometers, AERONET radiometers, AOD satellite pictures and PM10 ground
545 detectors was combined to describe the dust storm penetration and development over Israel. As a single
546 wavelength instrument, ceilometers cannot distinguish between aerosols types. Therefore, the measured
547 profiles were analyzed to distinguish between clouds and other aerosols. The ceilometer profiles are
548 unitless and therefore divided by a scale factor of $10^{-9} \text{ m}^{-1} \text{ sr}^{-1}$ enabling quantitative analysis (Kotthaus
549 et al., 2016). An example of the ability to distinguish attenuated backscatter profiles from clouds and dust
550 plume is given in Fig. 7 with reference to Fig. 8, as follows: High signals of attenuated backscatter, up
551 to $7 \times 10^{-1} \text{ m}^{-1} \text{ sr}^{-1}$ were received on 7.9.15 (Fig. 7a, indicated arrow no.1 in Fig. 8). Profiles containing
552 dust plume produced signals up to $4 \times 10^{-5} \text{ m}^{-1} \text{ sr}^{-1}$ were received on the 07.09.15 (Fig. 7b, indicated by
553 arrow no.2 in Fig. 8). The process on the 08.09.15 (Fig. 7c, indicated by arrow no.3 in Fig. 8) displays a
554 double layer dust plume, at 250 m ASL of $\sim 1 \times 10^{-4} \text{ m}^{-1} \text{ sr}^{-1}$ and 450 m ASL of $\sim 4 \times 10^{-5} \text{ m}^{-1} \text{ sr}^{-1}$. On 9.9.15
555 (Fig. 7d, indicated by arrow no.4 in Fig. 8) only a thin lofted plume is evident between 300-350 m ASL
556 of $\sim 1.5 \times 10^{-5} \text{ m}^{-1} \text{ sr}^{-1}$.

557

558

559

560

561

562

563

564

565

566

567

568

569

570

571

572

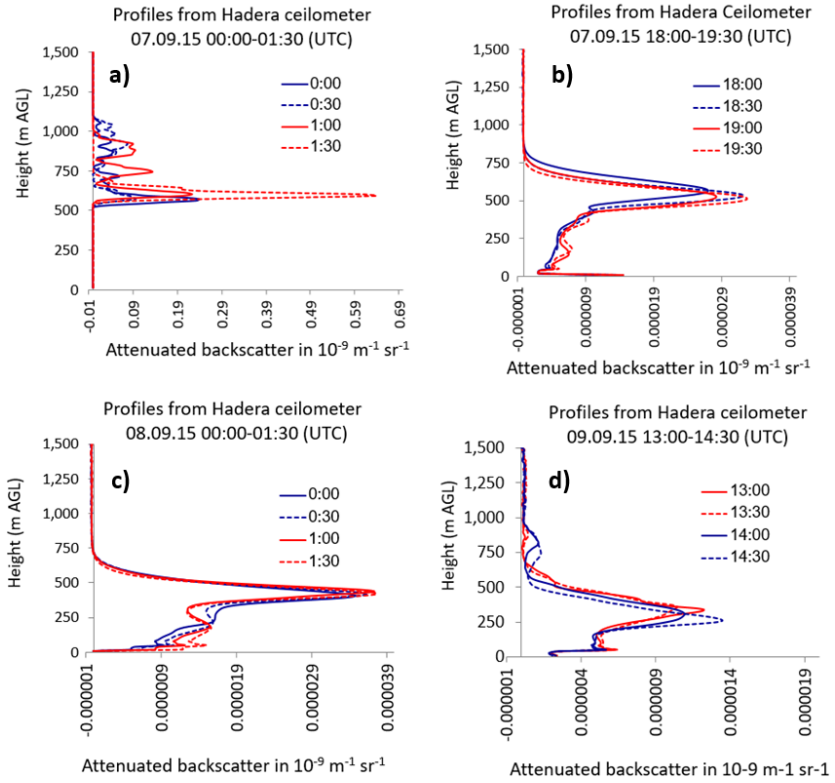
573

574

575

576

577



578

Formatted: Font: 12 pt, Font color: Auto

579

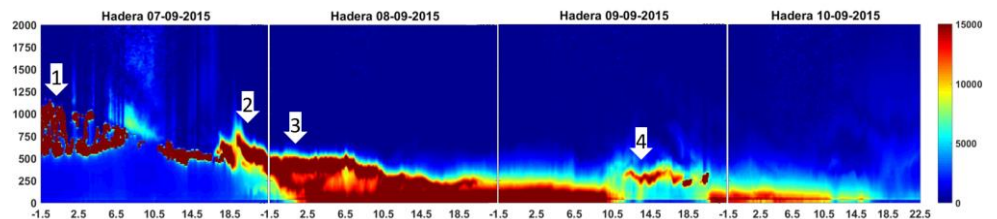
Figure 7. Hadera ceilometer attenuated backscatter profiles for cloud and dust plume detections indicated in Fig.8 by (a) arrow no.1 (clouds), (b) arrow no.2 (dust layer), (c) arrow no.3 (dust layer), d) arrow no.4 (dust layer).

581

582

583

584



585

586

587

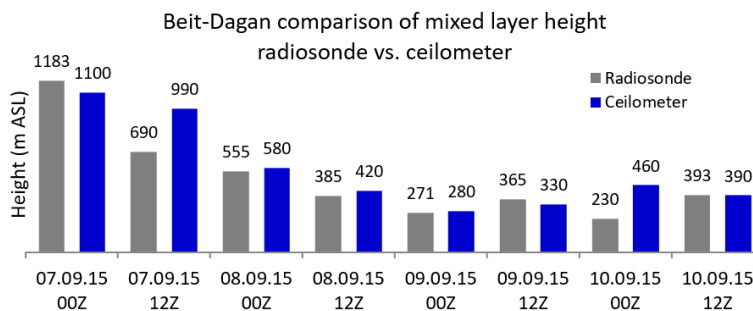
588

Figure 8. Hadera ceilometer attenuated backscatter plots for 07.09.15-10.09.15. y axis is the height up to 2000 m AGL, x axis is the time corrected from local time to UTC.

589 During the entire period of the dust event, both AERONET radiometers indicated growth of the coarse
590 particle fraction in the size distribution and high absorption in the UV (400nm) region (not shown). These
591 characteristics together with the satellite pictures indicated that the ceilometers tracked the dust entrance
592 and evolution.

593
594 Mamouri et al. (2016) performed a coarse estimation of the extinction based on visibility measurements
595 below 500m at three different locations in Cyprus. Here, the estimation was done by the Koschmieder
596 equation (Koschmieder 1924) based on the typical 40-50 sr LIDAR ratio for dust, visibility
597 measurements on the 8.9.15 of ~200 m (IMS reports). The estimated attenuated backscatter value
598 matched the order of magnitude measured using the Vaisala ceilometer CL31 scaling factor of 10^{-9} m^{-1}
599 sr^{-1} (not shown).

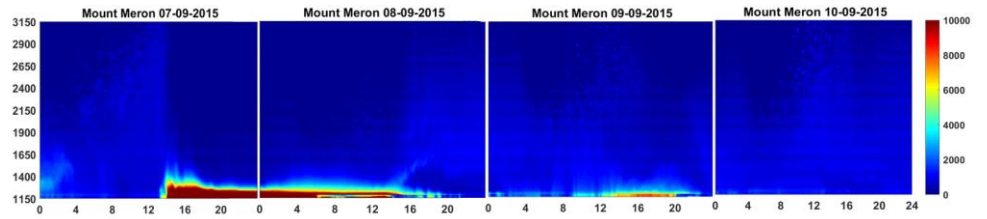
600 Ceilometers are not provided with an AOD upper limit value for signal reliability of the ceilometer
601 profiles. Therefore, the validity of the ceilometer measurements during high AOD levels (08.09.15-
602 10.09.15) was crucial. To verify ceilometer could measure correctly up 500 m AGL, MLH calculations
603 were related to the Beit Dagan radiosonde measurements which were comparable (Fig. 9).



608 **Figure 9.** The mixed layer height over central Israel (Beit Dagan site) between 07.09.15-10.09.15 at 00 UTC
609 and 12 UTC defined by adjacent radiosonde launches and ceilometer measurements, both in Beit Dagan site.

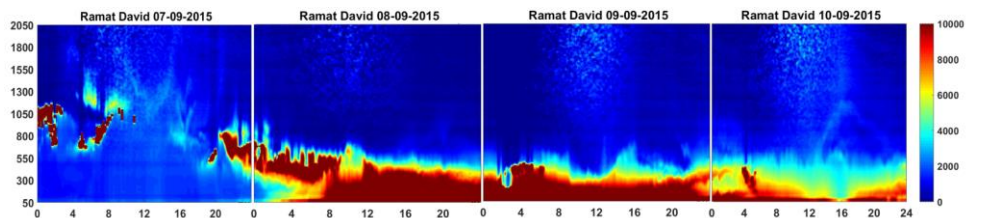
610
611
612 By the aforementioned tools, the dust event was analyzed as follows, providing consecutive ceilometer
613 plots between 07.09.15-10.09.15 (Fig. 8-16) from 8 sites (two for each region: north, shoreline, central
614 and southern Israel). Notice the plots are given in different scale in order to highlight the dust feature in
615 the different sites.

616
617



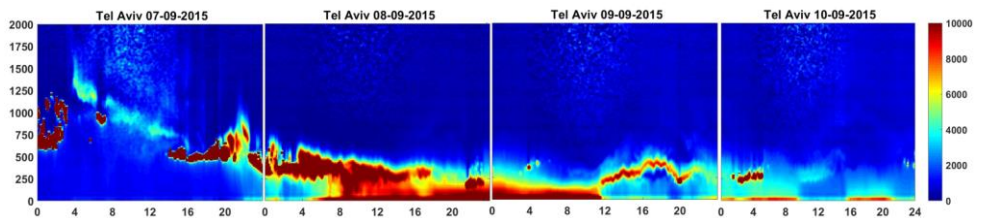
618
619
620
621

Figure 10. Same as Fig. 8 but for Mount Meron ceilometer site (Northern Israel, 1150 m ASL). The x axis is the time in UTC.



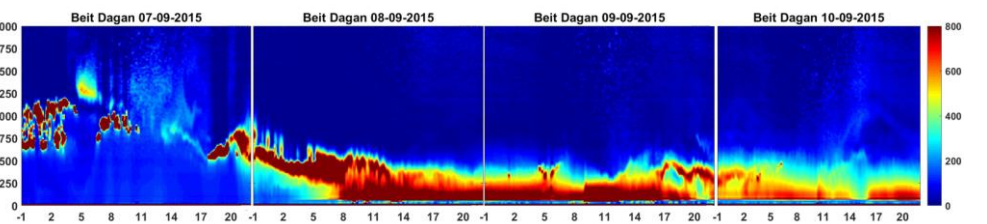
622
623
624
625

Figure 11. Same as Fig. 8 but for Ramat David ceilometer site (Northern Israel, 50 m ASL). The x axis is the time in UTC.



626
627
628
629
630

Figure 12. Same as Fig. 8 but for Tel Aviv ceilometer site (Israel shoreline, 5 m ASL). The x axis is the time in UTC.



631
632
633
634

Figure 13. Same as Fig. 8 but for Beit Dagan ceilometer site (Central Israel, 33 m ASL). The x axis is the measurement time corrected from local time to UTC.

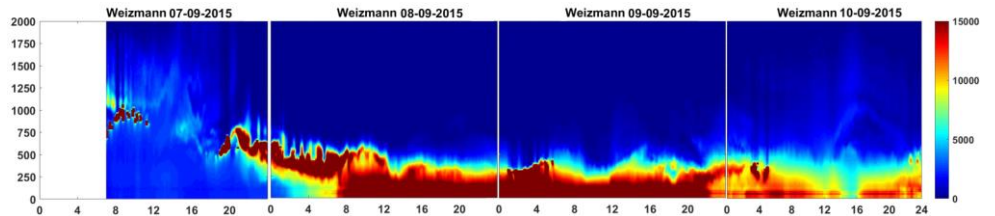


Figure 14. Same as Fig. 8 but for Weizmann ceilometer site in Rehovot (Central Israel, 60 m ASL). The x-axis is the time in UTC.

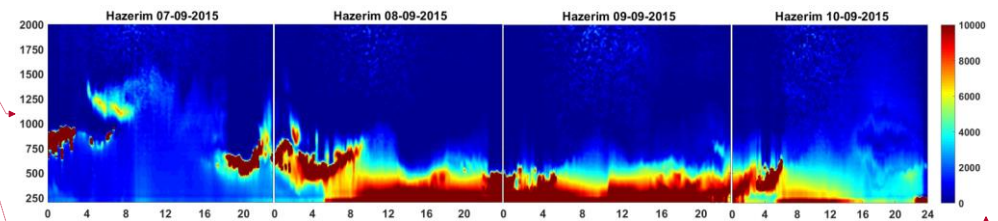


Figure 15. Same as Fig. 8 but for Hazerim ceilometer site (Southern Israel, 200 m ASL). The x-axis is the time in UTC.

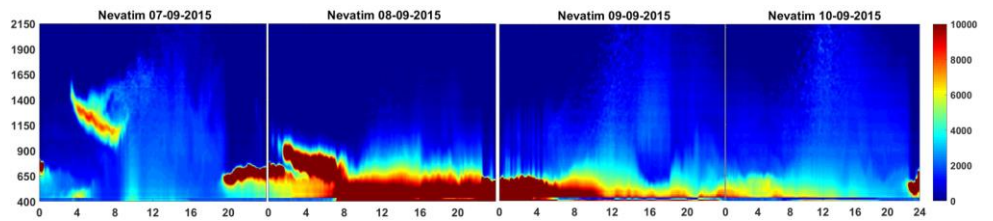


Figure 16. Same as Fig. 8 but for Nevatim ceilometer site (Southern Israel, 400 m ASL). The x-axis is the time in UTC.

Entrance of dust into Israel – 7 Sep 2015: Solomos et al. (2016) postulated that the dust storm was initially created as a dust front on the 06.09.15 as the result of a thermal low in Syria, north-east to Israel. This followed by a second front, generated by a thunder storm in northern Syria on the 07.09.15 giving rise to a fast running dust wall moving north-west then reaching Israel.

The AERONET (Fig. 6) and ceilometer plots (Fig. 8, 11-16) reveal that the first dust plume penetrated Israel at approximately 04:00 UTC at an elevated height of about 1500 m ASL. At this time, the ground station air monitoring 3-hourly PM10 concentration were still relatively low i.e., below 100 $\mu\text{g}/\text{m}^3$ (Fig. 5). The descending dust plume was measured by all ceilometers except for the Mount Meron ceilometer (Fig. 10). Indeed, the satellite pictures (Fig. 2 a, b) confirm that the first dust plume was fragmented and

658 had not reached the region of Mount Meron before 12 UTC. Fig. 2e shows the corresponding 925 mb
659 map including the deep RST intrusions to Syria and to Israel (Gasch et al., 2016).

660

661 The Mount Meron ceilometer, posted at 1150m ASL, captured the entrance of the second dust plume
662 descending to approximately 1000m ASL at around 13:00 UTC. By then, the PM10 3-h concentration
663 increased to $320 \mu\text{g}/\text{m}^3$ (5 times the average) in the southeastern monitoring station in Beer Sheva (270
664 m ASL; within the green zone, (Fig. 5) and $240 \mu\text{g}/\text{m}^3$ in one of the highest monitoring stations in
665 Jerusalem (800 m ASL; within the red zone, Fig. 4). Whereas in the shoreline, the PM10 concentrations
666 were still low (blue zone; Fig. 5). Next, we describe the decrease of aerosols aloft on mid-day.

667

668 ~~Noon decrease of aerosols aloft 7 Sep 2015:~~ The Israeli RS wind profiles on the 7.9.15 (not shown)
669 rotated from north east to the south east at 1000-2000 m altitudes ASL. The change in wind direction
670 disturbed the aforementioned dust plume descent, leading to dust dispersion over Israel. This is
671 illustrated by the significant decrease of the dust in the ceilometer measurements (clearly shown in Fig.
672 13-16 between 08-16 UTC) while the particle deposition (PM10) was rising (Fig. 5). The ICON-ART
673 model ran by Gasch et al., (2016) showed the dust plume split as it progressed to the south with one part
674 descended through the Golan Heights. And, the other stretched south along the Red Sea Trough, rotating
675 east as the wind altered along the trough margins. However, these model findings cannot explain the fact
676 that both the elevated plume and the ground measurements began simultaneously at about 04 UTC.

677

678 ~~2nd day of dust event 8 Sep 2015:~~ In the morning of 08.09.15, the AERONET in Sede Boker discloses
679 high AOD > 3 . Ceilometers across the country (except to the Mount Meron site) disclose high and
680 uneven vertically attenuated backscatter values of the dust in the atmosphere. This portioning occurred
681 at approximately 07-08 UTC (Fig. 8, 11-16), as the surface mixed layer breaks and the thermals build up
682 (Uzan and Alpert, 2012; Dayan et al., 2002). During the morning hours of the 08.09.15 the ground level
683 PM10 concentration increased up to $9,800 \mu\text{g}/\text{m}^3$ in Jerusalem which is 100 times over the 3 hourly
684 normal average. The highest levels were measured mainly in the elevated monitoring stations, located on
685 the high eastern strip of Israel (Fig. 5 and Table 4). These are represented only by the stations that were
686 available in the south center part of Israel (due to the lack of PM10 measurements in the north).
687 Radiosonde profiles show that the MLH subsides to 385 m ASL at 12 UTC (Fig. 9). The low MLH is
688 accompanied by the increase of PM10 concentrations in all 38 PM10 stations, with the highest hourly
689 value of $\sim 2,000 \mu\text{g}/\text{m}^3$ (Fig. 5).

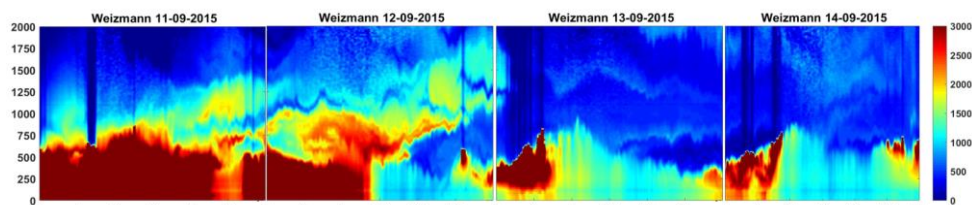
690

691 The aforementioned earlier studies of this dust event employing both models and satellite pictures, had
692 not clarified whether the descending plume was vertically mixed within the low MLH or rather merged
693 with a dust wall that reached Israel. The process of the plume mixing can be verified from the vertical
694 structures in Fig. 8-16 as follows. The ceilometers show that on the morning of the 08.09.15 (4-8 UTC)
695 the dust profiles appeared as two separate dust layers at near ground and aloft (~500 m ASL) that have
696 combined later in the morning (7-8 UTC).

697
698 3rd day of dust event – 9 Sep 2015: On the 09.09.15 a shallow MLH (Fig. 9) maintained the high PM10
699 concentrations e.g. 3,400 $\mu\text{g}/\text{m}^3$ in Hadera – 40 times over the average (Fig. 18) and high AOD > 3 (Fig
700 6). At approximately 11 UTC, the shoreline ceilometers (Tel Aviv and Hadera) revealed a discontinuous
701 structure of a dust arc at (Fig. 8,12) which was less evident in the inland ceilometers in Beit Dagan (Fig.
702 13) and Rehovot (Fig. 14). We presume the dust "arc" is a result of a dilution generated by the sea breeze
703 front (SBF). The SBF entered at about 11 UTC (evaluated by the Tel Aviv onshore meteorological
704 station, not shown) as limited radiative transmitted through the dense dust layer that had been covering
705 Israel. Furthermore, prevailing northerly winds on the 09.09.15 restrained the SBF progress inland (not
706 shown).

707
708 4th day of dust event – 10 Sep 2015: From 10.9.15 the ground level PM10 concentration decreased
709 considerably (Fig. 5). Respectively, the ceilometers (Fig. 8-16) and satellite pictures (Fig. 1) show a
710 decrease of the dust loads. Although ceilometer plots of the 10.09.15 reveal total clearance of the dust
711 plume, the AERONET measurements from 14.09.15 show the AOD did not resume to the lowest values,
712 prior to the dust storm. An example is given of the dust load dispersion between 11.09.15-14.09.15 in
713 Fig. 17 from the Weizmann Rehovot ceilometer.

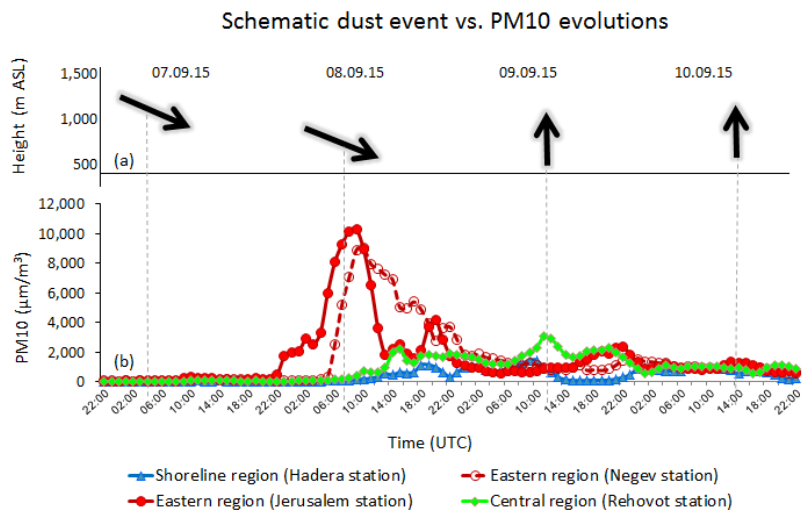
714
715
716



717 Figure 17. Weizmann ceilometer site in Rehovot (central Israel, 60 m AGL) attenuated backscatter plots
718 between 11.09.15 – 14.09.15. Y axis – heights up to 2000 m AGL, X axis – time in UTC.
719
720

721 A Schematic evolution of the dust event is given in Fig. 18 as a dust layer of ~250 m (Fig 11-13, 15-
 722 16) penetrated Israel at the height of ~1000-1500 m on 07.09.15-4 UTC. On the 08.09.17 the dust
 723 plume reached ground level height at about 08 UTC in the northern region (Fig 11, Ramat David
 724 ceilometer), central region (Fig 13-14, Beit Dagan and Weizmann ceilometers) and shoreline strip (Fig
 725 8 and 12, Hadera and Tel Aviv ceilometers). In the southern region (Hazerim and Nevatim ceilometers)
 726 the dust plume reached ground level earlier, beginning at 05 UTC. Correspondingly, an increase in
 727 PM10 concentration from the eastern region (Fig. 18) was measured by monitoring stations which are
 728 nearest to the southern ceilometers. The dissipation of the dust plume on 09.09.15-10.09.15 was
 729 revealed both by the dust features from the ceilometers plots (Fig. 8-16) and the decrease in PM10
 730 concentration from adjacent monitoring station.

731
 732



733
 734

735 **Figure 18.** A schematic illustration of the dust storm evolution as discovered by the ceilometer plots (a, top
 736 panel), compared to the PM10 concentration (b, bottom panel) measured on ground level from four representative
 737 air monitoring stations (Hadera, Negev, Jerusalem and Rehovot) for the four regions (Shoreline, south, east and
 738 central, respectively, Fig. 5). The representative stations were chosen adjacent to corresponding ceilometer sites
 739 (Hadera, Nevatim, Beit Dagan and Rehovot, respectively, Fig. 5)

740
 741
 742
 743
 744
 745
 746

747 **4. Conclusions and discussion**

748

749 Former research of the September 2015 dust event focused primarily on the synoptic evolution, outlined,
750 the meteorological features and analyzed the limitations of the models to forecast such a dominant and
751 unique event (Ginoux and Pu, 2016; Solomos et al, 2016; Parolari et al, 2016; Gasch et al, 2016; Jasmin,
752 2016; Mamouri et al, 2016). They had explained the dust storm progression by remote sensing means
753 either looking from ground up (AERONET, PM10) or from space down (satellite).

754

755 In due to power failure. In this study, for the first time, such an event is vertically analyzed using an array
756 of ceilometers deployed across Israel. The ceilometer array enabled us to improve the spatial the temporal
757 evaluation and evolution of the September 2015 dust storm over Israel we used AERONET Level 2.0
758 data (cloud screened and quality assured for instrument calibration) for AOD at 500 nm and the Ångstrom
759 Exponent defined by 440-870 nm.

760

761

762 **2.5 Global, direct and diffuse solar radiation measurements**

763

764 Global radiation measured in by IMS in 22 sites (Table. 6) by instrument type Kipp & Zonen pyranometer
765 CMP-11. Integrated solar radiation (W m⁻²) from 300 to 3000 nm is produced every 10 min. Diffuse and
766 direct radiation also measured in Beit Dagan (coastal region, 31 m ASL) and Beer Sheva (southern
767 region, 71 m ASL). For diffuse radiation, a ring is installed over the pyranometer to shade direct solar
768 radiation. Direct radiation is measured by a sun tracker pyrliometer.

769

770

771 **2.6 Satellite imagery**

772

773 **2.6.1 SEVIRI (MSG satellite)**

774

775 Meteosat Second Generation (MSG) is a new series of European geostationary satellites operated by
776 EUMETSAT (European Organization for the Exploitation of Meteorological Satellites). On board the
777 MSG is a 12-channel Spinning Enhanced Visible and Infrared Imager (SEVIRI) (Roebeling et al., 2006).
778 The combination of red, blue and green (RGB) channels (12-10.8 μm , green:10.8-8.7 μm , blue:10.8 μm ,
779 respectively) produce imagery of dust in pink or magenta, dry land in pale blue at daytime and pale green

780 at nighttime, thick high-level clouds in red-brown tones and thin high-level clouds nearly black
781 (<http://oiswww.eumetsat.int/>). Access to EUMETSAT imagery is given in
782 <https://www.eumetsat.int/website/home/Images/RealTimeImages/index.html>. Several studies (Romano
783 et al., 2013; Bennouna et al., 2009; Jolivet et al., 2008) compared AOD from MGS SEVIRI and
784 AERONET measurements clarified the uncertainty of MSG SEVIRI AOD decreases as AOD rises. For
785 continental aerosol type, errors do not exceed 10 % in viewing zenith angles between 20° and 50°.
786 probable for the study area considered here. Overall, the MSG SEVIRI AOD uncertainty it is expected
787 to be under 15% (Mei et al, 2012). North Africa Sand storm survey (NASCube: [lille1.fr](http://nascube.univ-</u>
788 <u><a href=)) obtains AOD by temperature anomalies of SEVIRI RGB by the difference in emissivity of dust
789 and desert surfaces during daytime.

790
791
792
793
794

795 **2.6.2 MODIS (Terra and Aqua satellites)**

796
797
798
799
800
801
802
803
804
805
806

807 **2.6.3 CALIOP (CALIPSO satellite)**

808
809
810
811
812
813

The MODerate resolution Imaging Spectrometer (MODIS) instrument flies aboard the Earth Observation
System's (EOS) Terra and Aqua polar-orbiting satellites, with Terra on a descending orbit (southward)
over the equator about 10:30 local sun time, and Aqua on an ascending orbit (northward) over the equator
about 13:30 local sun time. MODIS performs measurements by 36 channels between 412 to 14200 nm
whereas the aerosol retrieval makes use of seven channels (646, 855, 466, 553, 1243, 1632 and 2119 nm
central wavelength), and a number of other wavelength bands associated with screening procedures. As
land signals (AERONET) and the atmospheric signals are comparable at ~ 550 nm, errors of 0.01 in
assumed surface reflectance will lead to errors on the order of 0.1 in AOD retrieval (Remer et al., 2006).

The Cloud-Aerosol Lidar with Orthogonal Polarization (CALIOP) is a two-wavelength polarization lidar
(1064 and 532nm) that performs global profiling of aerosols and clouds in the troposphere and lower
stratosphere. CALIOP is the primary instrument on the Cloud-Aerosol Lidar and Infrared Pathfinder
Satellite Observations (CALIPSO) satellite. CALIOP is required to accurately measure signal returns
from the aerosol-free region between 30 and 35 km as well as the strongest cloud returns. Samples

814 acquired below 40 km for the 532-nm channel and below 30 km for the 1064-nm channel are downlinked
815 as profile data. Data used here was based on level 2 version 4-10 CALIPSO product, spatial resolution
816 of 5 km (20N-50N, 20E-50E) and vertical resolution of 60 m (limited up to 6 km).

819 **3. Results and discussion**

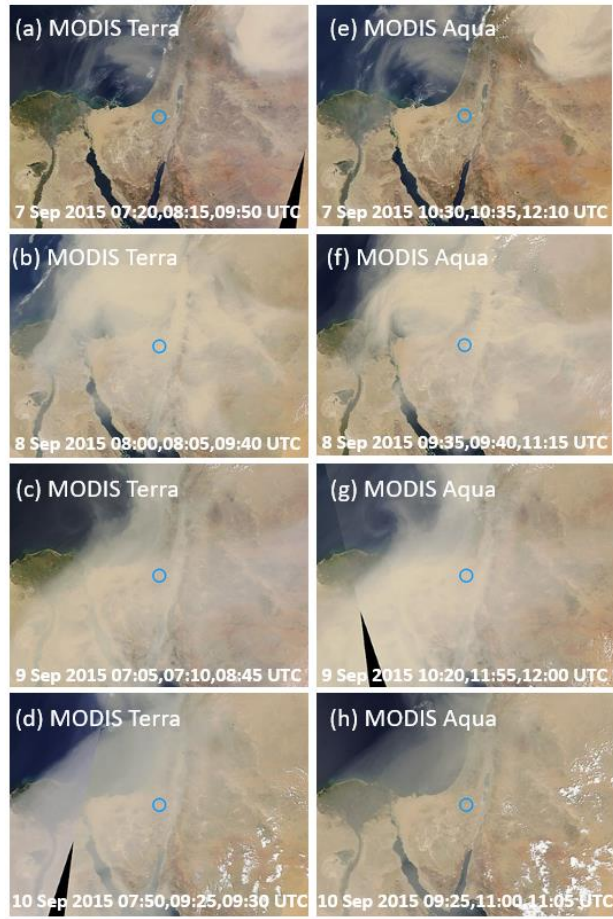
820
821 The following description of the dust event will proceed chronologically from 7 to 10 September and
822 include main findings of the instruments (Sect. 2). The order of the instruments described follow the most
823 interesting features revealed, not necessarily in the same order for each day.

824
825 On 7 September, images from MODIS Aqua (Fig. 4a) and MODIS Terra (Fig. 4e) taken between
826 07:20-12:10 UTC show that the dust plume progressed from northeast in a near-circular motion over the
827 Mediterranean Sea. The penetration of the dust plume to Israel was indicated at ~ 05 UTC by an increase
828 in AOD along a decrease in the Angström exponent (Fig. 5) from AERONET Sede Boker site. The
829 relationship between the Angström exponent decrease and the mineral dust was pointed out by Mamouri
830 et al., (2016). They studied the dust layer particle linear depolarization by an EARLINET lidar stationed
831 in Limassol Cyprus and concluded that the linear depolarization ratio of 0.25-0.32 on 7,10 September,
832 indicated the dominance of the mineral dust. In addition, an increase in the PM concentration started at
833 ~ 05 UTC (not shown) reaching the highest hourly values of 107 $\mu\text{g m}^{-3}$ PM_{2.5} (Table 5) and 491 $\mu\text{g m}^{-3}$
834 PM₁₀ (Table 6) only in the Jerusalem elevated sites and only at 22 UTC. This 17-hour gap is shown by
835 the ceilometers' plots (Fig. 6-12) of a downward motion of the dust plume from ~ 04 UTC in all
836 measuring sites except for the elevated Mount Meron site (1150 m ASL, Fig. 13). Following Gasch et al
837 (2017) cold pool outflows concept, the exception of Mount Meron site is supported by the MSG-SEVIRI
838 picture (Fig. 14) showing that the first dust plume was fragmented (Fig.14, red arrow) and the second
839 dust plume (Fig.14, black arrow) had not passed over Israel before 12 UTC.

840
841 The full picture of what happened on the 7 September can be further obtained from the MSG-
842 SEVIRI picture at 12 UTC that shows AOD to be still under 1 in most parts of Israel (Fig. 15). At the
843 same time, Beit Dagan radiosonde profiles show the MLH was still high (700 m ASL, Fig. 16). And,
844 ceilometers' profiles at 23 UTC (Fig. 17 a) show indications of typical cloud presence from 400 m ASL
845 in the shoreline site (Tel Aviv, 5 m ASL) and up to ~700 m ASL in the elevated southern site (Nevatim,
846 400 m ASL). Clouds are identified by the peak shape of the profiles (Uzan et al, 2016) and the high
847 attenuated backscatter of $10^{-1} \text{ m}^{-1} \text{ sr}^{-1}$ which in this case is 4 orders of magnitude higher than the

848 attenuated backscatter of the dust plume (shown in Fig 17 b-c). In spite of the still high MLH and the
849 cloud presence, the solar radiation measurements clearly indicates the significance of the dust plume
850 effect through the decrease of the daily direct radiation along with an increase of the diffuse radiation
851 (Fig. 18, see 7 September daily variation) measured both in central Israel (Beit Dagan) and southern
852 Israel (Beer Sheva).

853
854
855
856
857

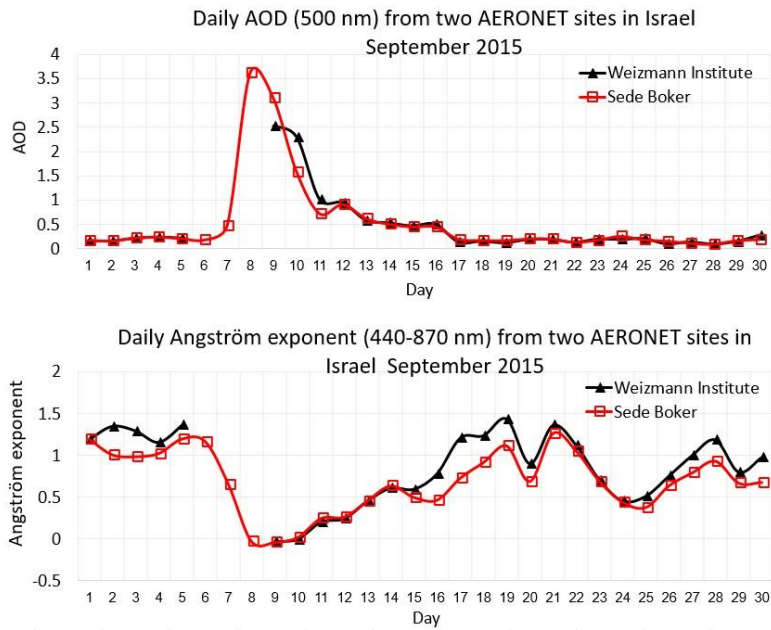


858

Formatted: Font: 12 pt, Font color: Auto

859
860
861
862
863
864
865
866
867
868
869
870
871

Figure 4. Pictures from MODIS terra (a-d) and MODIS Aqua (e-h). The date and time of overpass are indicated on each figure. Blue circle indicating the AERONET Sede Boker site. Source: <https://aeronet.gsfc.nasa.gov>.

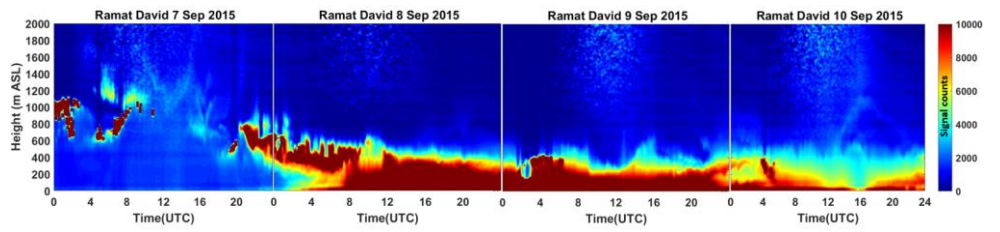


872
873
874
875
876
877

Formatted: Font: 12 pt, Font color: Auto

Figure 5. September 2015 daily average of AOD (top panel) and Angström exponent (bottom panel) from two AERONET sites in Israel (Sede Boker and Weizmann, see Fig.3). The Weizmann AERONET did not operate on 6-8 September due to power failure.

878
879
880
881
882
883
884
885
886
887

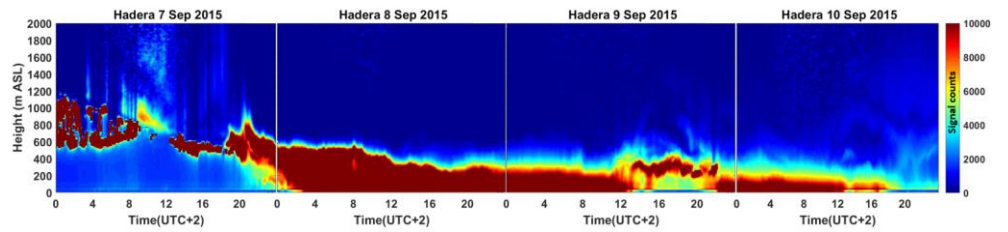


888

Formatted: Font: 12 pt, Font color: Auto

889
890
891

Figure 6. Ramat David ceilometer signal counts plots for 7-9 September 2015. Y-axis is the height up to 2000 m ASL, X-axis is the time in UTC, signal count scale range between 0-10,000.

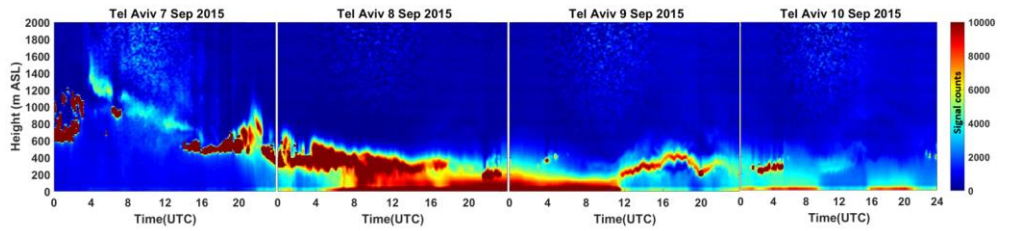


892

Formatted: Font: 12 pt, Font color: Auto

893
894
895
896

Figure 7. Hadera ceilometer signal counts plots for 7-9 September 2015. Y-axis is the height from site deployment to 2000 m ASL, X-axis is the time in LST (UTC+2), signal count scale range between 0-10,000.

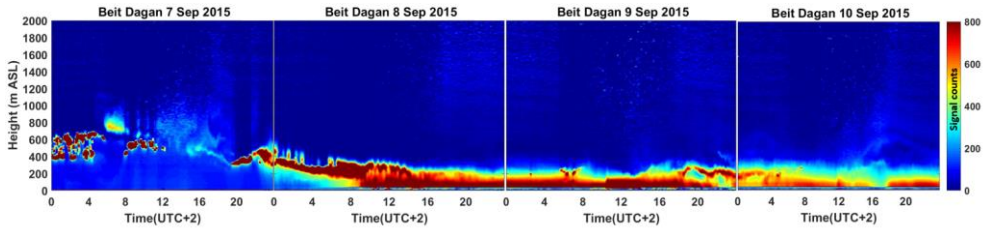


897

898 Figure 8. Tel Aviv ceilometer signal counts plots for 7-9 September 2015. Y-axis is the height from
 899 site deployment to 2000 m ASL, X-axis is the time in UTC, signal count scale range between 0-
 900 10,000.

901

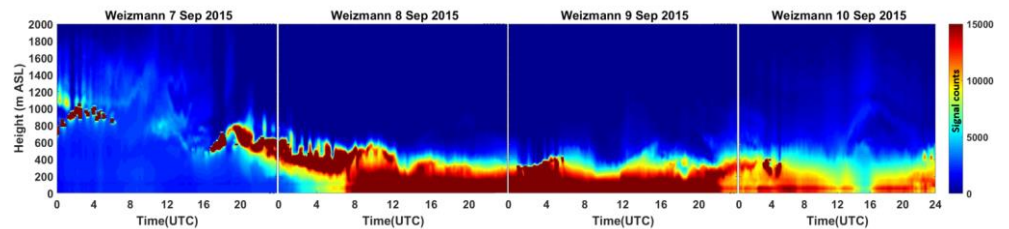
902



903

904 Figure 9. Beit Dagan ceilometer signal counts plots for 7-9 September 2015. Y-axis is the height from
 905 site deployment to 2000 m ASL, X-axis is in LST (UTC+2), signal count scale range between 0-800.

906



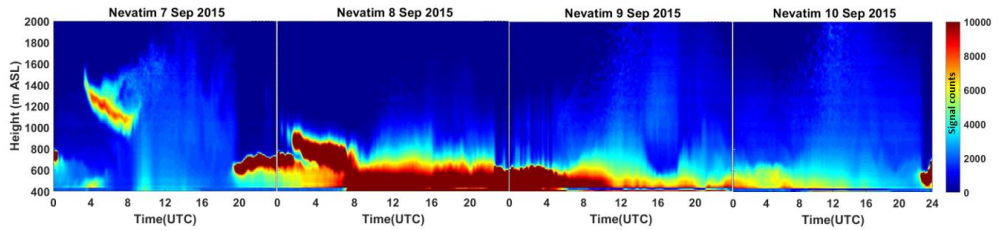
907

908 Figure 10. Weizmann ceilometer signal counts plots for 7-9 September 2015. Y-axis is the height from
 909 site deployment to 2000 m ASL, X-axis is in UTC, signal count scale range between 0-15,000.

910

911

Formatted: Font: 12 pt, Font color: Auto



912

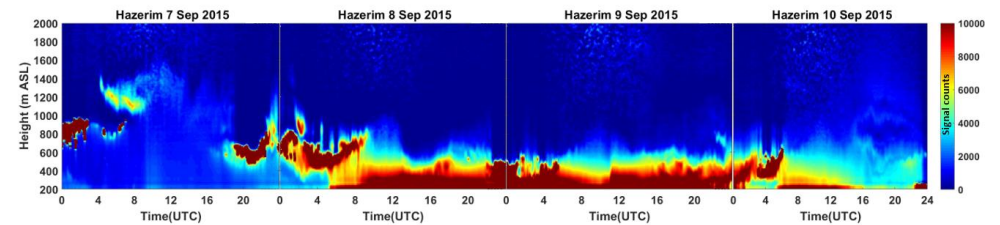
913 Figure 11. Nevatim ceilometer signal counts plots for 7-9 September 2015. Y-axis is the height from
 914 site deployment to 2000 m ASL, X-axis is the time in UTC, signal count scale range between 0-
 915 10,000.

916

917

918

919

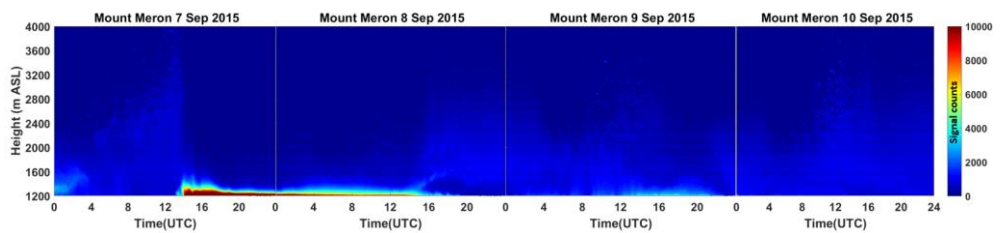


920

921 Figure 12. Hazerim ceilometer signal counts plots for 7-9 September 2015. Y-axis is the height from
 922 site deployment to 2000 m ASL, X-axis is the time in UTC, signal count scale range between 0-
 923 10,000.

924

925



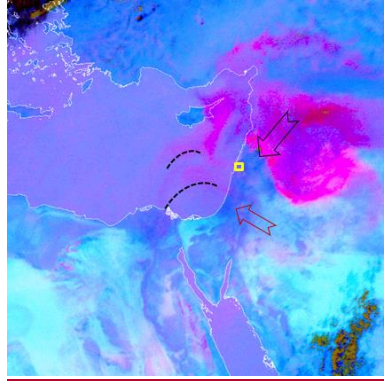
926

927 Figure 13. Mount Meron ceilometer signal counts plots for 7-9 September 2015. Y-axis is the height
 928 from site deployment to 2000 m ASL, X-axis is the time in UTC, signal count scale range between 0-
 929 10,000.

930

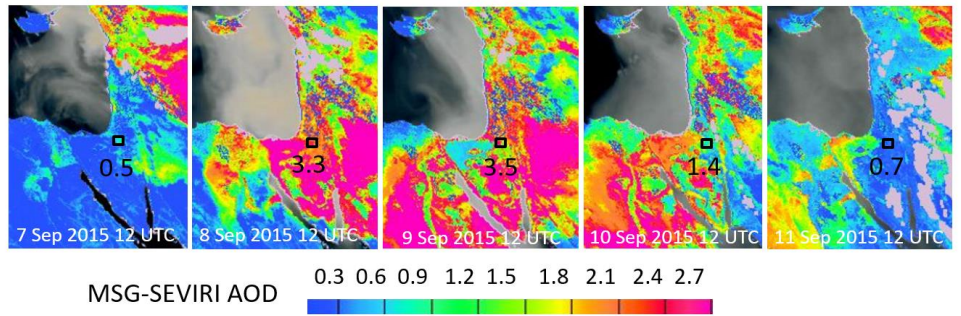
931

932



933

934 Figure 14. Picture from MSG-SEVIRI satellite of the dust RGB component (dust appears in pink
 935 colors) at 12 UTC 7 September 2015 with indications of Mount Meron ceilometer site (yellow
 936 square, Lon 33.0°, Lat 35.4°) and the dust plumes progression from east to west (red arrow and
 937 dashed lines) and from the northeast to southwest (black arrow).

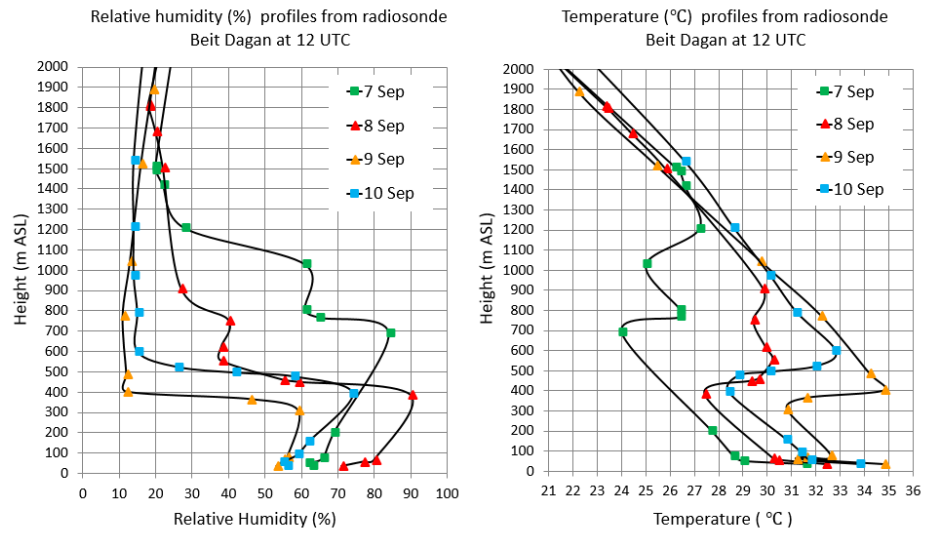


938

939 Figure 15. Aerosol Optical Depth (AOD) at 12 UTC 7-11 September 2015 analyzed by NAScube
 940 (Université de Lille) based on imagery from the MSG-SEVIRI satellite (by a combination of the SEVIRI
 941 IR8.7, IR10.8 and IR12.0 channels). The map includes indication of the Sede Boker AERONET site
 942 (black square) and its AOD value at 12 UTC.

944

945



946

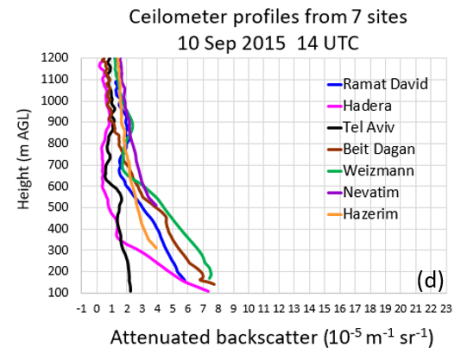
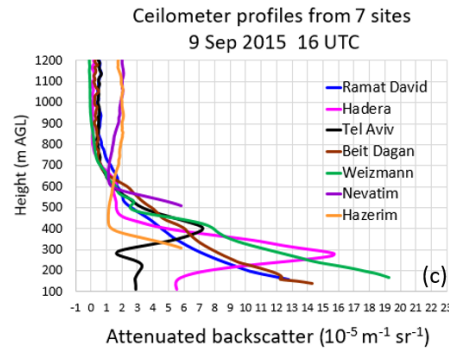
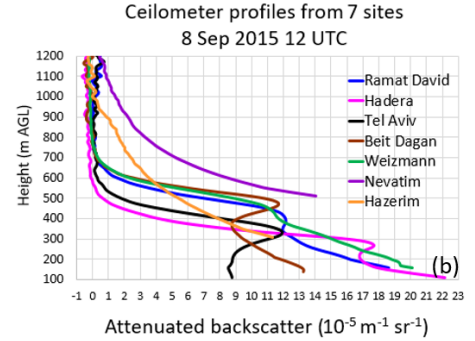
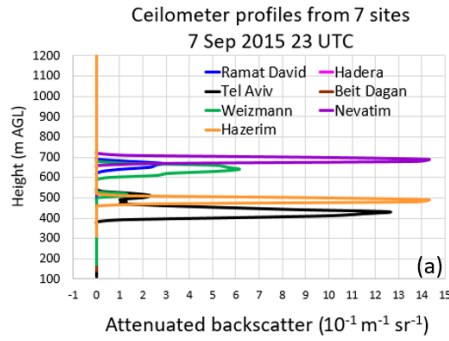
Formatted: Font: 12 pt, Font color: Auto

947

Figure 16. Radiosonde Beit Dagan profiles at 12 UTC between 7-10 September 2015 of relative humidity (left panel) and temperature (right panel).

948

949



950

951

952

953

954

955

956

957

958

959

960

Figure 17. Ceilometer attenuated backscatter profiles from 7 sites (Ramat David, Hadera, Tel Aviv, Beit Dagan, Weizmann, Nevatim and Hazerim, Fig. 3) at 23 UTC 7 Sep 2015 (a), 8 September 2015 at 12 UTC (b), 9 September 2015 at 16 UTC (c) and 10 September 2015 at 14 UTC (d). Notice each profile begins relative to the height of its' measuring site (ASL) including a deletion of the first 100 m AGL due to inaccuracies in the first range gates of the CL31 ceilometers (for details see Sect. 2.1). Fig (a) shows cloud detection therefore it has a different scale ($10^{-1} \text{ m}^{-1} \text{ sr}^{-1}$) and a different x-axis range.

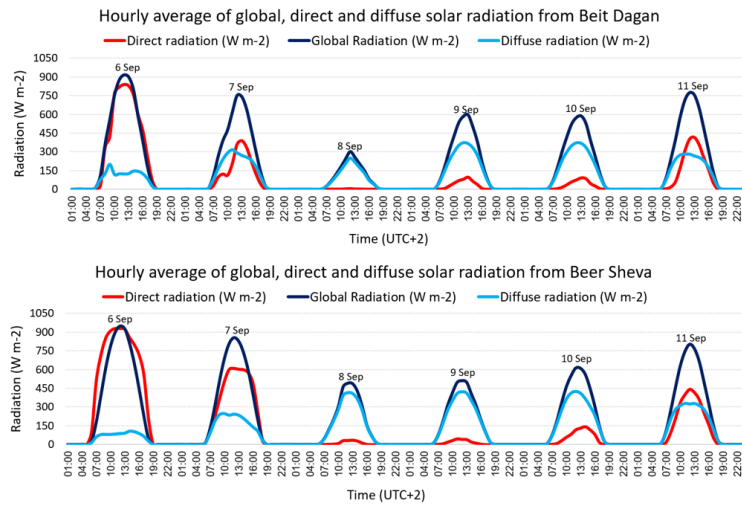


Figure 18. Hourly average of global, direct and diffuse solar radiation between 6-11 September 2015 from Beit Dagan and Beer Sheva.

961
962
963
964
965
966
967
968
969
970
971
972
973
974
975
976
977
978
979
980
981
982

The main phase (the peak) of the dust storm occurred on 8 September. Images from MODIS Aqua (Fig. 4b) and MODIS Terra (Fig. 4f) taken between 08:00-11:15 UTC show the dust storm prevalence over Israel. Ceilometers' plots detect the descending motion of the dust plume reached ground level at ~08 UTC (Fig. 6-12). Simultaneously, Sede Boker AERONET AOD measurements increased up to ~4 along with a negative Angström exponent (not shown).

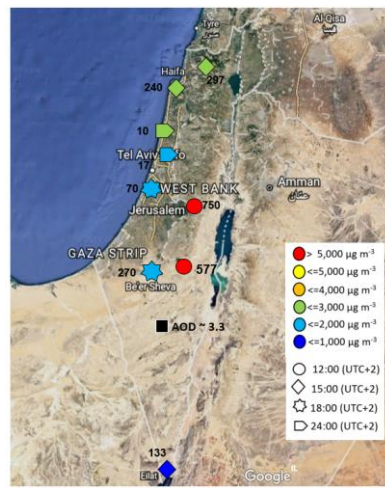
An hour later, at ~09 UTC, extreme maximum PM hourly values were measured in the elevated sites of Jerusalem Safra ($10,280 \mu\text{g m}^{-3}$ PM₁₀) and Jerusalem Bar Ilan ($3,063 \mu\text{g m}^{-3}$ PM_{2.5}). Whereby, in the coast and the lower northern regions, maximum PM values were measured only 14 hours later at ~23 UTC and were much lower (up to $3,459 \mu\text{g m}^{-3}$ PM₁₀ and $470 \mu\text{g m}^{-3}$ PM_{2.5}, see Tables 5-6). Fig. 19 illustrates the spatio-temporal variation of the PM₁₀ extreme values, beginning at ~12 UTC in the elevated Jerusalem sites and ending at midnight in the shoreline.

Ceilometer plots from Tel Aviv, Hadera (with plot range of 0-15,000, not shown here), Beit Dagan and Weizmann, reveal a two-layer shape, (beneath and above ~300 m ASL) starting from ~08 UTC. This two-layer shape later on combined into one dense layer. This pattern may explain the spatial variation and time delay between the extreme PM measurements in the elevated vs. lower sites.

983 Referring to satellite imagery on 8 September, MSG-SEVIRI at 12 UTC (Fig. 15) underestimated
984 AOD to be 2.7 while Sede Boker AERONET measured a higher value of 3.3. Furthermore, MODIS
985 images (Fig. 4a, 4b) show a dominant dust plume over Israel, while solar global radiation measurements
986 (Fig.20a) show significant spatial variations in the reduction of the global radiation measured in the
987 different regions. Minimum values down to 200 W m^{-2} were measured mainly in northern Israel. This
988 may infer the complex behavior of the dust dispersion in contrary to satellite imagery of a prevailing dust
989 storm over Israel. Additionally, in spite the extreme PM10 values of $9,031 \mu\text{g m}^{-3}$ measured in the
990 elevated southern site (Negev Mizrahi 577 m ASL, Table 6), the maximum global radiation in southern
991 Israel was still relatively high ($\sim 500 \text{ W m}^{-2}$).

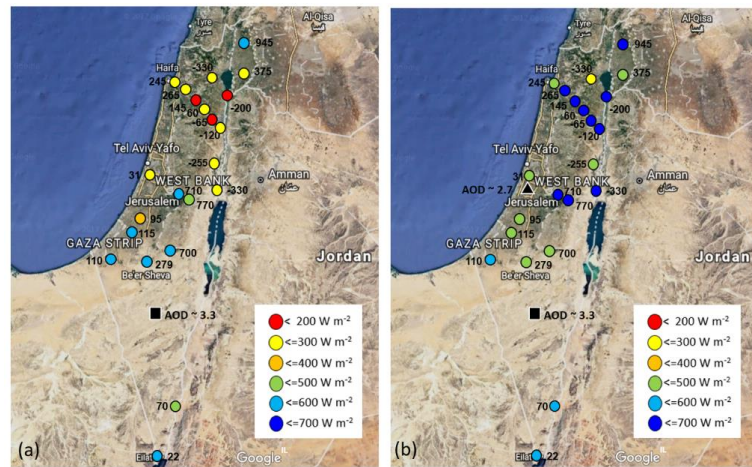
993 Overall, 8 September shows the highest PM concentrations and the lowest solar radiation levels
994 for this dust storm event. The solar radiation was composed mainly of diffuse radiation (Fig.18)
995 emphasizing the immense atmospheric dust loads preventing direct insolation. Surprisingly, the low solar
996 radiation was still able to warm the ground and generate a late and weak sea breeze front (not shown).
997 We assume the insufficient ground heating generated thermals that were too weak to create and inflate a
998 MLH. Therefore, we assume the low MLH (300 m ASL) revealed by the Beit Dagan profiles from 8
999 September (Fig.16) which may indicate the dust plume base height.

1000
1001
1002
1003



1004

1005 Figure 19. A map of PM10 maximum hourly concentration from 9 sites measured at 10 UTC on
 1006 8 September 2015. The map includes indications of the time of measurement (symbol shape),
 1007 concentration range (symbol color), height of measurement site (numbers in black) and
 1008 AERONET AOD from Sede Boker site.
 1009



1010 Figure 20. A map of maximum global solar radiation from 22 sites measured at 10 UTC (midday)
 1011 on 8 September 2015 (a) and 9 September 2015 (b). The map includes indications of radiation
 1012 range (see legend), height of measurement site (numbers in black) and AERONET AOD from
 1013 Sede Boker site (black square) and Weizmann site (black triangle). On 8 September Weizmann
 1014 AERONET did not operate.
 1015

1016 .

1017

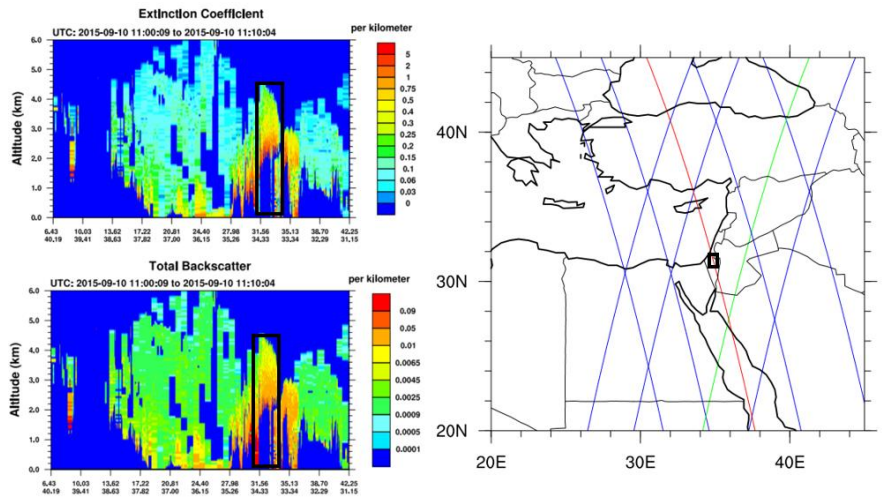
1018 On 9 September, MODIS images (Fig.4c and 4g) taken between 07:05-12:00 UTC show the dust
 1019 plume progression southward to Egypt (Fig. 4), indicated by Sede Boker AERONET AOD >3 and a
 1020 negative Angström exponent (Fig. 5). Again, an underestimation of AOD MSG-SEVIRI at 12 UTC
 1021 shows lower AOD~ 2.7 compared to Sede Boker AERONET AOD ~ 3.5 (Fig.15). In contrary to the
 1022 high AOD measurements, and the descend of the MLH down to ~ 350 m ASL (Fig.16), PM values did
 1023 not crease but rather decrease below $900 \mu\text{g m}^{-3}$ PM2.5 (Table 5) and $4050 \mu\text{g m}^{-3}$ PM10 (Table 6). The
 1024 drop in PM concentration gave rise to an increase of solar radiation of up to 400 W m^{-2} (Fig. 20 b). An
 1025 increase in solar radiation enables significant ground heating to temperature values measured prior to the
 1026 initiation of the dust storm (not shown). Thus, allowing generation of thermals and the creation of the
 1027 sea breeze cycle which eventually produced an arc shape dust ascent visible in mainly in Tel Aviv and

1028 Hadera coastal ceilometers beginning at ~ 12 UTC (Fig.7-8). Interestingly on 9 September, compared to
1029 the peak of the dust storm on the day before, we do not see a significant difference in solar radiation in
1030 southern Israel, which continued to be relatively high ~500 W m⁻² (Fig. 20b).

1031
1032 On 10 September, MODIS pictures from 7:50 -11:05 UTC (Fig. 4d and 4h) show the dust plume
1033 over Israel transported southeast from Syria-Iraq to Sinai-Egypt. The CALIPSO single overpass Israel at
1034 11:00-11:10 UTC revealed a dust layer between 2-4 km ASL (Fig.21). This corresponds with the
1035 EARLINET lidar measurements in Limassol, Cyprus (Mamouri et al., 2016) detecting a dust plume
1036 between 1-3 km ASL. We assume the CALIOP lidar did not produce data beneath 2 km ASL due to total
1037 attenuation. Fortunately, the ceilometers complement the dust profile (beneath 1~ 1 km ASL) showing a
1038 reduction both in signal counts (Fig. 6-12) and in attenuated backscatter profiles (Fig.17d) pointing out
1039 a reduction in atmospheric dust loads. AOD from MSG-SEVIRI and Sede Boker AEONET show a
1040 decrease down to (~1.5) and a low Angström exponent of ~0.5 indicating prevalence of mineral dust.

1041
1042 Furthermore, a profound reduction in PM values, down to a third of the values from the day before
1043 (Table 6), was measured mainly in southern Israel. Therefore, an increase in direct radiation (therefore
1044 an increase in global radiation as well) was measured in southern site as well (Fig.18). The reduction of
1045 dust loads may also be denoted by the orange background color of the photograph on the 8 September
1046 (Fig.1b) compared to the grey background visible on 10 September (Fig.1c). As the dust storm dissipated
1047 cloud formation was visible from at ~4 UTC by ceilometers plots from Ramat David (Fig.6), Tel Aviv
1048 (Fig.8), Weizmann (Fig.10) and Hazerim (Fig.11) (indicated by brown spots and evaluated by ceilometer
1049 profiles -not shown), otherwise not evident by MODIS imagery (Fig 4d, 4h).

1050
1051
1052
1053
1054
1055



1078 **Conclusions** Beginning from the dust plume penetration to Israel from north-east (~1-1.5 km AGL)
1079 on the 07.09.15 reaching ground level height on the 08.09.15, creating a very low (beneath 500 m AGL)
1080 and stable MLH. As a result, extreme AOD values comprised mainly of mineral dust (Fig. 6), and high
1081 ground level PM10 concentrations were measured across Israel (Fig. 5). The highest values PM10 (100
1082 times over the 3 hourly average) were measured on the 08.09.15 mainly in the elevated monitoring
1083 stations situated in the eastern strip of Israel. The clearance of the dust plume began in the shoreline on
1084 the 09.09.15 at approximately 11 UTC (Fig. 8) and continued on for several days until low AOD and
1085 high Angström values (indicating low content of mineral dust) finally resumed. During the clearing
1086 period, there were temporal and vertical differences in the dust plume evolution between the onshore and
1087 inland stations. These were attributed to the unusual late and weak sea breeze penetration due to the
1088 heavily opaque atmosphere. Detailed analysis of the various station vertical structure revealed the
1089 turbulent nature of the dust penetration attributed to the height and distance from seashore. These details
1090 were not revealed by the high resolution scale models.

1091
1092 The dust event measured in Cyprus (Mamouri et al., 2016) by an intensified LIDAR showed a structure
1093 of two dust layers, 1.5 and 4 km AGL. The complicated nature of the dust evolution and its creation,
1094 made it difficult to state if the same double layer structure reached Israel (and not measured by the CL31
1095 ceilometers due to high SNR above 2 km) or was it partially carried by the different prevailing wind
1096 regimes over Israel and Cyprus (therefore, not measured even in the elevated Mount Meron site, 1150 m
1097 AGL).

1098
1099 Finally, this research emphasized the importance of LIDAR networks close to dust source areas such as
1100 the EM as a tool to improve forecast details and validate forecast models.

1101 4.

1102
1103 A very severe dust storm struck the EM on September 2015. Previous investigations including in
1104 situ and remote sensing measurements and models discussed the initiation of the dust storm in the Syrian-
1105 Iraqi border, the limitations of the models to forecast this unique event, and several aspects of its transport
1106 over the EM. The analysis concentrated mainly on the upper level of the atmosphere and analyzed
1107 specific time segments of the dust storm period. The benefit here is the provision of vertical profiles of
1108 the dust in the lower part of the troposphere and the continuous measurements at 8 sites in Israel.

1109

1110 This study confirmed that the dust storm entered Israel on 7 September and showed the gradual
1111 downfall of the dust plume from ~1000m ASL on 7 September down to ~400 m ASL on 8 September.
1112 The detailed ceilometer profiles and auxiliary instruments enabled to separate the dust storm into two
1113 dust layers (beneath and above 1 km) and show a complex dispersion which would have been challenging
1114 for meso-scale model simulations. As the dust plume descended towards ground level on 8 September,
1115 PM concentration increased in the elevated stations (up to 10,280 $\mu\text{g m}^{-3}$ PM10) and radiation decreased
1116 down to $\sim 200 \text{ W m}^{-2}$ mainly in the northern region. On 9 September as the dust plume diluted, in spite
1117 of the high AOD >3 , the global radiation (mainly comprised of diffuse radiation) increased, thus enabling
1118 the ground heating and the creation of a late sea breeze circulation (~ 12 UTC) visible as dust arcs near
1119 the coast sites (Tel Aviv, Hadera and Beit Dagan). On 10 September, the dust plume motion continued
1120 southwest to Egypt, with indication of a dust layer between 2-4 km measured by CALIPSO overpass.
1121 The progress of the dust storm from the Syria-Iraqi border (origin) southwest to Egypt over Israel,
1122 continued in two levels. The lower level (up to 1 km ASL) dissipated at 13 September while the level
1123 aloft (above 1 km ASL) was observed until 17 September.

1124

Formatted: Font: 12 pt, Font color: Auto

Formatted: Normal

Formatted: Font: 18 pt, Font color: Auto

Formatted: Font color: Auto

Formatted: Font color: Auto

5. Data availability

1128 PM10 measurements- Israeli Environmental ministry air quality monthly reports:

1129 <http://www.svivaaqm.net>~~http://www.svivaaqm.net,~~

1130

1131 [Israeli Environmental ministry air quality monthly reports \(in Hebrew\):](http://www.sviva.gov.il/subjectsEnv/SvivaAir/AirQualityData/NationalAirMonitoring/Pages/AirMonitoringReports.aspx)

1132 [http://www.sviva.gov.il/subjectsEnv/SvivaAir/AirQualityData/NationalAirMonitoring/Pages/AirMonitoringReports.aspx.](http://www.sviva.gov.il/subjectsEnv/SvivaAir/AirQualityData/NationalAirMonitoring/Pages/AirMonitoringReports.aspx)

1133

Formatted: Font color: Auto

1135 Weather reports- Israeli Meteorological Service ~~monthly reports: <http://www.ims.gov.il>.~~ [September monthly report \(in Hebrew\):](http://www.ims.gov.il)

1136 <http://www.ims.gov.il/IMS/CLIMATE/ClimateSummary/2015/hazesep+2015.htm>

1137

Formatted: Font color: Auto

1139 Radiosonde profiles –University of Wyoming:

1140 <http://weather.uwyo.edu/upperair/sounding.html>~~http://weather.uwyo.edu/upperair/sounding.html.~~

1141

Formatted: Font color: Auto

1142 AERONET data- <https://aeronet.gsfc.nasa.gov>.

1143

1144 Meteosat Second Generation Spacecraft pictures:

1145 http://nascube.univ-lille1.fr/cgi-bin/NAS3_v2.cgi,

1146 <https://www.eumetsat.int/website/home/Images/RealTimeImages/index.html>

1147

1148 Ceilometer profiles- the data is owned by ~~the Israeli defense force and the Israeli meteorological~~
1149 ~~service-governmental offices~~. The data is not online and provided by request.

1150

1151

1152 **Author contribution**

1153

1154 Leenes Uzan carried out the research and prepared the manuscript under the careful guidance of Smadar
1155 Egert and Pinhas Alpert. The authors declare that they have no conflict of interest.

1156

1157 **Acknowledgements**

1158

1159 We wish to thank the Israeli Meteorological Service (IMS), the Israeli Air Force (IDF), ~~the~~
1160 ~~Weizmann institute of science, the~~ Association of towns for environmental protection (Sharon-Carmel) ~~and~~
1161 ~~Rafat Qubaj from the department of Earth and Planetary Science in the Weizmann institute of Science,~~ for
1162 their ~~ceilometerceilometers'~~ data ~~and collaboration~~. Special thanks to ~~Anat Baharad, for the assistance with~~
1163 ~~the MATLAB scripts, to~~ Nir Stav (IMS) and Dr. Yoav Levy (IMS) for their fruitful advice ~~and data~~, ~~Anat~~
1164 ~~Baharad (IMS) for computer assistance and Pavel Kunin from the Tel Aviv university, for the CALIPSO~~
1165 ~~images~~. We thank the principal investigators Prof. Arnon Karnieli and Prof. Yinon Rudich for their effort in
1166 establishing and maintaining Sede-~~Boker~~ and Weizmann AERONET sites. We wish to thank the institutes
1167 that provide open site data reduction: ~~Université de Lille~~, ~~NAScube site~~, Wyoming University Radiosonde
1168 site and Israeli ministry of Environmental protection for the ~~PM10PM~~ data. ~~Expense~~ ~~Partial funding~~ of this
1169 research was ~~partly funded~~ ~~made~~ by the Virtual Institute DESERVE (Dead Sea Research Venue).

1170

1171

1172

References

1173
1174
1175
1176
1177
1178
1179
1180
1181
1182
1183
1184
1185
1186
1187
1188
1189
1190
1191
1192
1193
1194
1195
1196
1197
1198
1199
1200
1201
1202
1203
1204
1205

Alpert P., Osetinsky I., Ziv B. and Shafir H.: A new seasons definition based on the classified daily synoptic systems: An example for the Eastern Mediterranean, *Int. J. Climatol.* 24,1013-1021, 2004.

Alpert, P., Ziv, B.: The Sharav cyclone-observations and some theoretical considerations, *Int. J. Geoph. Res.*, 94, 18495-18514, 1998.

[Ansmann, A., Petzold, A., Kandler, K., Tegen, I.N.A., Wendisch, M., Mueller, D., Weinzierl, B., Mueller, T. and Heintzenberg, J.: Saharan Mineral Dust Experiments SAMUM-1 and SAMUM-2: what have we learned? *Tellus B.* 63\(4\), 403-429, 2011.](#)

[Bennouna, Y.S., De Leeuw, G., Piazzola, J. and Kusmierczyk-Michulec, J.: Aerosol remote sensing over the ocean using MSG-SEVIRI visible images. *Journal of Geophysical Research: Atmospheres.* 114\(D23\), 2009.](#)

Continuous measurement of PM10 suspended particulate matter (SPM) in ambient air, Center for Environmental Research Information Office of Research and Development U.S. Environmental Protection Agency Cincinnati, OH 45268 June 1999.

Dayan U., Lifshitz-Golden B., and Pick K.: Spatial and structural variation of the atmospheric boundary layer during summer in Israel-profiler and rawinsonde measurements, *J. Appl. Meteo.* 41, 447-457, 2002.

Derimian, Y., Karnieli, A., Kaufman, Y.J., Andreae, M.O., Andreae, T.W., Dubovik, O., Maenhaut, W., Koren, I. and Holben, B.N.: Dust and pollution aerosols over the Negev desert, Israel: Properties, transport, and radiative effect, *J. Geophys. Res.*, 111, D05205 (1-14), 2006.

Donner, L.J., Wyman, B.L., Hemler, R.S., Horowitz, L.W., Ming, Y., Zhao, M., Golaz, J.C., Ginoux, P., Lin, S.J., Schwarzkopf, M.D. and Austin, J.: The dynamical core, physical parameterizations, and basic simulation characteristics of the atmospheric component AM3 of the GFDL global coupled model CM3, *Journal of Climate*, 24(13), 3484-3519, 2011.

1206 Dubovik, O., A. Smirnov, B. N. Holben, M. D. King, Y. J. Kaufman, T. F. Eck, and Slutsker I.:
1207 Accuracy assessments of aerosol optical properties retrieved from Aerosol Robotic Network
1208 (AERONET) Sun and sky radiance measurements, J. Geophys. Res., 105(D8), 9791–9806, 2000.

1209

1210 Gasch, P., Rieger, D., Walter, C., Khain, P., Levi, Y., Knippertz, P., and Vogel, B.: ~~An~~
1211 analysis Revealing the meteorological drivers of the September 2015 severe dust event in the Eastern
1212 Mediterranean, Atmos. Chem. Phys. ~~Discuss., in review.~~, 17, 13573-13604, 2017.

1213

1214

1215 Haeffelin M., Angelini F., et al: Evaluation of Mixing –Height Retrievals from Automatic Profiling
1216 Lidars and Ceilometers in View of Future Integrated Networks in Europe. Boundary-layer Meteorol.,
1217 143.49-75, 2012.

1218

1219 Holben, B.N., Eck, T.F., Slutsker, I., Tanre, D., Buis, J.P., Setzer, A., Vermote, E., Reagan, J.A.,
1220 Kaufman, Y.J., Nakajima, T. and Lavenu, F.: AERONET—A federated instrument network and data
1221 archive for aerosol characterization. Remote sensing of environment, 66(1), 1-16, 1998.

1222

1223 Hsu, N.C., Jeong, M.J., Bettenhausen, C., Sayer, A.M., Hansell, R., Seftor, C.S., Huang, J. and Tsay,
1224 S.C.: Enhanced Deep Blue aerosol retrieval algorithm: The second generation. Journal of
1225 Geophysical Research: Atmospheres, 118(16), 9296-9315, 2013.

1224

1245 Jasim, F.H., Investigation of the 6-9 September 2015 Dust Storm over Middle East, AJER, 5 (11),
1246 201-207, 2016.

1247

1248 Jolivet, D., Ramon, D., Bernard, E., Deschamps, P.Y., Riedi, J., Nicolas, J.M. and Hagolle, O.:
1249 Aerosol monitoring over land using MSG/SEVIRI. In Proceeding of the EUMETSAT
1250 Meteorological Satellite Conference, Darmstadt, Germany ,8-12, 2008.

1251

1252 Kaskaoutis, D.G., Kambezidis, H.D., Nastos, P.T. and Kosmopoulos, P.G.: Study on an intense dust
1253 storm over Greece. Atmospheric Environment, 42(29), 6884-6896, 2008.

1254

1255 Koschmieder H.: Theorie der horizontalen sichtweite, Beitrage zur Physik der Freien Atmosphere
1256 12, 33–55,171–181, 1924.

1257

1258

1259 [Kotthaus, S., O'Connor, E., Münkel, C., Charlton-Perez, C., Gabey, A. M., and Grimmond, C. S. B.: Recommendations for processing atmospheric attenuated backscatter profiles from Vaisala CL31 Ceilometers. Atmos. Meas. Tech., 9, 3769-3791, 2016.](#)

1262

1263 ~~[Koschmieder H.: Theorie der horizontalen sichtweite, Beitrage zur Physik der Freien Atmosphäre 12, 33-55, 171-181, 1924.](#)~~

1265

1266 Levi Y., Shilo E., Setter I.: Climatology of a summer coastal boundary layer with 1290-MHz wind profiler radar and a WRF simulation. J. Appl. Meteo., 50(9), 1815-1826, 2011.

1268

1269 Mamouri, R.E., Ansmann, A., Nisantzi, A., Solomos, S., Kallos, G. and Hadjimitsis, D.G.: Extreme dust storm over the eastern Mediterranean in September 2015: satellite, [LIDARlidar](#), and surface observations in the Cyprus region, Atmos. Chem. Phys., 16(21), 13711-13724, 2016.

1272

1273 [Mei, L., Xue, Y., de Leeuw, G., Holzer-Popp, T., Guang, J., Li, Y., Yang, L., Xu, H., Xu, X., Li, C. and Wang, Y.: Retrieval of aerosol optical depth over land based on a time series technique using MSG/SEVIRI data. Atmospheric Chemistry and Physics, 12\(19\), 9167–9185, 2012.](#)

1276

1277 [Mona, L., Liu, Z., Müller, D., Omar, A., Papayannis, A., Pappalardo, G., Sugimoto, N. and Vaughan, M.: Lidar measurements for desert dust characterization: an overview. Advances in Meteorology, 2012.](#)

1279

1280 [Münkel C., Emeis S., Muller J. W., Schäfer K.: Aerosol concentration measurements with a \[LIDARlidar\]\(#\) ceilometer: results of a one year measuring campaign, Remote sensing of Clouds and the Atmosphere VIII, 5235, 486-496, 2004.](#)

1284

1285 [Münkel, C., Schäfer, K. and Emeis, S.: Adding confidence levels and error bars to mixing layer heights detected by ceilometer, In Proc. SPIE, Vol. 8177, 817708-1, 2011.](#)

1287

1288 [Papayannis, A., Amiridis, V., Mona, L., Tsaknakis, G., Balis, D., Bösenberg, J., Chaikovski, A., De Tomasi, F., Grigorov, I., Mattis, I. and Mitev, V.: Systematic lidar observations of Saharan dust over Europe in the frame of EARLINET \(2000–2002\). Journal of Geophysical Research: Atmospheres, 113\(D10\), 2008.](#)

1291

Formatted: Font color: Auto

1292 Parolari, A.J., Li, D., Bou-Zeid, E., Katul, G.G. and Assouline, S.: Climate, not conflict, explains
1293 extreme Middle East dust storm, Environ. Res. Lett, 11, 114013, 2016.
1294

1295
1296 Pu, B. and Ginoux, P.: The impact of the Pacific Decadal Oscillation on springtime dust activity in
1297 Syria, Atmos. Chem. Phys., 16(21), 13431-13448, 2016.
1298

1299 [Rao, P.G., Hatwar, H.R., Al-Sulaiti, M.H. and Al-Mulla, A.H.: Summer shamals over the Arabian](#)
1300 [Gulf. Weather, 58\(12\), 471-478, 2003.](#)
1301

1302 [Remer, L.A., Tanre, D., Kaufman, Y.J., Levy, R. and Mattoo, S.: Algorithm for remote sensing of](#)
1303 [tropospheric aerosol from MODIS: Collection 005. National Aeronautics and Space](#)
1304 [Administration, 1490, 2006.](#)
1305

1306 [Rieger, D., Bangert, M., Bischoff-Gauss, I., Förstner, J., Lundgren, K., Reinert, D., Schröter, J.,](#)
1307 [Vogel, H., Zängl, G., Ruhnke, R. and Vogel, B.: ICON-ART 1.0-a new online-coupled model system](#)
1308 [from the global to regional scale. Geosci. Model Dev., 8, 1659–1676, 2015](#)
1309

1310 [Roebeling, R. A., Feijt A. J., and Stammes P.: Cloud property retrievals for climate monitoring:](#)
1311 [Implications of differences between Spinning Enhanced Visible and Infrared Imager \(SEVIRI\) on](#)
1312 [METEOSAT-8 and Advanced Very High Resolution Radiometer \(AVHRR\) on NOAA-17, J.](#)
1313 [Geophys. Res., 111\(D20\), 2006.](#)
1314

1315 [Romano, F., Ricciardelli, E., Cimini, D., Di Paola, F. and Viggiano, M.: Dust Detection and Optical](#)
1316 [Depth Retrieval Using MSG-SEVIRI Data. Atmosphere, 4\(1\), 35-47,2013.](#)
1317

Formatted: Font color: Auto

1318 Solomos, S., Ansmann, A., Mamouri, R.-E., Biniotoglou, I., Patlakas, P., Marinou, E., and Amiridis,
1319 V.: Remote sensing and modeling analysis of the extreme dust storm hitting Middle East and Eastern
1320 Mediterranean in September 2015, Atmos. Chem. Phys., 17, 4063-4079, 2017.
1321

1322 Stull R. B.: An introduction to boundary layer meteorology, Kluwer Academic publishers,
1323 Netherlands, 666p, 1988.

Formatted: Font color: Auto

1324
1325 Uzan L., Alpert P.: The coastal boundary layer and air pollution- A high temporal resolution analysis
1326 in the East Mediterranean Coast, [TOASJThe open atmospheric science journal](#), 6 ,9-18, 2012.

Formatted: Font color: Auto

Formatted: Font color: Auto

1327
1328
1329
1330
1331
1332
1333
1334
1335
1336
1337
1338
1339
1340
1341
1342
1343
1344
1345
1346
1347
1348
1349
1350
1351
1352
1353
1354
1355
1356
1357
1358
1359
1360

Uzan, L., Egert, S. and Alpert, P.: Ceilometer evaluation of the eastern Mediterranean summer boundary layer height—first study of two Israeli sites. *Atmos. Meas. Tech.*, 9(9), 4387–4398, 2016.

Vaisala ceilometer CL31 user's guide M210482EN-B, October, 2004.

[Wang, Y. Q.: MeteoInfo: GIS software for meteorological data visualization and analysis. *Met. Apps*, 21, 360–368, 2014.](#)

Wiegner M. and Gasteiger J.: Correction of water vapor absorption for aerosol remote sensing with ceilometers, *Atmos. Meas. Tech.*, 8, 3971–3984, 2015.

Wiegner, M., Madonna, F., Binietoglou, I., Forkel, R., Gasteiger, J., Geiß, A., Pappalardo, G., Schäfer, K. and Thomas, W.: What is the benefit of ceilometers for aerosol remote sensing? An answer from EARLINET, *Atmos. Meas. Tech.*, 7(7), 1979–1997, 2014.

Winker, D.M., Vaughan, M.A., Omar, A., Hu, Y., Powell, K.A., Liu, Z., Hunt, W.H. and Young, S.A.: Overview of the CALIPSO mission and CALIOP data processing algorithms. *Journal of Atmospheric and Oceanic Technology*, 26(11), 2310–2323, 2009.

1361
1362
1363
1364

365 Table 1. ~~A list of~~The publications on the September 2015 dust event

Publications	Title	Main Tool	Main outcome
Pu, B. and Ginoux, P (2016)	The impact of the Pacific Decadal Oscillation on springtime dust activity in Syria	MODIS Terra MODIS Aqua DOD AOD, GFDL-AM3 model	Model underestimation in the EM due to inaccurate soil moisture
Parolari et al. (2016)	Climate, not conflict, explains extreme Middle East dust storm-	WRF model	Unusual low level westerly wind spread to the EM, to reversely transport the previously eastward particles back to the EM.
Mamouri et al. (2016)	Extreme dust storm over the eastern Mediterranean in September 2015: satellite, LIDAR lidar, and surface observations in the Cyprus region-	MODIS, EARLINET profiles and PM10	Dust plumes from Syria entered the EM in a double layer structure, pointing to multiple dust sources
Solomos Stavros et al. (2016)	Remote sensing and modeling analysis of the extreme dust storm hitting Middle East and Eastern Mediterranean in September 2015-	RAMS model EARLINET LIDAR lidar, MSG and CALIPSO.	Low model ability to simulate the event, due to inaccuracies in model physical processes.
Jasim, F.H. (2016) Gasch et al. (2017)	An analysis Investigation of the 6-9 September 2015 severe dust event in the Eastern Mediterranean Dust Storm over Middle East	ICON-ART Satellite MSG-SEVIRI, Meteoinfo model	Two dust storms simultaneously, from northern Syria and Sinai desert created by two low pressure systems An unusual early active Red Sea Trough with meso-scale convective systems generating cold pool outflows producing the dust storm. Model lacked development of a supercritical flow to produce excessive wind speeds-
Gasch et al. (2017) Jasim, F.H. (2016)	Investigation An analysis of the 6-9 September 2015 Dust	Satellite MSG-SEVIRI, Meteoinfo ICON-ART model	An unusual early active Red Sea Trough with meso-scale convective systems generating

Storm over Middle East, severe dust event in the Eastern Mediterranean

cold-pool outflows producing the dust storm. Model lacked development of a super critical flow to produce excessive wind speeds. Two dust storms simultaneously, from northern Syria and Sinai desert created by two low pressure systems.

1366
1367
1368
1369
1370
1371

Table 2. Ceilometer CL31/Ceilometers locations

Location	Site	Long/Lat	Distance from shoreline (km)	Height (m AGL)
Mount Meron	Northern	33.0/35.4	31	1,150
Ramat David	Northern	32.7/35.2	24	50
Hadera	Onshore	32.5/34.9	3.5	10
Tel Aviv	Onshore	32.1/34.8	0.05	5
Beit Dagan	Inland	32.0/34.8	7.5	33
Weizmann	Inland	31.9/34.8	11.5	60
Nevatim	Southern	31.2/34.9	44	400
Hazerim	Southern	31.2/34.7	70	200

*Ceilometer Weizmann is a CL51

1374

1375

1376

1377

1378

Table 3. Some detail on Israel and Cyprus radiosonde detail/Ceilometers configurations

Site Location	# Station	Lon/Lat	Type	Time	Height (m ASL)
Israel	40179	34.8/32.0		12:00	35
		resolution(sec)	resolution (m)		
Mount Merc	CL31	16	10	7.7	
Ramat Davi	CL31	16	10	7.7	
Hadera	CL31	16	10	7.7	
Tel Aviv	CL31	16	10	7.7	
Beit Dagan	CL31	15	10	7.7	
CyprusWeizm	17607CL51	33.4/35.2	161	06:00	
nn		15.4	16		
Nevatim	CL31	16	10	7.7	

Hazerim CL31 16 10 7.

1379 * Height range depends on sky conditions and is limited as AOD increases.
 1380 * In all ceilometers but in Beit Dagan site, data acquisition was limited to 4.5 km based on the BLview firmware
 1381
 1382
 1383

1384
 1385
 1386
 1387 Table 4. Numbers & heights of PM10 measurement sites-Ceilometer technical information

Region	Location	Total Number of Stations	Highest Station		Lowest Station		Type	Engine
			Receiver	Transmitter	Receiver	Firmware		
Beit Dagan	(m ASL)	9	CLE311	CLR311	CLT311			1.72
			CLRE321	CLT521			1.03	
			CL51		133			
East		9	960		57			
Center		16	305		21			
Shoreline		12	75		0			
South	Weizmann	1	CL51		133			CLE3

1388
 1389
 1390
 1391
 1392
 1393 Table 5. Hourly maximum concentration of PM2.5, collected from 21 monitoring sites, between 7-10
 1394 September 2015. The values are ranked from low (dark green) to high (dark red) values.

No.	Site	Height (m ASL)	Region	PM2.5 ($\mu\text{g m}^{-3}$)			
				7-Sep-15	8-Sep-15	9-Sep-15	10-Sep-15
1	Kefar Masarik	8	North	52	378	389	378
2	Ahuza	280	North	36	743	650	419
3	Newe Shaanan	240	North	43	400	466	525
4	Nesher	90	North	43	564	496	349
5	Kiryat Biyalic	25	North	53	424	703	447
6	Kiryat Binyamin	5	North	40	223	412	256
7	Kiryat Tivon	201	North	47	413	416	300
8	Afula	57	North	44	836	550	405
9	Raanana	54	Coast	38	173	291	229
10	Antolonsky	34	Coast	32	470	626	386
11	Ashdod	25	Coast	36	303	750	332
12	Ironi D	12	Coast	34	424	507	327
13	Tel aviv Central Station	29	Coast	41	716	803	451
14	Ashkelon	25	Coast	61	182	537	119
15	Jerusalem Efrata	749	Mountain	106	2285	434	403
16	Jerusalem Bar Ilan	770	Mountain	107	3063	641	518
17	Gedera	70	South	34	433	683	308
18	Nir Israel	30	South	25	363	638	228
19	Kiryat Gvaram	95	South	42	376	870	300
20	Sede Yoav	105	South	45	323	245	228
21	Negev Mizrahi	577	South	42	1748	526	317

1396
1397
1398
1399
1400
1401
1402
1403
1404
1405
1406
1407
1408
1409
1410
1411
1412
1413
1414
1415

Table 6. Hourly maximum concentration of PM10, collected from 31 monitoring sites, between 7-10 September 2015. The values are ranked from low (dark green) to high (dark red) values.

No.	Site	Height (m ASL)	Region	PM10 ($\mu\text{g m}^{-3}$)			
				7-Sep-15	8-Sep-15	9-Sep-15	10-Sep-15
1	Galil Maaravi	297	North	114	3130	1987	1562
2	Karmelia	215	North	39	1120	1008	765
3	Newe Shaanan	240	North	104	3459	2471	1518
4	Haifa Port	0	North	78	1600	1965	1699
5	Nesher	90	North	117	3265	2746	1270
6	Kiryat Haim	0	North	82	1161	1625	1088
7	Afula	57	North	97	3239	2322	1961
8	Um El Kotof	0	Coast	99	2025	2028	1630
9	Orot Rabin	0	Coast	58	1152	1455	999
10	Barta	0	Coast	112	2540	2345	1612
11	Qysaria	19	Coast	54	1067	2116	1272
12	Rehuvot	70	Coast	88	2236	3045	1257
13	Givataim	0	Coast	112	1909	4014	1484
14	Yad Avner	77	Coast	61	1738	2902	1252
15	Ameil	20	Coast	96	2027	3472	1321
16	Shikun Lamed	17	Coast	51	1701	3244	1097
17	Station	29	Coast	87	1420	2176	998
18	Ashkelon	29	Coast	117	953	1692	551
19	Ariel	546	Mountain	128	2723	1481	1358
20	Jerusalem Efrata	770	Mountain	273	7820	1630	1437
21	Jerusalem Bar Ilan	749	Mountain	181	5588	1191	966
22	Jerusalem Safra	797	Mountain	491	10280	2389	1780
23	Gush Ezion	960	Mountain	310	6230	1679	1119
24	Erez	80	South	44	1000	1000	718
25	Beit Shemesh	350	South	115	2097	1943	1788
26	Caray Yosef	260	South	85	1047	784	594
27	Modiin	267	South	185	2701	2245	1980
28	Bat Hadar	54	South	65	1342	2563	841
29	Nir Galim	0	South	94	1479	2292	1027
30	Negev Mizrahi	577	South	183	9031	2806	1730
31	Eilat	0	South	275	1867	1592	1684

1416

1417

1418

1419

1420

1421

Formatted: Font color: Auto 1422

Formatted: Indent: Before: 0", After: -0.23" 1423